1992

New pathways to tungsten and molybdenum oxides, nitrides and azides

Michael Richard Close
Iowa State University

INFORMATION TO USERS

This manuscript has been reproduced from the microfilm master. UMI films the text directly from the original or copy submitted. Thus, some thesis and dissertation copies are in typewriter face, while others may be from any type of computer printer.

The quality of this reproduction is dependent upon the quality of the copy submitted. Broken or indistinct print, colored or poor quality illustrations and photographs, print bleedthrough, substandard margins, and improper alignment can adversely affect reproduction.

In the unlikely event that the author did not send UMI a complete manuscript and there are missing pages, these will be noted. Also, if unauthorized copyright material had to be removed, a note will indicate the deletion.

Oversize materials (e.g., maps, drawings, charts) are reproduced by sectioning the original, beginning at the upper left-hand corner and continuing from left to right in equal sections with small overlaps. Each original is also photographed in one exposure and is included in reduced form at the back of the book.

Photographs included in the original manuscript have been reproduced xerographically in this copy. Higher quality 6" x 9" black and white photographic prints are available for any photographs or illustrations appearing in this copy for an additional charge. Contact UMI directly to order.

U·M·I

University Microfilms International
A Bell & Howell Information Company
300 North Zeeb Road, Ann Arbor, MI 48106-1346 USA
313/761-4700 800/521-0600

Order Number 9311484

New pathways to tungsten and molybdenum oxides, nitrides and azides

Close, Michael Richard, Ph.D.

Iowa State University, 1992

U·M·I
300 N. Zeeb Rd.
Ann Arbor, MI 48106

New pathways to tungsten and molybdenum oxides, nitrides and azides

by

Michael Richard Close

A Dissertation Submitted to the
Graduate Faculty in Partial Fulfillment of the
Requirements for the Degree of
DOCTOR OF PHILOSOPHY

Department: Chemistry
Major: Inorganic Chemistry

Approved:

Signature was redacted for privacy.

In Charge of Major Work

Signature was redacted for privacy.

For the Major Department

Signature was redacted for privacy.

For the Graduate College

Iowa State University
Ames, Iowa

1992

TABLE OF CONTENTS

LIST OF TABLES

LIST OF FIGURES

GENERAL INTRODUCTION

The interest in new materials and their properties has produced a synergistic collaboration between chemistry and material science resulting in new methodologies[1-4] for the preparation of ceramics[5] and refractory metal oxides, carbides and nitrides[6]. Traditional processing of ceramics utilize high temperatures and long reaction periods in order to obtain the required diffusion rates for the completion of the reaction. Increased purity and lower processing temperatures[7] are obtainable by utilization of molecular precursors designed for the application. One example of new methodologies is sol-gel processing[8] which offers the advantage of mixing the elements on an atomic level prior to heat processing which lowers the diffusion distance required for final phase formation and potentially lowers the temperatures at which these ceramics can be processed. It is through the use of molecular precursors coupled with appropriate processing techniques that metastable (thermodynamically unstable and kinetically stable) compounds which cannot be obtained using conventional processing techniques can be produced.

Molybdenum and tungsten nitrides (MN_x $x \leq 1$) have been made by heating the metal oxides in flowing ammonia at high temperatures[9], reaction of the metal halide[10] ($MoCl_5$) with ammonia at 400-800 °C, reactive sputtering and ion implantation[11], and nitrogen plasma reactions[12]. All of these reactions are

conducted at temperatures above 400 °C resulting in a metal nitride with a metal oxidation state of 3+ or lower. The thermodynamic studies of Lyutaya[13] and Lakhtin[14] demonstrated that the Gibbs free energy of formation (ΔG_f°) of Mo_2N is inversely related to temperature. The decomposition of metal nitrides is enthalpically and entropically driven due to the exothermic formation of N_2 (N≡N bond energy is 934 Kj/mol) and the evolution of gas, respectively. The decomposition of a transition metal dinitride can be represented by the following scheme:

$$MN_2 \text{ --------> } MN + 1/2\ N_2$$

$$2MN \text{ --------> } M_2N + 1/2\ N_2$$

$$M_2N \text{ --------> } 2M + 1/2\ N_2$$

This sequence of decomposition is simplified but it does establish the stability order, generally, in the tungsten and molybdenum nitrides. Relatively few reports of tungsten and molybdenum nitrides in oxidation states higher than (III) have been given. WN_2 was reported by Khitrova[15] to form as a result of nitriding thin films of tungsten with ammonia at elevated temperatures. The metal was quenched and only the thinnest regions of the film displayed the rhombohedral, WN_2, as characterized by TEM. A higher nitride of molybdenum, identified as a gold colored conductive compound with the stoichiometry, Mo_2N_3, was prepared by the chemical vapor deposition (CVD) of $Mo(NMe_2)_4$ in

ammonia gas.[16]

Part of this work focuses on the synthesis, reactivity and thermal decomposition of tungsten and molybdenum nitride and azide compounds to yield higher nitrides of the metals, not obtainable using conventional processing. A project relating to tungsten oxides grew out of the nitride research when it was discovered that a hexagonal tungsten oxide bronze phase could be prepared from tungsten nitrido and imido reactants.[17] Upon further investigation, the parameters of hexagonal phase formation were elucidated and a detailed structural study, utilizing neutron powder diffraction, was completed for the bronze and will be reported hereafter.

Explanation of Dissertation Format

This dissertation consists of four sections, each of which are formatted for publication in a technical journal. However, each section would be subject to modification, prior to submission. The references cited in the general introduction are found at the end of the dissertation, while each section contains an independent listing of references cited in that section.

SECTION I. SYNTHESIS, CHARACTERIZATION AND STRUCTURE OF THE TUNGSTEN-NITROGEN HETEROCYCLE: $[WNCl_3]_4$

INTRODUCTION

One of the fundamental objectives of this research is to synthesize molecular reactants that can be converted to desired high oxidation state metal nitrides of tungsten which are metastable (thermodynamically unstable). $WNCl_3$ represents a potentially significant intermediate between WCl_6 and a desired product, WN_2. $WNCl_3$ was prepared initially by Kurt Dehnicke et al.[1] in 1965 by the reaction of WCl_6 and chlorine azide (ClN_3) in carbon tetrachloride at 30 °C. More recent studies have utilized trimethylsilylazide[2] and tris(trimethylsilyl)amine[3] as the nitriding reactants for the formation of $MNCl_3$ from tungsten or molybdenum halides. Since the initial preparation of $MNCl_3$ (M=Mo,W)[1], which was characterized by infrared spectroscopy, X-ray powder diffraction and elemental analysis, $[MoNCl_3]_4$[4], $[MoNCl_3 \cdot OPCl_3]_4$[5], $[WNCl_3 \cdot OPCl_3]_4 \cdot 2OPCl_3$[6], $[WNCl_3 \cdot 0.5HN_3]_4$[7] and $[WNCl_3 \cdot NCPh]_4 \cdot 3CH_2Cl_2$[8] represent some of the tetrameric compounds that have been characterized structurally by single crystal X-ray diffraction methods. $WNCl_3$ was formulated as a polymer $[WNCl_3]_\infty$ in a 1981 review of metal nitride multiple bonding[9]. Two possibilities for polymeric $WNCl_3$ are readily apparent. One would possess an infinite planar zig-zag chain geometry which has yet to be observed and the other would contain a linear chain similar to those found in $ReNCl_4$[10] and $WN(t\text{-}BuO)_3$[11]. The crystal structure of $WNCl_3$ as a compound uncoordinated by

other ligands has been conspicuously absent from the literature.

In order to fully utilize $WNCl_3$ as a starting material for tungsten nitride synthesis, a new method for production of $WNCl_3$ has been developed which yields relatively pure $WNCl_3$ in high yields. The structure of $[WNCl_3]_4$ has been determined by single crystal X-ray methods. Three different compounds of $WNCl_3$ have been identified by single crystal and powder X-ray diffraction and the differences in structure attributed to the interactions of solvent molecules with the $[WNCl_3]_4$ units. The solvent appears to coordinate to the tungsten, trans to the W-N multiple bond. This coordination seems to disrupt the packing and inter-chloride linking of adjacent tetrameric $[WNCl_3]_4$units.

EXPERIMENTAL SECTION

Materials

All the materials reported in this section are extremely reactive with oxygen and water. Manipulations of oxygen- and water-sensitive compounds were performed under inert atmosphere conditions using standard drybox, vacuum and Schlenk techniques.

Dichloromethane and 1,2-dichloroethane (DCE) were dried by refluxing the solvents over phosphorus(V) oxide or calcium hydride for greater than 6 hours to remove all water, degassed by three freeze-evacuate-thaw cycles and vacuum distilled onto 3 Å molecular sieves, which had been heated to 250 °C under dynamic vacuum, prior to use. The organic solvents were transferred for further reactions by either vacuum distillation or syringe with an inert gas flow. Tungsten hexachloride was obtained from Pressure Chemical Co. and sublimed using a three chamber sublimation tube to remove the tungsten oxychlorides ($WOCl_4$, WO_2Cl_2) by sublimation to the outer chamber, then subliming the purified WCl_6 into a central chamber and isolating it in a dry-box. Trimethylsilylazide (TMSA) was obtained from Petrarch Chemical Co. and transferred to a solvent flask and stored in the dark, under vacuum, to avoid photolytic decomposition of the azide.

Analytical Procedures

Tungsten was determined using a gravimetric procedure in which the tungsten containing material was weighed, by difference, into tared ceramic crucibles and treated with nitric acid to convert all of the tungsten containing material to WO_3. The crucibles were then heated to 820 °C for 1 to 10 hours, allowed to cool in a desiccator and reweighed. This process was repeated until constant weight was achieved.

Chloride was determined by use of a potentiometric titration. In the drybox, the chloride containing material was weighed, by difference, into dried, 250 mL beakers which were then covered with Parafilm and subsequently taken into a fume hood where the samples were treated with 1 to 3 M sodium or potassium hydroxide and heated to facilitate decomposition. If the samples did not decompose completely, hydrogen peroxide was added which, in every case, decomposed the samples entirely. The hydrogen peroxide was decomposed by boiling the solutions for an additional 1 to 3 hours. The cooled, basic solutions were then acidified with 1 M nitric acid to a methyl red endpoint and chloride was determined using a potentiometric titration with a standardized silver nitrate solution.

Synthesis

In a typical preparation, a solution of DCE (15 mL) and TMSA (2.34 mL, 17.6 mmole, 2.03 g) was added drop-wise (approximately 3 drops/sec) to a refluxing solution of WCl_6 (6.975 g, 17.6 mmole) in DCE (80 mL), which was mixed with a rotating magnetic stirring bar. During the reaction the color of the solution remained purple but the color of the particulate solid changed from purple to brown-orange after 2 days. The reaction solution was allowed to continue at refluxing temperature for three days, after which the mixture was filtered using a porous ceramic filter in an evacuable pyrex tube. The solid $WNCl_3$, isolated on the frit, was extracted with clean DCE for approximately 2 days to eliminate any silane compounds or remaining WCl_6. The solid was then dried under vacuum for a period not less than 12 hours and isolated in a drybox. A typical yield was 4.20 g (78.5%). The $WNCl_3$ was then heated under dynamic vacuum at 160 °C for 12 hours to eliminate DCE and WCl_6. Anal. Calcd for $WNCl_3$: W, 60.43; Cl, 34.96; W:Cl, 1:3.00. Found (before heating): W, 55.18; Cl, 32.53; W:Cl, 1:3.06. Found (after heating): W, 60.32; Cl, 34.60; W:Cl, 1:2.98. IR (Nujol, cm^{-1}) of $WNCl_3$ (before heating): 1082 s, (υ(W≡N));[12], 685 s, (υ(C-Cl)); 400 s, 385 s, 371 s, 358 s, 315 s, (υ(W-Cl)). IR of $WNCl_3$ (after heating): 1082 s, (υ(W≡N)); 399 s, 374 s, 361 s, 356 sh, 331 s, 309 s υ(W-Cl).

Physical Measurements

Infrared spectra were obtained from a IBM IR/90 or a Bomem MB-Series Fourier Transform infrared spectrometer. The samples were prepared as Nujol mulls and pressed between CsI plates. The spectra were recorded separately for the mid-IR (4000-600 cm^{-1}) and far IR (600-200 cm^{-1}) in the case of the IBM spectrometer and from 4000 to 185 cm^{-1} with the Bomem spectrometer. Most of the spectral baselines were normalized, using non-linear baseline algorithms.

X-ray powder diffraction data were obtained from an Enraf-Nonius Delft triple-focusing Guinier camera using copper $K\alpha_1$, radiation (λ=1.54056), a Philips ADP3520 X-ray powder diffractometer or a Scintag θ-θ diffractometer using Cu $K\alpha_1$,$K\alpha_2$ averaged radiation. Two air-tight chambers for x-ray powder diffraction were designed and built to accommodate air-reactive materials. A cylindrical sample holder (Figure I-1) was developed for the Philips diffractometer. The powdered, air-sensitive samples were mounted by pressing the powders into a recessed square or circular region (created by sandblasting a quartz slide with the appropriate template) in the single crystal quartz plate (obtained from Gem Dugout)[13], with a microscope slide to insure that the surface of the powder and the quartz plate were coplanar. The surface of the quartz plate in the holder was designed to align with the mounting tab on the

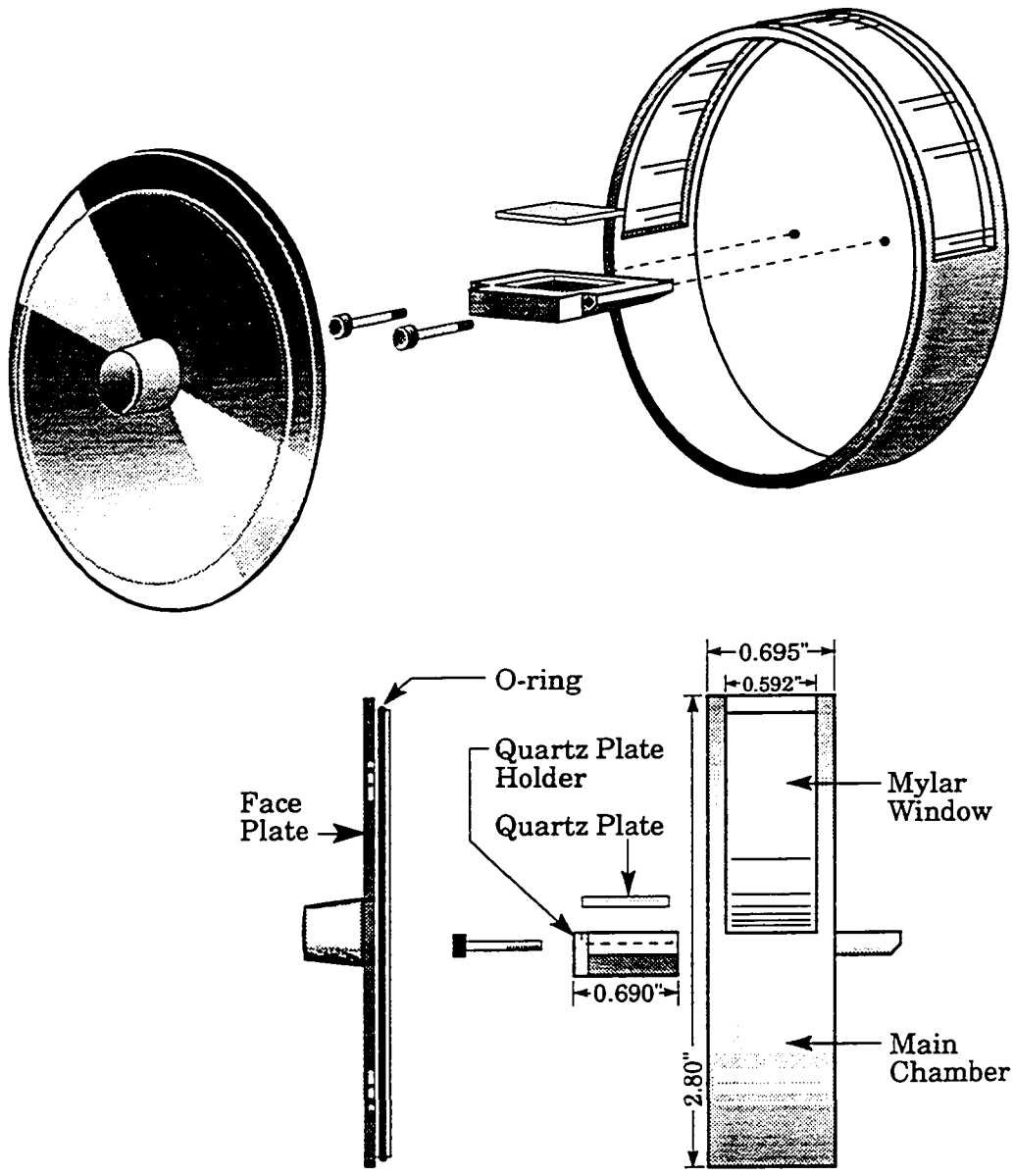

Figure I-1. Mylar-windowed aluminum sample holder for X-ray powder diffraction analyses of water and oxygen reactive compounds. Designed for use with a Philips ADP3520 diffractometer

rear of the main chamber to insure proper elevation of the sample with respect to the X-ray focal distance. After the quartz plate was placed in the sample holder, the chamber was closed with an o-ring sealed face plate which creates a positive pressure in the holder. Thus, even with the Mylar window, an effective barrier to water vapor and oxygen diffusion was maintained for greater than 24 hours for most of materials tested. The Scintag environment cell had to be modified in accordance with the diffractometer geometry (see Fig. I-2). Similar principles were used in the design of the Scintag cell as those used in the Philips cell. However the following difference is worth noting. The positive pressure produced within the Scintag cell will not be as great as that in the Philips cell. But with the use of tightening screws, the o-ring can form a tighter seal in the Scintag cell and therefore should represent an improvement over the Philips cell.

Crystal Growth and Mounting

Numerous attempts were made to obtain crystals of $WNCl_3$. Cooling saturated solutions and layering non-polar solvents on top of saturated solutions of $WNCl_3$ produced only finely divided powders. It was during the final heating step in the $WNCl_3$ synthesis that small (10 to 30 micron) orange crystallites were observed to form in the cooler end of the tube. In order to produce larger

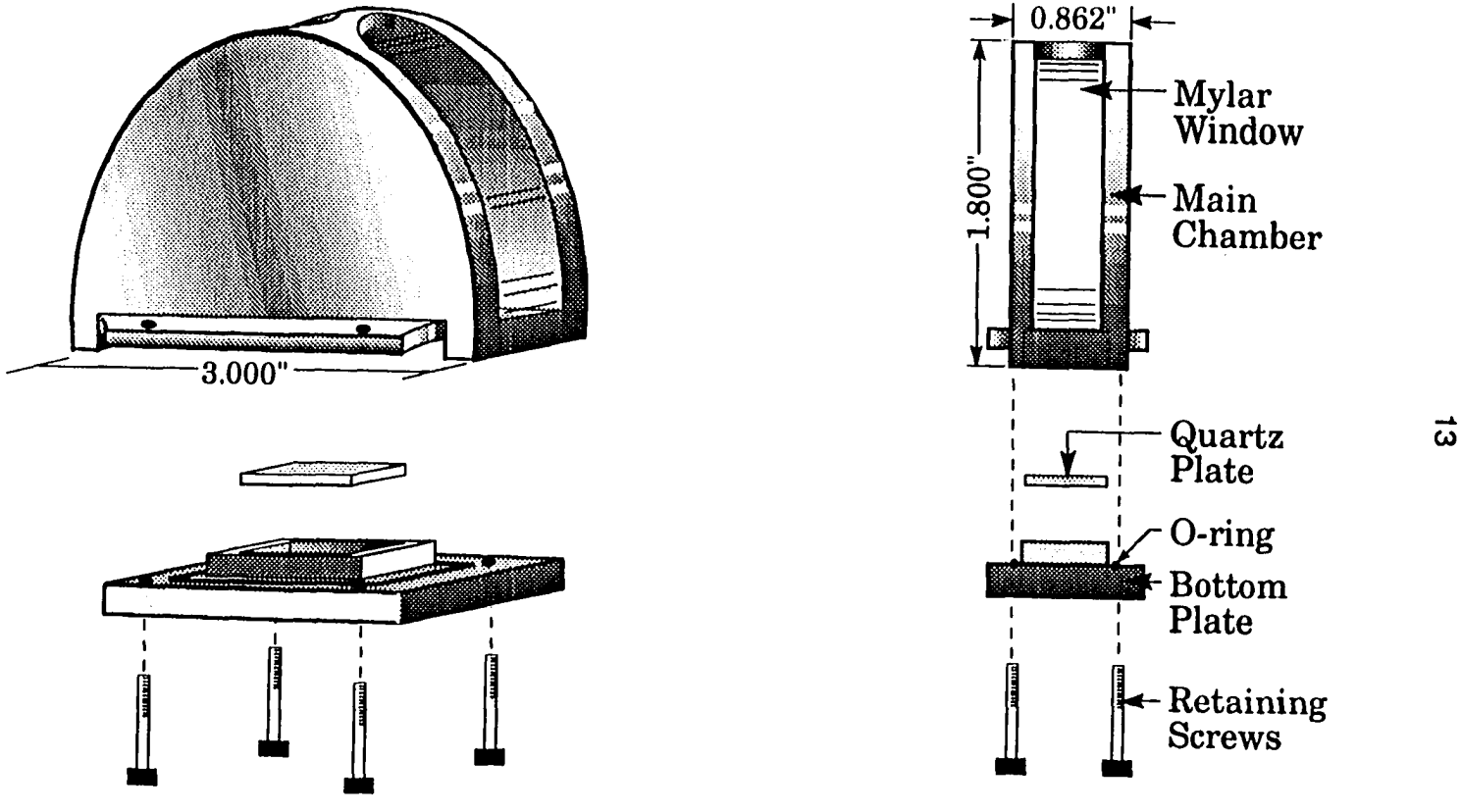

Figure I-2. Mylar-windowed aluminum sample holder for X-ray powder diffraction analyses of air reactive compounds. Designed for use with a Scintag θ-θ diffractometer using copper radiation

crystals, small samples of $WNCl_3$ (15 mg) were sealed under vacuum in 15 cm by 1 cm (outer diameter) pyrex tubes and placed in a two zone furnace under a thermal gradient of 10 °C at several temperatures ranging from a 160 to 170 °C gradient to a 290 to 300 °C gradient. It was found that crystallites of sufficientsize (3 to 400 micron) for single crystal x-ray diffraction could be obtained by sublimation of the $WNCl_3$, using a thermal gradient of 290/300 °C for 3 days. In sublimation experiments conducted above 200 °C only a small amount of the $WNCl_3$ actually sublimed while the rest decomposed to a non-volatile black solid. The crystals were mounted in 0.5 mm capillary tubes with Apiezon grease using a microscope drybox in Dr. J. D. Corbett's group. The crystallites had a platelet geometry with dimensions 300 x 400 x 50 microns.

Data Collection and Structural Determination

Data were collected at room temperature with an Enraf-Nonius CAD4 diffractometer. Lattice parameters were determined from 15 reflections with $18.5 < 2\theta < 32.4°$. Graphite-monochromated Mo Kα radiation was used to collect the data with a two-theta range of 4 to 60°. The θ-2θ scan technique was used. The data were corrected for Lorentz and polarization effects. The transmission factors, based on Ψ scans, varied from .99 to .25, which was reflective of the crystal platelet geometry. An empirical absorption correction

was made based on the Psi scans. The intensities of three standard reflections were constant throughout the data collection, therefore a standard correction was not applied. 5742 reflections were collected, of which 2399 were unique with $F_o^2/\sigma F_o^2 > 3$. The structure was solved by Patterson methods (SHELXS86)[14] and refined by full matrix least-square techniques using TEXSAN[15] programs to R=0.041 and R_w=0.049. All atoms were located and refined anisotropically. The final electron density difference map contained many peaks, with the highest being at 6.4 e/Å^3. All the large difference Fourier peaks were near the tungsten atoms with distances less than 1.00 Å from tungsten. An improved absorption correction would be needed to provide a better fit of the data.

Details of the data collection are given in Table I-1 . Final atomic positional parameters and selected bond distances and angles are given in Tables I-2 and I-3 respectively. The anisotropic temperature factors are listed in Table I-4.

Table I-1. Crystal Data Summary for $[WNCl_3]_4$

Compound	$[WNCl_3]$
Formula Weight	396.57
Space Group	$P\bar{1}$
a, Å	7.7517(9)
b, Å	8.143(1)
c, Å	9.114(1)
α, deg	98.71(2)
β, deg	107.52(2)
γ, deg	110.40(2)
V, $Å^3$	492.6(4)
Z	4
d_{calc}, g/cm^3	4.10
Crystal size, mm	0.4 x 0.2 x 0.1
μ(MoKα), cm^{-1}	254.3
Data collection instrument	Enraf-Nonius CAD4
Radiation (monochromated in incident beam)	MoKα(λ=0.71073Å)
Orientation reflections, number, range (2Θ)	15, 18.5 < 2Θ < 32.4
Temperature, °C	22(1)
Scan method	Θ-2Θ
Data collection range, 2Θ, deg	4.0 to 60.0
No. data, collected	5742
unique	4945
with $F_o^2 > 3\sigma(F_o^2)$	2399
Number of parameters refined	92
Trans. factors, max., min. (psi-scans)	0.999, 0.25
R^a	0.041
$R_w{}^b$	0.049
Quality-of-fit indicator[c]	1.38
Largest shift/esd, final cycle	0.01
Largest peak, $e/Å^3$	6.4(3)

a $R=\Sigma||F_o| - |F_c||/\Sigma|F_o|$

b $R_w=[\Sigma w(|F_o| - |F_c|)^2/\Sigma w|F_o|^2]^{1/2}$; $w=1/\sigma^2(|F_o|)$

c Quality-of-fit$=[\Sigma w(|F_o| - |F_c|)^2/(N_{obs}-N_{parm})]^{1/2}$

Table I-2. Positional Atomic Parameters and Isotropic Temperature Factors for $[WNCl_3]_4$

Atom	x	y	z	B(Å^2)[a]
W(1)	0.13376(4)	0.36229(4)	0.12713(3)	1.164(5)
W(2)	0.01355(4)	0.05435(4)	0.72568(3)	1.201(5)
Cl(1)	0.3233(3)	0.0473(3)	0.3865(3)	2.38(4)
Cl(2)	0.1921(3)	0.6484(3)	-0.0158(2)	1.98(4)
Cl(3)	-0.3145(3)	-0.0400(3)	0.2057(3)	2.59(4)
Cl(4)	0.4498(3)	0.4064(3)	0.1612(3)	2.61(4)
Cl(5)	0.0758(3)	0.2311(3)	0.5535(2)	2.13(4)
Cl(6)	0.2188(3)	0.5798(3)	0.3531(2)	2.64(4)
N(1)	0.0605(8)	0.1734(8)	0.1892(6)	1.3(1)
N(2)	-0.0643(9)	0.7845(8)	0.1061(7)	1.6(1)

[a]Anisotropically refined atoms are given in the form of the isotropic equivalent displacement parameter defined as: (4/3) * [a^2*B(1,1) + b^2*B(2,2) + c^2*B(3,3) + ab(cos gamma)*B(1,2) + ac(cos beta)*B(1,3) + bc(cos alpha)*B(2,3)]inst2>

Table I-3. Selected Bond Distances and Bond Angles for $[WNCl_3]_4$

Bond Distances in Angstroms[a]

Atom 1	Atom 2	Distance	Atom 1	Atom 2	Distance
W(1)	Cl(2)	2.386(2)	W(2)	Cl(1)	2.275(2)
W(1)	Cl(4)	2.263(2)	W(2)	Cl(3)	2.276(2)
W(1)	Cl(6)	2.253(2)	W(2)	Cl(5)	2.328(2)
W(1)	N(1)	1.690(6)	W(2)	N(1)	2.081(6)
W(1)	N(2)	2.081(6)	W(2)	N(2)	1.702(6)

Bond Angles in Degrees

Atom 1	Atom 2	Atom 3	Angle	Atom 1	Atom 2	Atom 3	Angle
Cl(2)	W(1)	Cl(4)	160.81(7)	Cl(1)	W(2)	Cl(5)	94.94(7)
Cl(2)	W(1)	Cl(6)	92.80(8)	Cl(1)	W(2)	N(1)	82.3(2)
Cl(2)	W(1)	N(1)	95.0(2)	Cl(1)	W(2)	N(2)	99.7(2)
Cl(2)	W(1)	N(2)	83.5(2)	Cl(3)	W(2)	Cl(5)	93.55(8)
Cl(4)	W(1)	Cl(6)	95.41(8)	Cl(3)	W(2)	N(1)	82.7(2)
Cl(4)	W(1)	N(1)	100.6(2)	Cl(3)	W(2)	N(2)	98.6(2)
Cl(4)	W(1)	N(2)	84.3(2)	Cl(5)	W(2)	N(1)	160.1(2)
Cl(6)	W(1)	N(1)	100.0(2)	Cl(5)	W(2)	N(2)	101.7(2)
Cl(6)	W(1)	N(2)	165.8(2)	N(1)	W(2)	N(2)	98.2(2)
N(1)	W(1)	N(2)	94.0(2)	W(1)	N(1)	W(2)	176.8(3)
Cl(1)	W(2)	Cl(3)	157.85(8)	W(1)	N(2)	W(2)	165.6(4)

[a]Numbers in parentheses are estimated standard deviations in the least significant digits.

Table I-4. Table of General Displacement Parameter Expressions for $[WNCl_3]_4$[a]

Atom	B(1,1)	B(2,2)	B(3,3)	B(1,2)	B(1,3)	B(2,3)	B eqv
W(1)	1.523(7)	0.776(8)	1.207(7)	0.531(6)	0.489(6)	0.260(7)	1.16 4(5)
W(2)	1.688(7)	0.887(8)	1.144(7)	0.587(6)	0.635(6)	0.287(7)	1.20 1(5)
Cl(1)	1.83(5)	2.11(6)	2.95(7)	0.93(4)	0.45(5)	0.72(6)	2.38 (4)
Cl(2)	1.74(4)	1.91(6)	2.70(5)	0.87(4)	0.98(4)	1.19(5)	1.98 (4)
Cl(3)	1.95(5)	2.74(7)	3.12(7)	1.13(4)	0.90(5)	0.72(6)	2.59 (4)
Cl(4)	1.81(5)	2.80(8)	3.24(7)	0.97(5)	0.96(5)	0.90(6)	2.61 (4)
Cl(5)	3.53(6)	1.24(6)	1.87(5)	0.90(4)	1.40(4)	0.59(4)	2.13 (4)
Cl(6)	4.02(7)	1.61(6)	1.92(6)	1.32(5)	0.81(5)	-0.20(5)	2.64 (4)
N(1)	1.7(2)	1.0(2)	1.2(2)	0.6(1)	0.6(1)	0.4(1)	1.3(1)
N(2)	2.2(2)	0.7(2)	1.4(2)	0.4(1)	0.5(1)	0.2(1)	1.6(1)

[a]The form of the anisotropic displacement parameter is:
$\exp[-0.25\{h^2a^2B(1,1) + k^2b^2B(2,2) + l^2c^2B(3,3) + 2hkabB(1,2) + 2hlacB(1,3) + 2klbcB(2,3)\}]$ where a,b, and c are reciprocal lattice constants.

RESULTS AND DISCUSSION

Synthesis of $[WNCl_3]_4$

The following reactions define the pathway to formation of $WNCl_3$:

$$WCl_6 + (CH_3)_3SiN_3 \xrightarrow[84°C]{DCE} W(N_3)Cl_5 + (CH_3)_3SiCl$$

$$W(N_3)Cl_5 \xrightarrow[84°C]{DCE} WNCl_3 + N_2 + Cl_2$$

The intermediate, $W(N_3)Cl_5$, is relatively stable. When the reaction is conducted in refluxing dichloromethane (DCM) at 40 °C, decomposition of the azide intermediate does not occur after 6 days, whereas the reaction when conducted in refluxing DCE at 84 °C, leads to ready decomposition of the azide after 2 days. It was noted by Dehnicke and coworkers[3] that an insoluble dimer forms between $WNCl_3$ and WCl_6 below 80 °C which has the formula W_2NCl_9. The formation of a compound with high chloride content was substantiated in early reactions where high chloride analyses were obtained for the products. In order to avoid the formation of the dimer, a TMSA/DCE solution was added directly to a refluxing DCE solution of WCl_6. The dimer did not form and relatively pure $WNCl_3$ was produced in yields above 75 percent. The mid-IR

spectrum of the $WNCl_3$ always contained an unexpected band at 685 cm^{-1} which was assigned to a C-Cl mode of bound DCE. Heating the $WNCl_3$ to 160°C under dynamic vacuum was required to remove all of the DCE (Fig. I-3). The DCE was identified by ^1H NMR of the volatile components in deuterated chloroform from heating $WNCl_3$ to 160 °C under dynamic vacuum. DCE was the only ^1H NMR-active volatile material isolated from this heating experiment.

Structure of $[WNCl_3]_4$

$[WNCl_3]_4$ is a tetramer in which the four tungsten and four nitrogen atoms define one plane (Fig. I-4). There are essentially two significantly different tungsten-nitrogen bond lengths forming an alternated multiple bond/single bond ring system. The multiple bond (formally a triple bond), which has been assigned a bond order of 2.2 by Goubeau[13] in the molybdenum analog, has a bond distance of 1.696 Å (ave), whereas 2.081 Å is the distance of the W-N single bond. The coordination around tungsten in the discrete tetramer is a distorted square pyramid where three basal chlorides and one nitrogen atom define a plane below the tungsten atom. A chloride atom from an adjacent tetramer is weakly bonded (d(W-Cl)=2.850 Å ave.) in the sixth site, trans to the W-N multiple bond, which results in a distorted octahedral coordination around tungsten. It is this sixth site that is potentially occupied by

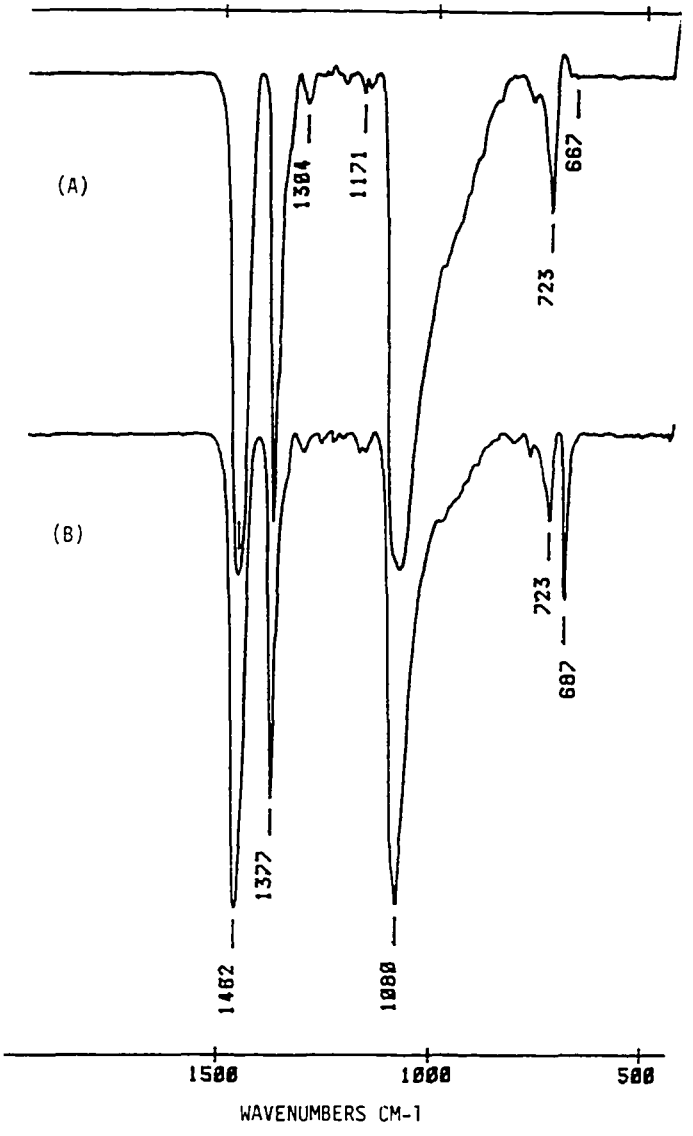

Figure I-3. Mid-infrared Nujol mull spectrum of $WNCl_3$ heated to 160 °C under dynamic vacuum for 3 hours (A) and corresponding spectrum of unheated $WNCl_3$ isolated after vacuum drying (B). The peak at 685 cm^{-1} is attributed to υ(C-Cl) and is eliminated by heating the product. The peak at 1080 cm^{-1} is due to the stretching mode of the W-N multiple bond. All other peaks arise from Nujol oil

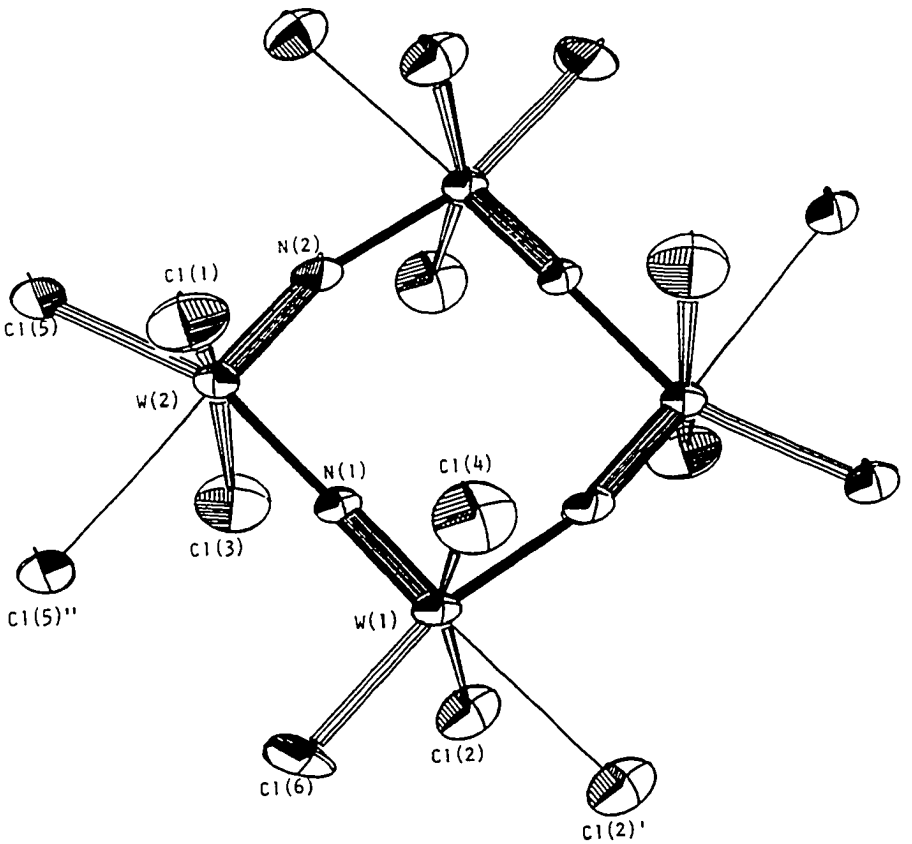

Figure I-4. Ortep drawing of $[WNCl_3]_4$ with 80% thermal ellipsoids. The view is along the 100 direction. Cl(2)' and Cl(5)" are chlorides from adjacent tetramers. An inversion center lies at the center of the W-N ring

chlorine from DCE and probably accounts for the tenacious retention of DCE. Coordination of $WNCl_3$ by basic ligands occurs in this trans position as verified by several recent papers[9] and should be the site of initial coordination of reactive molecules such as ammonia or trimethylsilylazide. Because of the strong tungsten-nitrogen multiple bond, any coordinated ligand in the sixth position would be weakly bound, due to the trans effect.

The extended interactions of $WNCl_3$ in the solid state are of two types. Along the b axis the inter-ring chloride bridges lie in the plane of the tungsten-nitrogen heterocycles, whereas the chloride bridges along the c axis are normal to the plane of the ring. This difference in packing predicts a variation in W-N multiple bond distances due to the difference in tungsten-chloride inter-tetramer dative bond distances between the parallel (along $\vec{b}$) and normal (along $\vec{c}$) bridges. Based on the trans relationship between the dative chloride bond and the W-N multiple bond, one would predict an inverse relationship between the two bond distances. The tungsten heterocycle does not show a significant difference in the W-N multiple bond distances, d(W(1)-N(1)) = 1.690 (6), d(W(2)-N(2)) = 1.702 (6) Å, which would correspond to a difference in the dative bond distances (d(W(1)-Cl(X') = 2.805 (3), d(W(2)-Cl(X") = 2.895 (3) Å). The molybdenum analog (2) does show the observed trend (Table I-5) but the Mo-N multiple bond distances are within 3 σ of each other and therefore a meaningful conclusion cannot be determined. The extended interactions of the

Table I-5. Comparison of Bond Lengths in Selected $[MNCl_3]$ Tetramers. Distances Given in Angstroms

Bonds	$[WNCl_3]_4$ (1)	$[MoNCl_3]_4$ (2)	$[WNCl_3 \cdot 0.5HN_3]_4$ (3)	$[WNCl_3 \cdot NCPh]_4$ (4)	$[WNCl_3 \cdot OPCl_3]_4 \cdot 2OPCl_3$ (5)
M(1)-N(1)	1.690(6)	1.672(10)	1.69(3)	1.65(2)	1.671(2)
M(1)-N(2)	2.081(6)	2.198(11)	2.11(3)	2.08(2)	2.169(3)
M(1)-Cl(2)	2.386(2)	2.379(7)	2.30(1)	2.280(6)	2.287(3)
M(1)-Cl(4)	2.263(2)	2.270(5)	2.28(1)	2.291(6)	2.318(3)
M(1)-Cl(6)	2.253(2)	2.241(10)	2.27(1)	2.270(6)	2.336(3)
M(1)-X'[a]	2.805(3)	2.822(7)	2.44(2)	2.49(2)	2.379(2)
M(2)-N(1)	2.081(6)	2.143(10)	2.08(3)	2.11(2)	2.163(2)
M(2)-N(2)	1.702(6)	1.638(11)	1.68(3)	2.28(2)	1.648(3)
M(2)-Cl(1)	2.275(2)	2.278(9)	2.26(1)	2.283(6)	2.318(2)
M(2)-Cl(3)	2.276(2)	2.276(5)	2.38(1)	2.324(6)	2.359(3)
M(2)-Cl(5)	2.328(2)	2.316(6)	2.30(1)	2.315(6)	2.323(3)
M(2)-X"*	2.895(3)	2.937(7)	2.80(2)	2.28(2)	2.316(3)

[a]Both X'and X" represent Cl, N or O atoms weakly bonded trans to the metal nitrogen multiple bond. For molecules (1) and (2) X',X"=Cl; (3) and (4) X',X"=N; (5a) and (5b) X',X"=O.

tetrameric units can be seen in Figures I-5 to I-7.

The bond lengths and angles of $WNCl_3$ are similar to those in previously prepared tungsten and molybdenum nitride tetramers (Table I-5), within statistical deviation. The exception is found in the length of the M-N single bond and the M-Cl" dative bond, which are shorter in $WNCl_3$ relative to $MoNCl_3$. This lengthening of the two bonds may reflect a slightly stonger M≡N bond for $MoNCl_3$.

$WNCl_3$ was initially investigated by x-ray powder diffraction[1]. In this study, powders of $WNCl_3$ were characterized by x-ray diffraction using the environment cell for the Philips diffractometer described previously in this section. A comparison between the x-ray powder data reported by Dehnicke[1] for $WNCl_3$, a spectrum of the unheated $WNCl_3$ prepared in this investigation, a spectrum of $WNCl_3$ heated to 160 °C under dynamic vacuum and a calculated powder pattern using the GSAS[14] diffraction software based on the unit cell information obtained from the $[WNCl_3]_4$ structural solution indicates that there are at least three separate crystallographic modifications for $WNCl_3$ (Fig. I-8). The particular modification appears to be dependent on the method of preparation. Many reflections were observed for each form of $WNCl_3$, which indicates that each crystallizes in a lower symmetry group, probably triclinic, based on the number of lines in each spectrum. The diffraction pattern of the heated $WNCl_3$ and the simulated pattern are essentially the same. Because

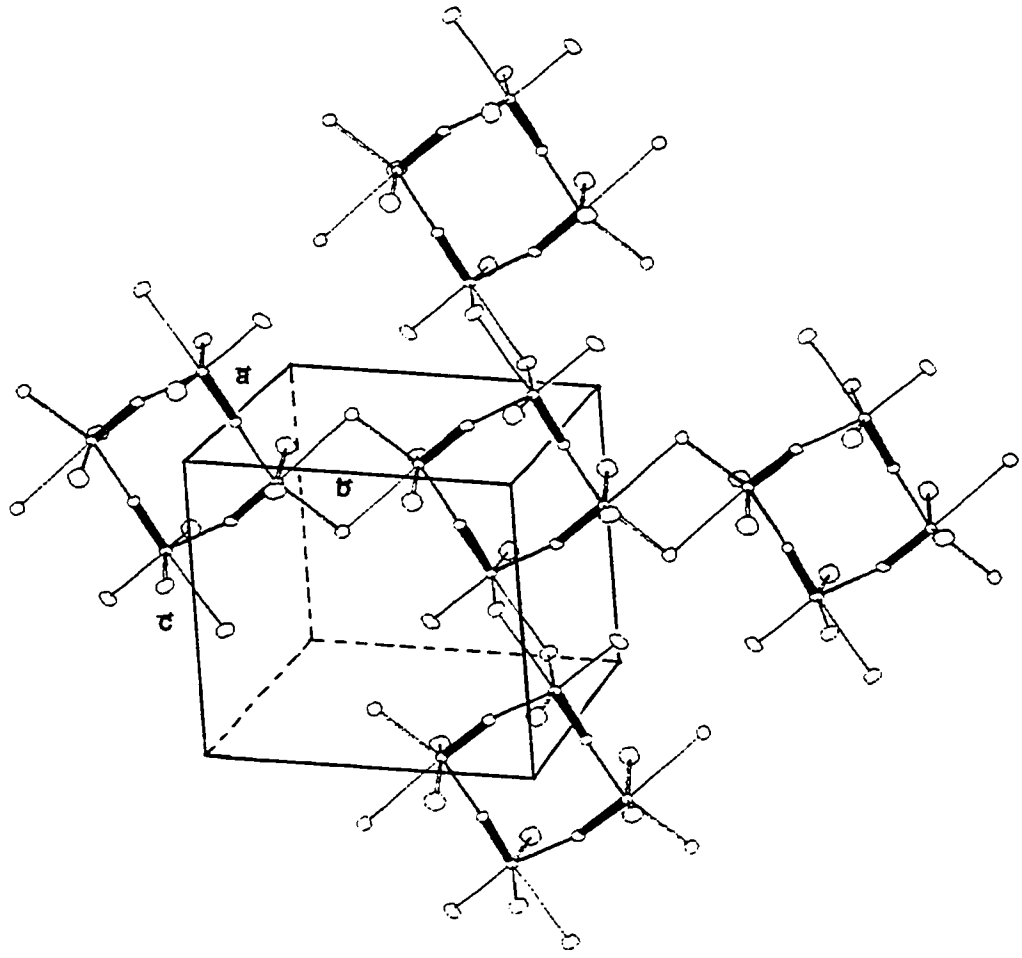

Figure I-5. Ortep drawing of the extended interactions of the $WNCl_3$ tetramers with unit cell representation. The viewing direction is perpendicular to the plane formed by the b and c axes

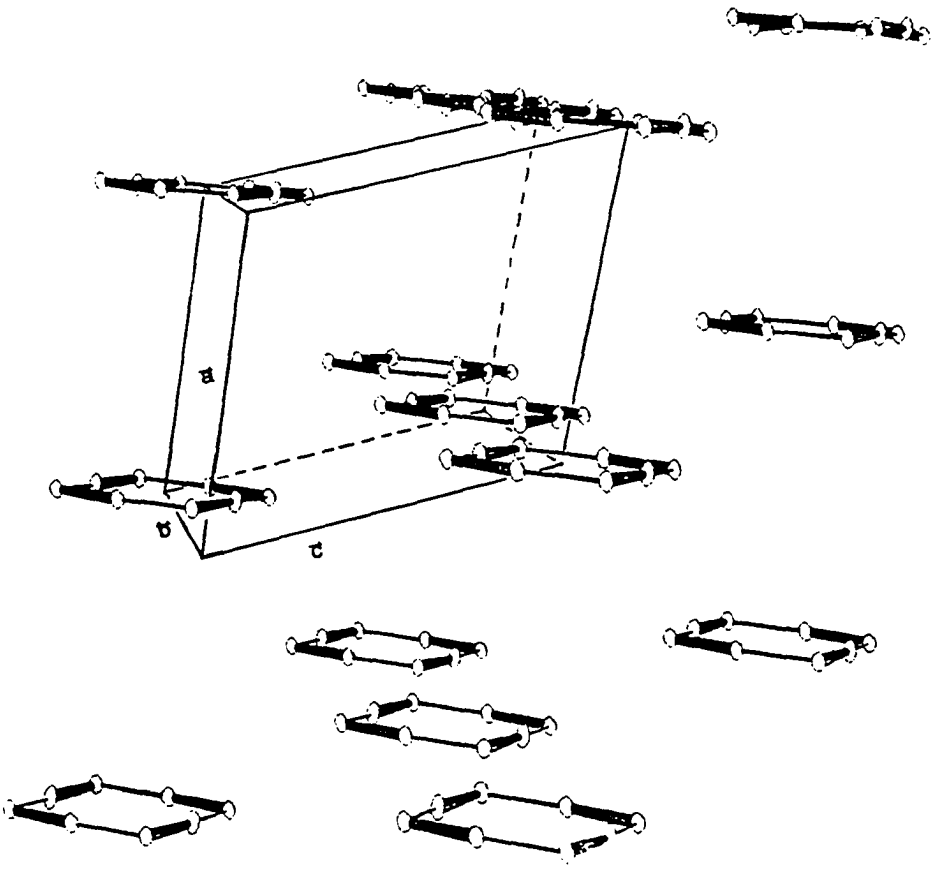

Figure I-6. Ortep diagram of the tetrameric tungsten-nitrogen rings with the chloride atoms removed for clarity. The rings that are connected, running along the b axis, are in the same plane whereas the W-N heterocycles along $\vec{c}$ stack in a stair-step fashion

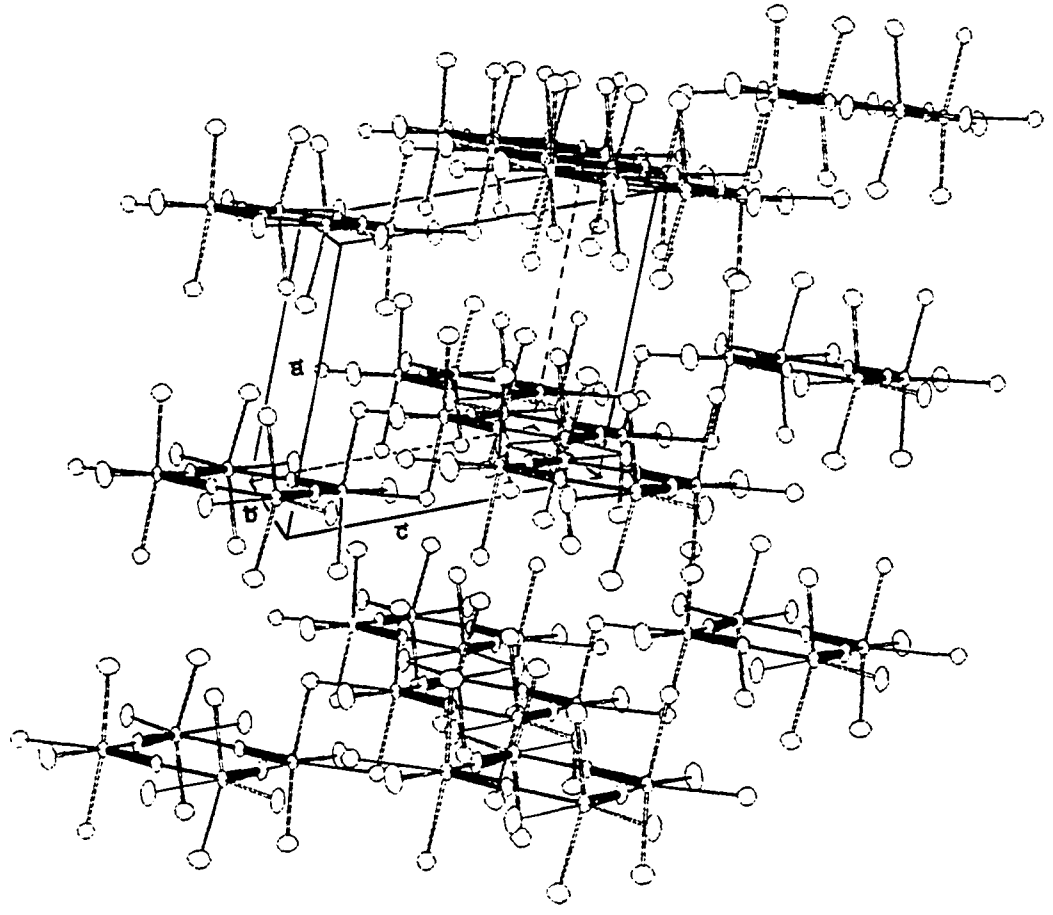

Figure I-7. Ortep diagram showing the extended interactions of $[WNCl_3]_4$ with the same perspective as Fig. I-6. The inter-ring chloride bridges are parallel to the W-N rings along $\vec{b}$ and perpendicular to rings along $\vec{c}$

extraneous solvent molecules coordinating trans to the multiply bonded nitrogen appear to cause a disruption of the inter-tetramer W-Cl linkage, it is likely that the structural variations are due to solvent molecules coordinating in these trans positions. The differences between the heated and unheated $WNCl_3$ X-ray powder data reflect this. After the tungsten, chloride and nitrogen percentages were subtracted from the unheated $WNCl_3$ mass, 8.2 % of the material remained. The only other compound in the unheated $WNCl_3$ was found to be DCE. If the DCE comprises the remaining 8.2 % in $WNCl_3$, the ratio of DCE to $[WNCl_3]_4$ was found to be 1.1:1. This indictes that, on the average, approximately one molecule of DCE is coordinating to each $WNCl_3$ tetramer. Three variations of the $WNCl_3$ extended lattice have been presented. Based on these variations it is likely that many other modifications may be possible as the nature and amount of coordinating solvent in the extended lattice is varied.

Physical Measurements

Infrared spectroscopy has been used extensively to characterize the molybdenum and tungsten tetramers. The utility of IR is based on the strong stretching mode of the metal-nitrogen multiple bond which is found at 1082 cm^{-1} in the tungsten case and at 1045 cm^{-1} for molybdenum. The original 1966 paper on the synthesis and characterization of

$MNCl_3$[X] (M=W,Mo) and a review of metal nitrides 15 years later reports the tungsten-nitrogen multiple bond stretching modes with bands at 1068 and 1084 cm^{-1} in the IR spectra. The IR spectra for every sample of $WNCl_3$ synthesized in this work has shown only a single band for the W-N stretching mode. The IR spectrum for single crystals of $WNCl_3$ in a Nujol mull is shown in Figure I-9. This fundamental difference in IR stretching modes between Dehnicke's original work and this report indicates that the $WNCl_3$ produced in this work differs from that prepared by Dehnicke[1] not only in the way the tetramers are packed in the lattice but also possibly in the tungsten-nitrogen connectivity.

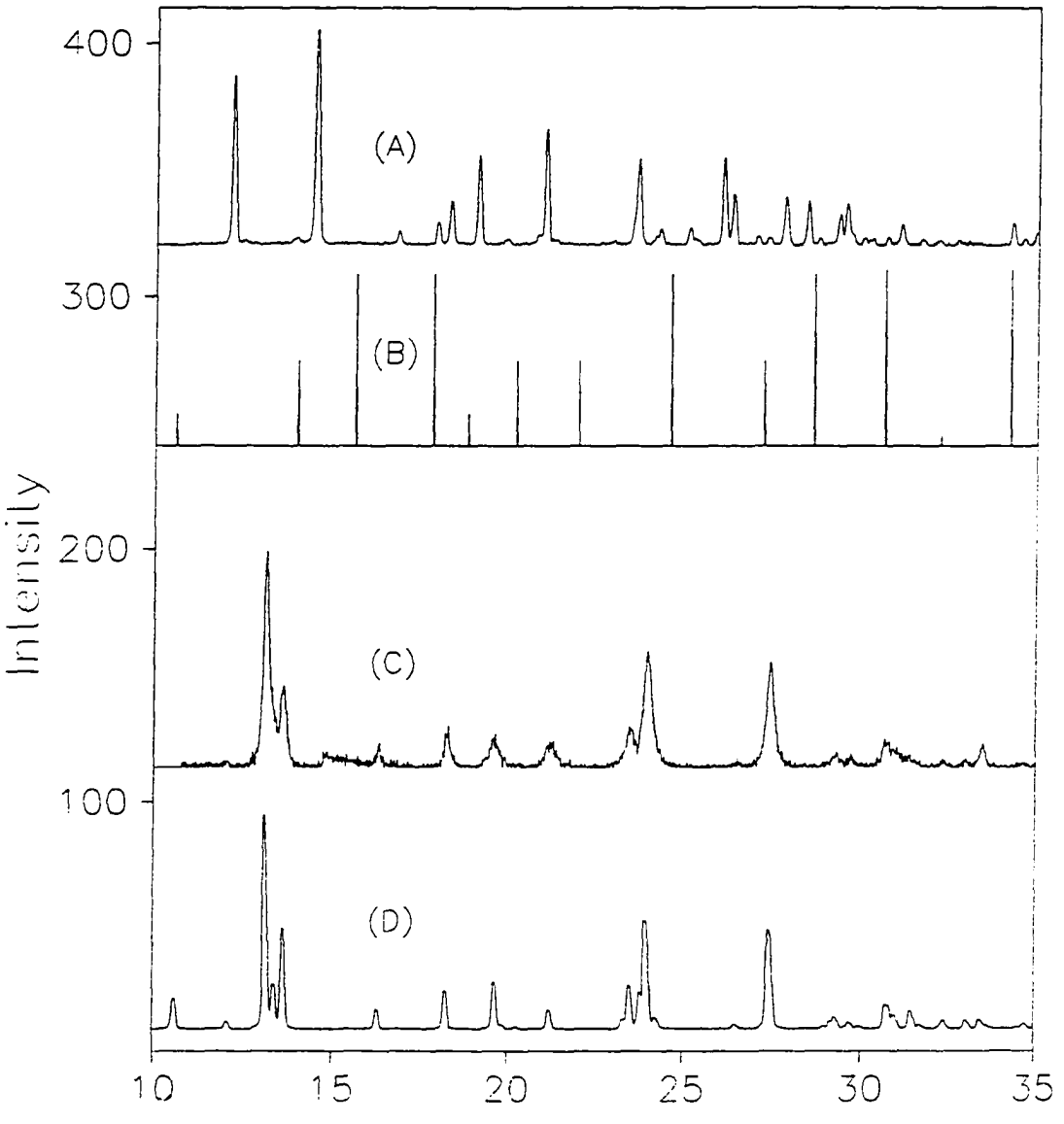

Figure I-8. Comparisons of the experimental and calculated X-ray powder diffraction for $[WNCl_3]_4$. (A) X-ray diffraction of unheated $WNCl_3$ (with included DCE). (B) Simulated X-ray pattern for $WNCl_3$ as reported by Dehnicke[1]. (C) X-ray pattern of $WNCl_3$ which has been heated to 160 °C under dynamic vacuum for 3 hours. (D) Calculated X-ray pattern using single crystal data from refinement

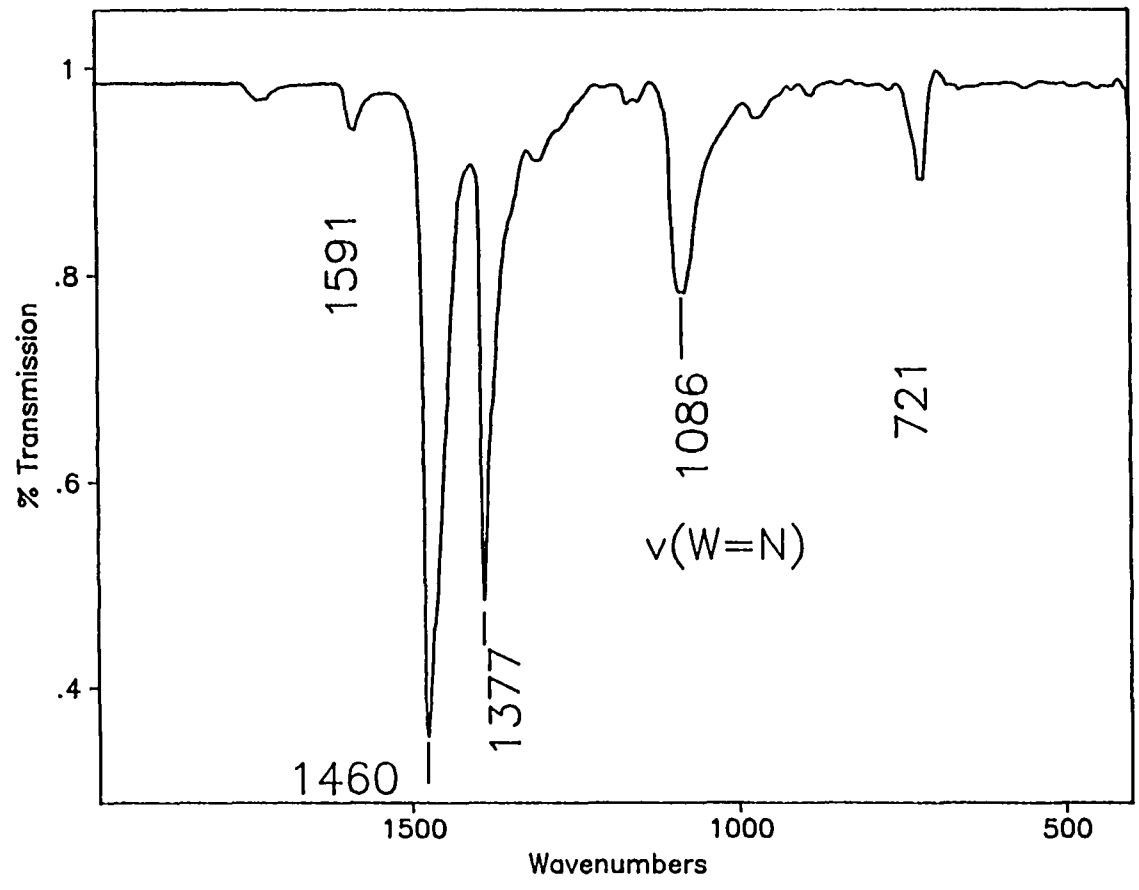

Figure I-9. Mid IR spectrum (Nujol) of $WNCl_3$ single crystals formed by vacuum sublimation. The peak at 1086 cm^{-1} is the stretching mode of the tungsten-nitrogen multiple bond (Nujol oil accounts for all other peaks)

CONCLUSION

A new synthetic approach to $WNCl_3$ has been developed in which dimer formation and impurities are minimized. This procedure is relatively convenient and minimizes the formation of an insoluble dimer between WCl_6 and $WNCl_3$ by allowing the reaction to proceed only at temperatures above 80 °C. Uncoordinated $[WNCl_3]_4$ has been structurally characterized for the first time and is comparable to the previous molybdenum and tungsten nitride-trichloride tetramers except for a difference in the W-N single bond lengths. The $WNCl_3$ tetramer has been shown to form in three independent structural variations, depending on the reaction conditions. This difference in structure has been attributed to a disruption of the packing of tetrameric $WNCl_3$ units by the interaction of chlorinated hydrocarbons in the trans position to the W-N multiple bond.

REFERENCES

(1) Dehnicke, K.; Strähle, J. *Z. Anorg. Chem.* **1965**, 339, 171.

(2) (a) Chatt, J.; Dilworth, J. R.; *J. Chem. Soc. Chem. Commun.* **1974**, 517
(b) Schweda, E.; Strähle, J. *Z. Naturforsch. B* **1980**, 35, 1146.

(3) Godmeyer, T.; Berg, A.; Gross, H.-D.; Müller,U.; Dehnicke, K. *Z Naturforsch.* **1985**, 40B, 999-1004.

(4) Strähle, J. *Z. Anorg. Allg. Chem.* **1970**, 375, 238.

(5) Strähle, J; Weiher, U; Dehnicke, K. *Z. Naturforsch. B 33* **1978**, 1347.

(6) Musterle, W; Strähle, J.; Liebelt, W; Dehnicke, K. *Z. Naturforsch. B 34* **1979**, 942.

(7) Walker, Von I.; Strähle, J. *Z. Anorg. Allg. Chem.* **1982**, 487, 26.

(8) Ergezinger, C; El-Kholi, A.; Müller, U.; Dehnicke, K. *Z. Anorg. Allg. Chem.* **1989**, 568, 55-61.

(9) Dehnicke, K; Strähle, J. *Angew. Chem., Int. Ed. Engl.* **1981**, 20, 413.

(10) Liese, W.; Dehnicke, K.; Walker, I.; Strähle, J. *Z. Naturforsch. B* **1979**, 34, 693.

(11) Chisholm, M. H.; Hoffman, D. M.; Huffman, J. C. *Inorg. Chem.* **1983**, 22, 2903.

(12) The designations for IR spectra peak intensities are: s = strong, m = medium, w = weak, sh = shoulder.

(13) Gem Dugout, c/o Deane Smith, 1652 Princeton Dr., State College, PA 16803.

(14) Sheldrick, G.M. In: Crystallographic Computing 3, G.M. Sheldrick, C. Kruger, R. Goddard, Oxford University Press, 1985, pp. 175-189

(15) "TEXSAN TEXRAY Structure Analysis Computer Software Package" Molecular Structure Corporation, The Woodlands, TX, 1985.

(16) Goubeau, J. *Angew. Chem.* 1966, 78, 565.

SECTION II. REACTIVITY OF $[WNCl_3]_4$ WITH SELECTED NITRIDING AGENTS TO YIELD TUNGSTEN NITRIDES, AMIDES, AND AZIDES

INTRODUCTION

Binary tungsten nitrides have been investigated generally for their interesting electrical and refractory properties. Thin films of binary tungsten nitrides WN_x ($x \leq 1$) have been developed for use in electronic devices, especially as Schottky gates to GaAs semiconductors.[1,2] Some tungsten nitrides have been shown to be superconductors, with higher superconducting transition temperatures than the pure metal.[3] The cubic β-W_2N phase is a refractory solid, and as such has applications in cutting tools, wear-resistant parts and materials constucted for elevated temperature use. Conventionally, tungsten nitrides are made by the reaction of the pure metal (usually finely powdered) and ammonia.[4] By using this technique or the reaction with WO_3 only W_2N is produced, with no indication of higher nitrides formed.[5] The formation of N≡N and lower nitrides in the thermal decomposition of MN accounts for the thermal instability in higher nitrides, WN_x ($x \geq 1$), relative to binary tungsten oxides. WN_2 has been synthesized as a thin film by treatment of thin tungsten sputter-coated films at 750 °C for 3 hours with rapidly flowing ammonia and subsequent rapid cooling. The resulting WN_2 was characterized by TEM.[6] WN_2 has not been synthesized in bulk quantities. Due to the thermodynamic instability of WN_2, low temperature reactions of activated tungsten compounds with appropriate nitriding agents may be necessary for its

formation. As mentioned in Section I, $WNCl_3$ represents a potentially significant intermediate in the pathway to higher tungsten nitrides (WN_x $1 \leq x \leq 2$). The conversion of $WNCl_3$ to a binary nitride, WN_y ($0 < y \leq 2$), has not been reported; in fact, most of the work with $WNCl_3$ has focused on the preparation and characterization of molecular $WNCl_3$ adducts, such as $[WNCl_3 \cdot 0.5HN_3]_4$[7], $WNCl_3$(2,2'-bipyridine)[8] and $[WNCl_3(CH_3CN)]_4$[9]. The first step in the reaction of $WNCl_3$ and basic molecules usually involves coordination of the reactant molecule to the tungsten site, trans to the tungsten-nitrogen multiple bond, although reaction at the nitride site with Me_3P was observed in the formation of $[W(NPMe_3)Cl_2(PMe_3)_3]Cl$[10] from the reaction of $WNCl_3$ and Me_3P in deuterated methylene chloride. In $WNCl_3$, trans coordination of basic ligands to the tungsten center causes perturbations in the W≡N infrared stretching frequency.[11] For example, the infrared spectrum of $[WNCl_3 \cdot 0.5HN_3]_4$[12] shows two peaks attributed to υ(W≡N) at 1082 and 1050 cm^{-1}, while the corresponding W≡N stretching modes for the uncoordinated compound, $WNCl_3$[9] are shifted to higher frequencies, at 1084 and 1068 cm^{-1}, respectively. The displacement of Cl in the weakly bound trans site of $WNCl_3$ appears to be the preferred site for coordination of basic reactive molecules and atoms. In attempts to synthesize higher tungsten nitrides, this study focuses on the reactivity of $WNCl_3$ with ammonia, trimethylsilylazide and lithium nitride in coordinating and non-coordinating solvents.

EXPERIMENTAL

General Considerations

All the materials reported in this section are extremely reactive to oxygen and water. Manipulations of oxygen- and water-sensitive compounds were performed under inert atmosphere conditions using standard drybox, vacuum and Schlenk techniques.

Materials

Anhydrous ammonia (99.9%) was obtained from Matheson Gas Products Co. and purified additionally by sodium metal dissolved into liquid ammonia. 1,2-dichloroethane (DCE), dichloromethane (DCM), pyridine and butyronitrile were dried by refluxing the solvent over phosphorus (V) oxide or calcium hydride for greater than 6 hours to remove all water, degassed by three freeze-evacuate-thaw cycles and vacuum distilled onto 3 Å molecular sieves prior to use. The organic solvents were transferred for further reactions by either vacuum distillation or syringe with an inert gas flow. $[WNCl_3]_4$ was prepared in this laboratory according to a procedure modified from the literature[13] Tungsten hexachloride was obtained from Pressure Chemical and sublimed using a three chamber sublimation tube to remove initially the tungsten

oxychlorides ($WOCl_4$, WO_2Cl_2) by sublimation to the outer chamber, then subliming the purified WCl_6 into a central chamber and isolating it in a dry-box. Trimethylsilylazide (TMSA) was obtained from Hüls Petrarch Systems, Inc. and transferred to a solvent flask and stored in the dark, under vacuum, to avoid photolytic decomposition of the azide. Lithium nitride was obtained from Strem Chemical, Inc. and stored in a dry box prior to use.

Analytical Procedures

Tungsten was determined using a gravimetric procedure as detailed in Section I of this report. Chloride was determined by use of a standard potentiometric titration with standardized $AgNO_3$. A Cambridge S-200 Scanning Electron Microscope (SEM) coupled to a Tracor Northern Micro Z II Energy Dispersive Spectrometer (EDS) with a Beryllium or ultra-thin carbon window was used to determine relative tungsten and chloride concentrations. The ultra-thin window was used for light atom determinations. Nitrogen composition was determined by the Dumas combustion method[14] on a Carlo Erba Instruments NA 1500 Nitrogen/Carbon/Sulfur Analyzer.

For two of the compounds herein reported, a temperature-programmed pyrolysis was conducted in which the volatile decomposition products were analyzed with a Finnigan Automated Gas Chromatograph/EI-CI Mass

Spectrometer System. In these decomposition studies, approximately 2-4 mg. of sample were placed in specially prepared pyrex reaction tubes which were centered in a tube furnace vertically and then connected to the ionization area of the mass spectrometer by a capillary tube, minimizing the evacuable volume. The material was allowed to heat at a controlled rate and a correlation was established between the measured temperature and the ion current detected by the mass spectrometer for the volatile components of pyrolysis.

Syntheses

In the reactions that follow, each product with a unique combination of reactants will be labeled with a unique numerical designation. If the reactants are the same and only the solvent is varied, each of these reactions will be labeled with the same number but a different letter descriptor.

$WNCl_3$ + NH_3(l) ---> (1A). 1.0 gm. of $WNCl_3$ was placed in a 100 mL round bottom flask and sodium purified ammonia was vacuum distilled onto $WNCl_3$. The ammonia was brought to -40 °C slowly because of the exothermic nature of the ammonolysis. $WNCl_3$ was then reacted in liquid ammonia at -40 °C (the temperature was maintained by a 2-isopropanol low temperature bath). The liquid ammonia and $WNCl_3$ were allowed to interact for 1 hour, after which time, the ammonia was allowed to boil off, leaving a mixture of black and white

solids, **1A** and ammonium chloride, respectively. The separation of the two solids was accomplished by either washing the ammonium chloride with liquid ammonia in a ceramic filtering apparatus designed for this purpose or by decanting the ammonium chloride dissolved in liquid ammonia using an evacuable tube with a side arm. While the decanting process was quicker, the filtering procedure was more effective at removing all the ammonium chloride; therefore the material obtained in the preceding reaction was filtered. There was a slight solubility of the black product in the ammonia therefore the yields were lowered. Based on a molecular formula of $WN(NH_2)_2Cl(NH3)_2$ for the black product, **1A**, the average yield of the ammonolysis was 54%. Elemental analyses for W and Cl, mid and far infrared spectra and X-ray powder data were obtained for **1A**. Anal. Calc. for $WClN_5H_{10}$: W, 61.41; Cl, 11.84. W:Cl. Found: W, 61.4; Cl, 11.4. Infrared spectrum (Nujol, cm^{-1}) for **1A** (Fig. II-1): 3000-3200 m, υ(N-H); 1599 m, 1302 m and 1261 m, $\delta_s(NH_3$ or $NH_2)$; the broad peak around 802 cannot be conclusively assigned but the absorption most closely corresponds to $\rho_r(NH_3)$; 430 - 406 s, υ(W-N); and the weak narrow peak at 350 corresponds to υ(W-Cl). Powders of **1A** are deep black and are amorphous to X-ray diffraction. The X-ray diffraction data indicate a complete lack of crystallinity, as evidenced by the featureless powder pattern.

$WNCl_3$ + pyridine + $9NH_3$ ---> (1B). In a reaction closely related to **1A**, $WNCl_3$ (0.315 g, 0.00104 mol) was dissolved completely in 50 mL of

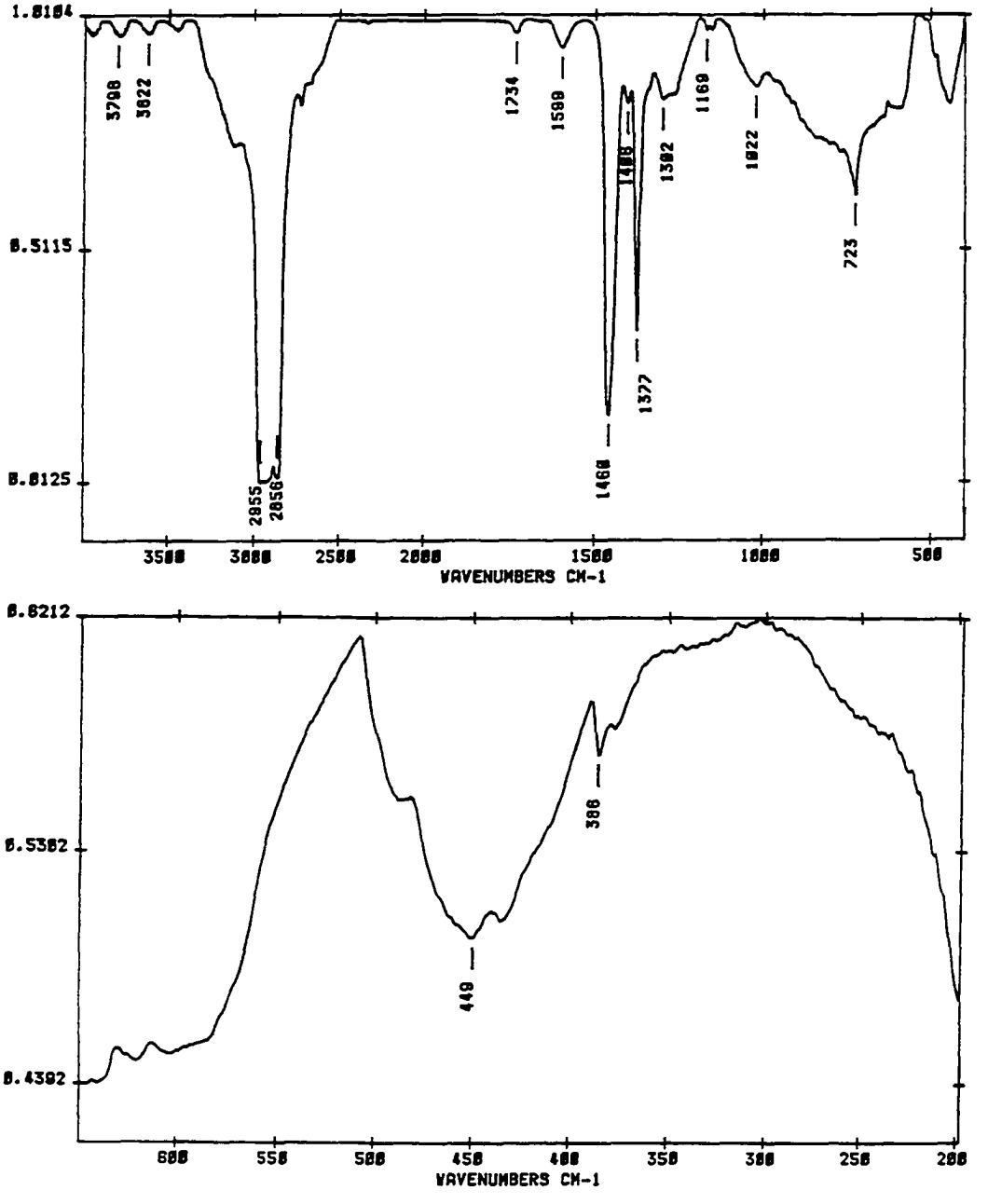

Figure II-1. Mid and far IR spectra (Nujol) for **1A** which was formed by the ammonolyses of $WNCl_3$ in liquid ammonia at -40 °C

pyridine at room temperature. Dried liquid ammonia (0.101 mL, 0.0098 mol) was measured in a calibrated vacuum tube and added slowly to the $WNCl_3$. The addition was accomplished by connecting the flask containing the purple $WNCl_3$/pyridine solution to that of the ammonia, freezing the ammonia and the pyridine solution, evacuating the system, allowing the pyridine to liquify and then letting the slush bath for the ammonia warm to room temperature. This slow addition allowed the gaseous ammonia to react with the pyridine adduct of $WNCl_3$ and over the course of 5 days a deeply colored precipitate slowly settled from the solution. The product was isolated on a ceramic frit and exposed to vacuum for 12 hours to eliminate solvent and residual ammonia. The resulting orange-brown solid was insoluble in pyridine. The X-ray powder pattern revealed a small amount of ammonium chloride present in the material, while the bulk material was amorphous. Infrared spectrum (Nujol, cm^{-1}) for B1 (Fig. II-2): 3000-3200 s, υ(N-H); 1600 w, 1300 m, and 1261 m, $\delta_s(NH_3$ or $NH_2)$; 1019.8 m, υ(W≡N); the broad peak around 802 cannot be conclusively assigned but the absorption best corresponds to $\rho_r(NH_3)$. 430 - 406 s, υ(W-N). The small peak around 350 corresponds to the W-Cl stretching frequency.

$WNCl_3$ + $(CH_3)_3SiN_3$ --<DCE>--> (2A), (2A'). A 1,2-dichloroethane (DCE) solution of trimethylsilylazide (0.220 mL, 1.68 mmol) was added dropwise to a stirring suspension of $WNCl_3$ (510 mg, 1.68 mmol) in 30 mL of DCE at room temperature. The reaction was mixed for 20 hours under vacuum at

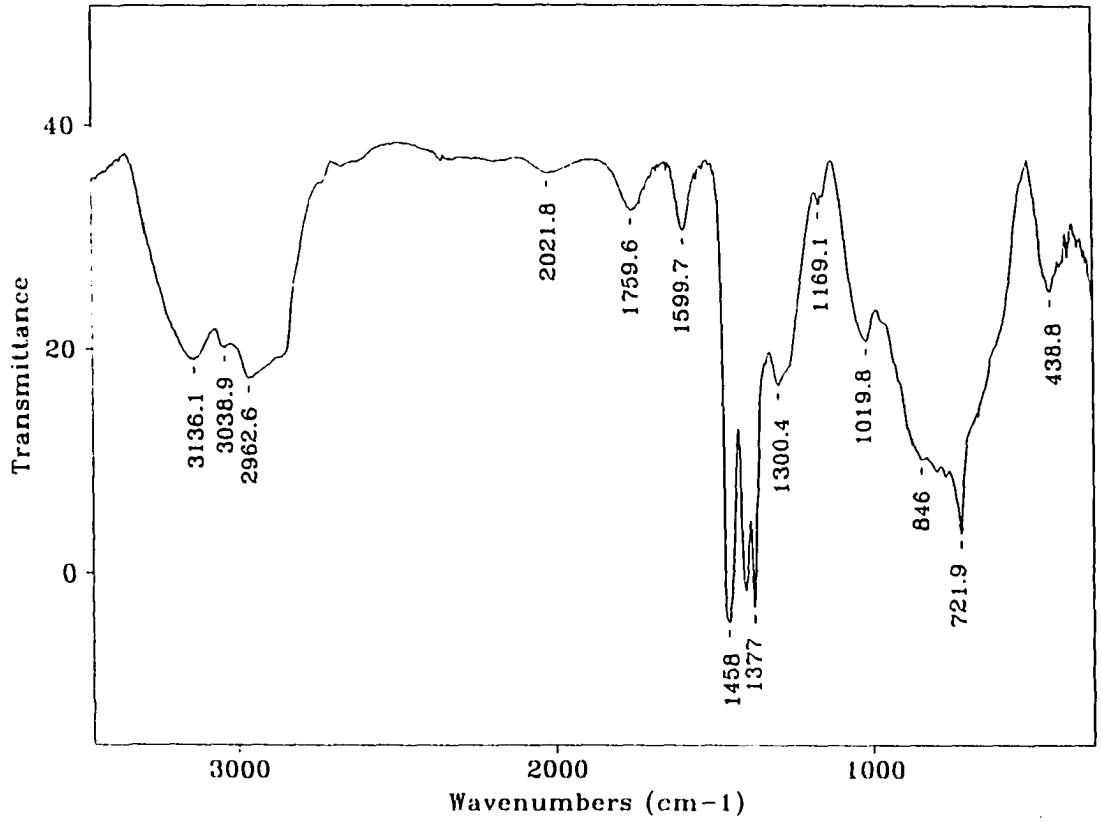

Figure II-2. IR spectra (Nujol) for 1B which was formed by the ammonolyses of $WNCl_3$ in pyridine by 9 moles of ammonia gas

reflux temperature then heated to 84 °C (reflux) and allowed to react for four days. Upon addition of the trimethylsilylazide (TMSA), the solution changed from orange to red and remained red for the duration of the room temperature reaction (**2A**). **2A** was isolated by extracting, with a syringe, a small amount of the reaction mixture prior to heating. The solution was then transferred under flowing argon to a dried sealable tube and transferred to a drybox. After the mixture was refluxed, the color of the solution changed from red to brown (**2A'**). Yield for **2A'**: 0.726 g. Anal. Found for **2A'**: W = 60.47, Cl = 21.45%. IR (Nujol, cm^{-1}) for 2A: 2129, 2091 m ($\upsilon_a(N_3)$), 1261 m-w ($\upsilon_s(N_3)$), 1076 s ($\upsilon(W{\equiv}N)$), 802 m-w, 669 w, 399, 378, 362, 332 s (υ(W-Cl)). IR (Nujol, cm^{-1}) for **2A'**: 2129, 2091 m ($\upsilon_a(N_3)$), 1261 m-w ($\upsilon_s(N_3)$), 1076 s ($\upsilon(W{\equiv}N)$), 802 m-w, 669 w, 442 s (υ(W-N)), 399, 385 s (υ(W-Cl)). **2A** and **2A'** are very similar in their IR absorption spectra. The difference is seen primarily in the peak at 442 cm^{-1} corresponding to an azide nitrogen bound to the tungsten center (see Fig. II-3, 4). The X-ray diffraction data for **2A'** exhibits several weak peaks indicating a degree of crystallinity. The X-ray data do not correspond to the $WNCl_3$ reactant (see Fig. II-5). A mass spectrum of the volatile components obtained from heating **2A'** to 500 °C in a dynamic vacuum was obtained (see Fig. II-6).

$WNCl_3$ + $(CH_3)_3SiN_3$ --<pyridine>--> (2B). $WNCl_3$ (648 mg, 2.13 mm) was dissolved completely in 50 mL of pyridine creating a deep red solution.

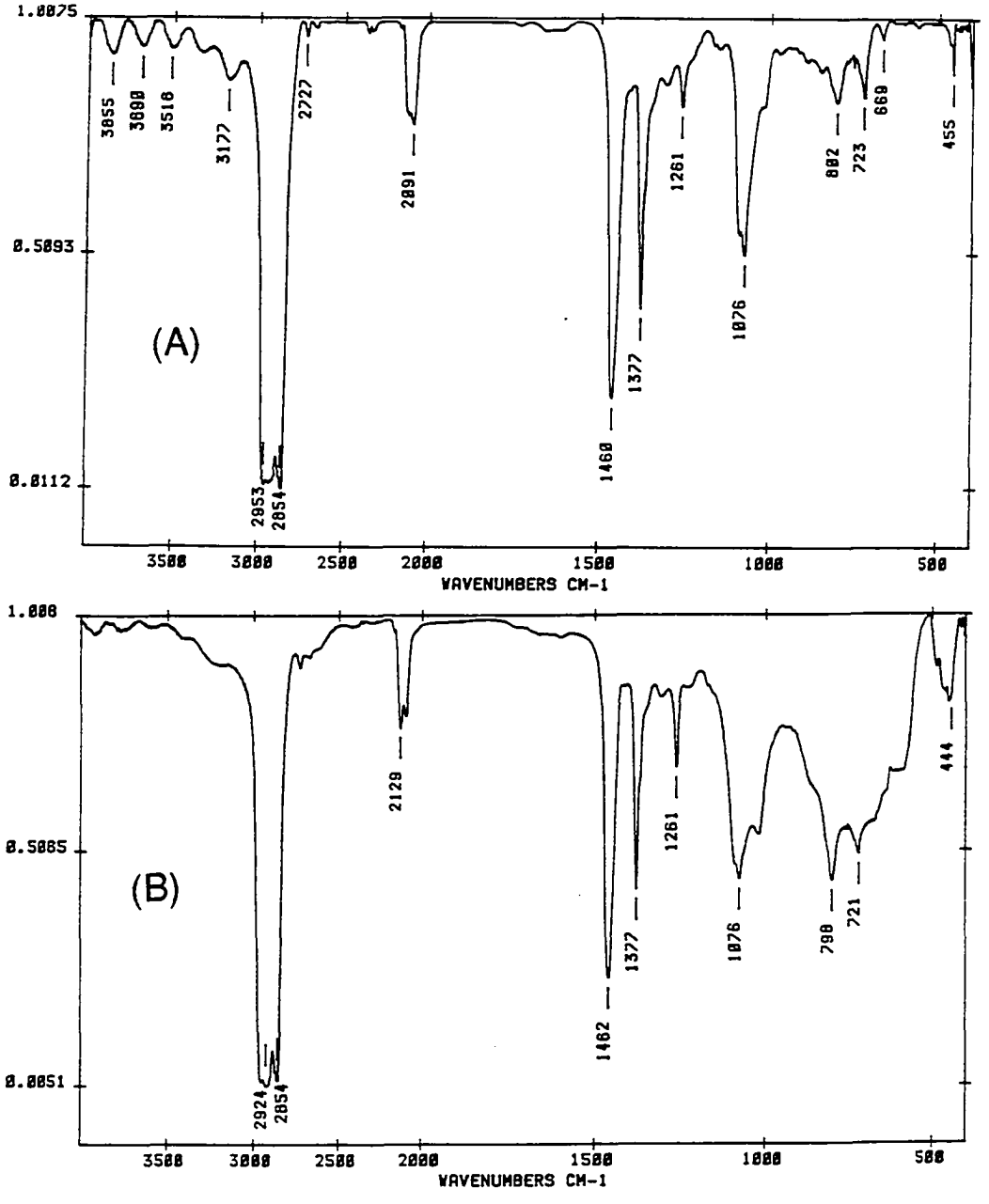

Figure II-3. Mid IR spectra (Nujol) of **2A** (A) and **2A'** (B). Differences in the spectra are seen in the regions around 1076, 798 and 444 cm^{-1} which indicates further reaction of the silyl- azide with the $WNCl_3$ tetramer in (B) relative to (A)

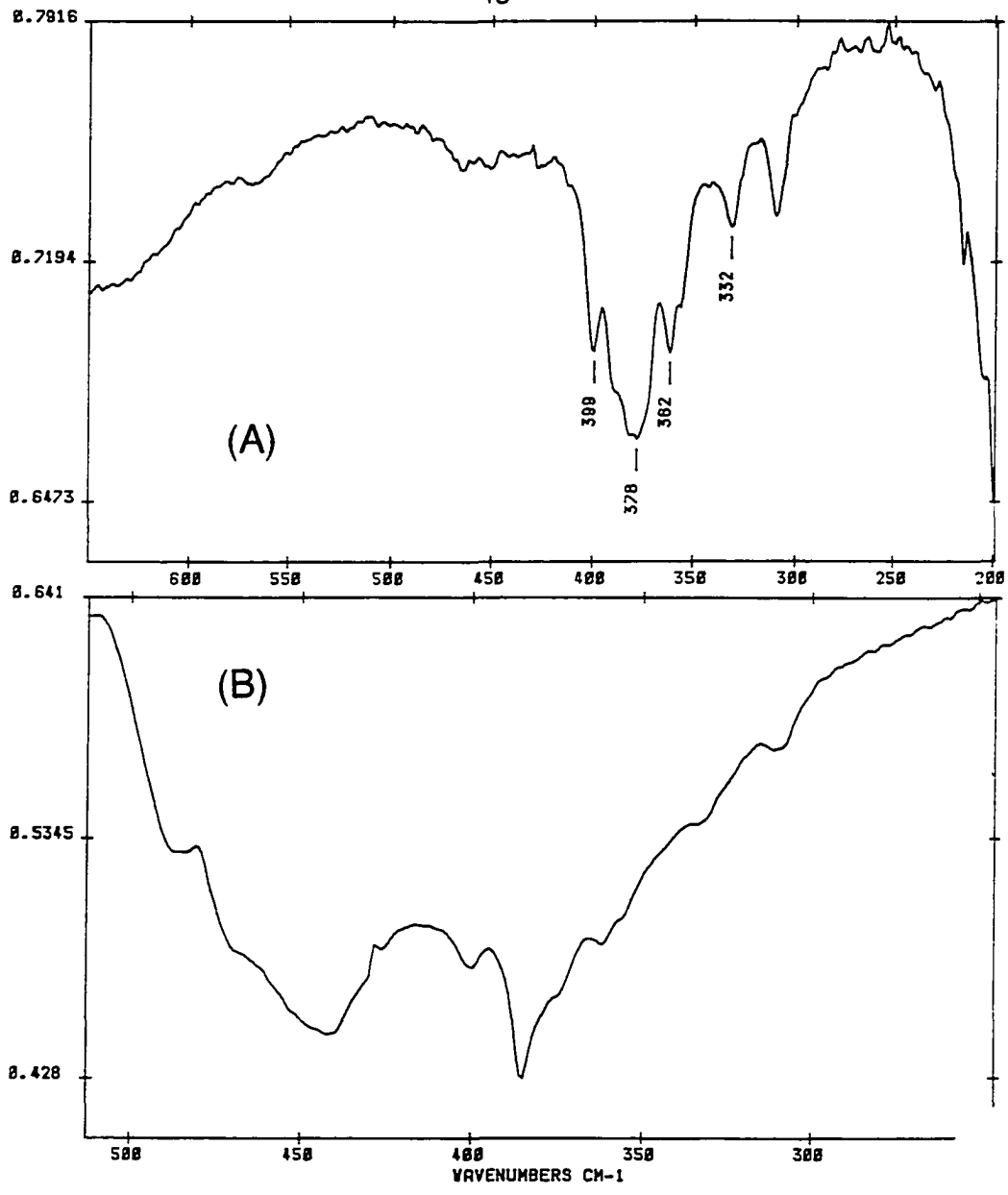

Figure II-4. Far IR spectra (Nujol) of **2A** (A) and **2A'** (B). A significant difference in the two spectra is the lack of a W-N stretching mode at ca. 450 cm^{-1} in (A) relative to (B). This indicates that (B) has the azide anion bound to the tungsten whereas it is likely that in (A), TMSA is bound as a ligand to the $WNCl_3$ tetramer in the trans position to the W-N multiple bond

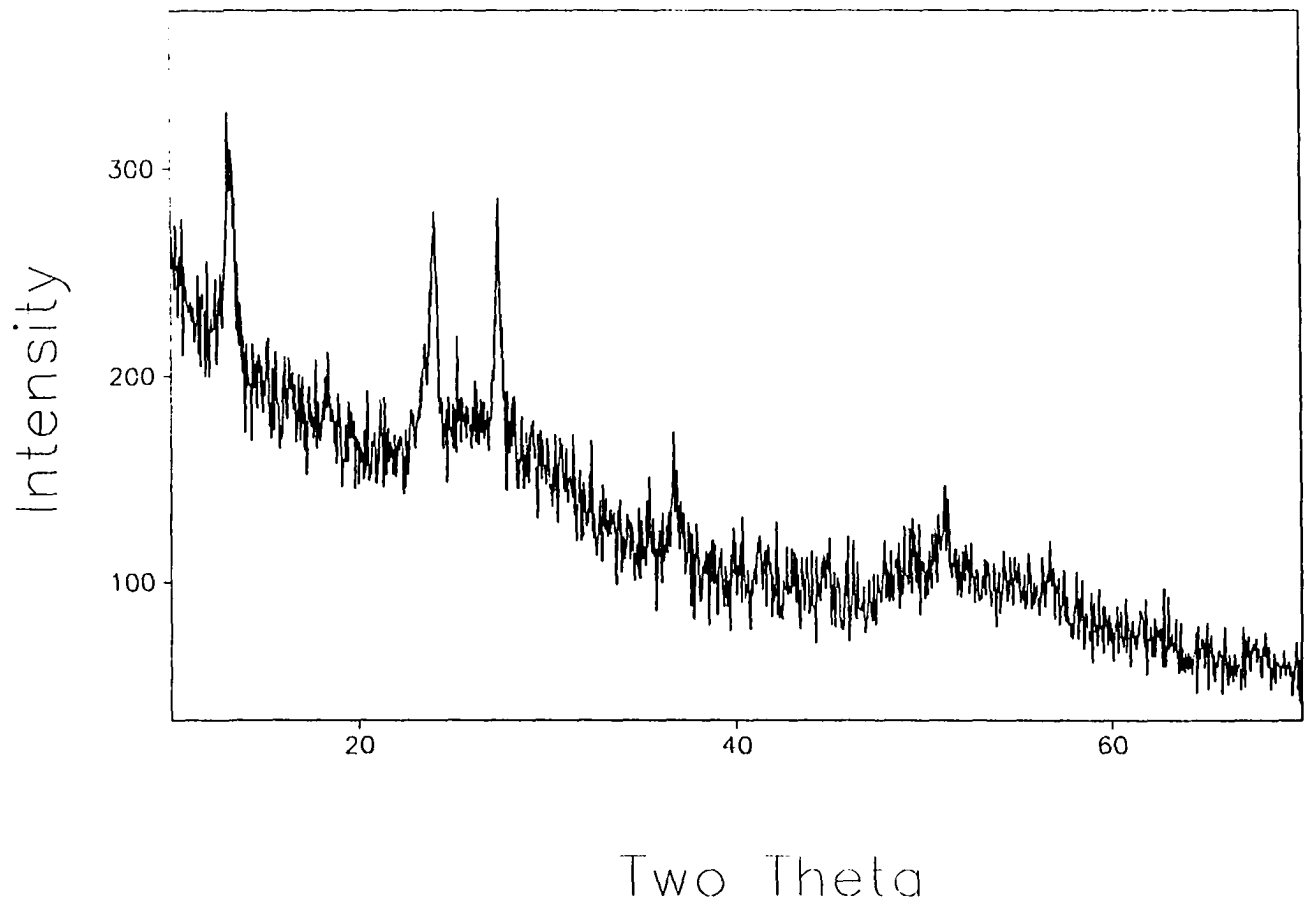

Figure II-5. X-ray diffraction data for $WN(N_3)Clx$ (**2A'**) from the reaction of $WNCl_3$ and trimethylsilylazide in DCE. The bragg diffraction does not correspond to the starting material, $WNCl_3$

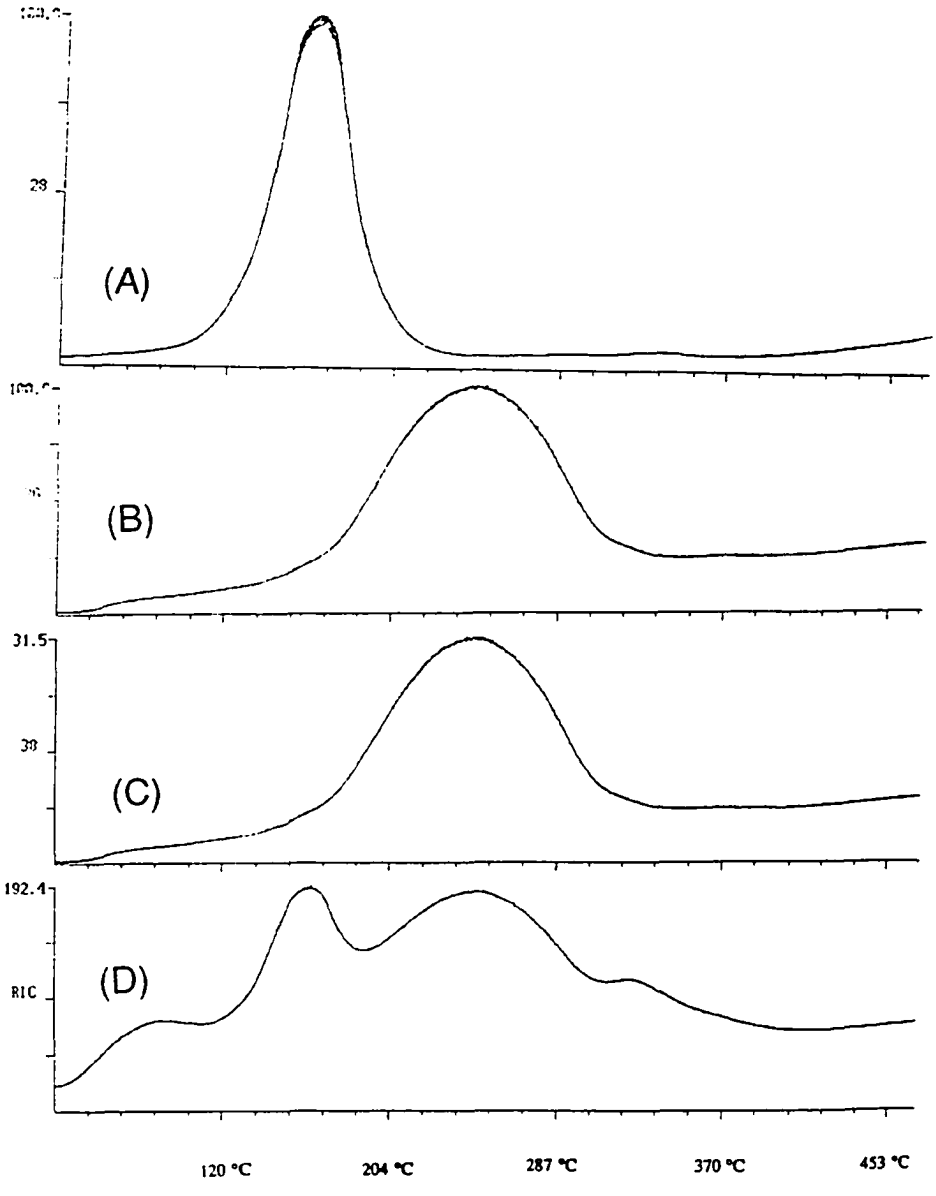

Figure II-6. Mass spectra correlation with the thermolysis of **2A'** in dynamic vacuum. The ion currents correspond to molecular weights of 28 (A), 36 (B) and 38 (C) for N_2, $H^{35}Cl$ and $H^{37}Cl$ respectively. N_2 and Cl account for most of the total ion current (D) although DCE and trimethylsilyl fragments were also present but not shown

The pyridine was removed from the solid under reduced pressure. In order to break the oil formed when the pyridine was distilled and to increase the refluxing temperature for the reaction, 30 - 40 mL of chlorobenzene (CB) were added to the solution when the pyridine volume was reduced to 15 ml. Me_3SiN_3 (0.281 mL, 2.13 mm) was added, by syringe, to the pyridine/chlorobenzene/$WNCl_3$ mixture at room temperature. As the TMSA was added, the solution did not bubble as it does when WCl_6 was reacted with the same reagent, but the solution did change from rose-red to violet upon TMSA addition. The reactants were mixed at ambient temperature for 12 hours, then the reaction mixture was heated to refluxing chlorobenzene temperature (130°C) for ca. 20 hours. The higher temperature was used in an effort to decompose the tungsten azido compound identified as **2A** and **2A'**. Elemental analyses were not available for this material but the IR spectra (see Fig. II-7, 8) of **2B** show peaks at 1020 and 311 cm^{-1} corresponding to the stretching modes of the W-N multiple bond and the W-Cl vibration, respectively. The IR asymmetric stretching mode of the azide group in the 2000 - 2100 cm^{-1} region was not observed for this compound.

$WNCl_3$ + $(CH_3)_3SiN_3$ --<butyronitrile>--> (2C, 2C'). Approximately 40 mL of butyronitrile was vacuum transferred onto $WNCl_3$ (535 g, .176 mmol) and allowed to warm to room temperature. Trimethylsilylazide (0.231 mL, 0.176 mmol) was added, by syringe, to the mixing solution of $WNCl_3$. Immediately

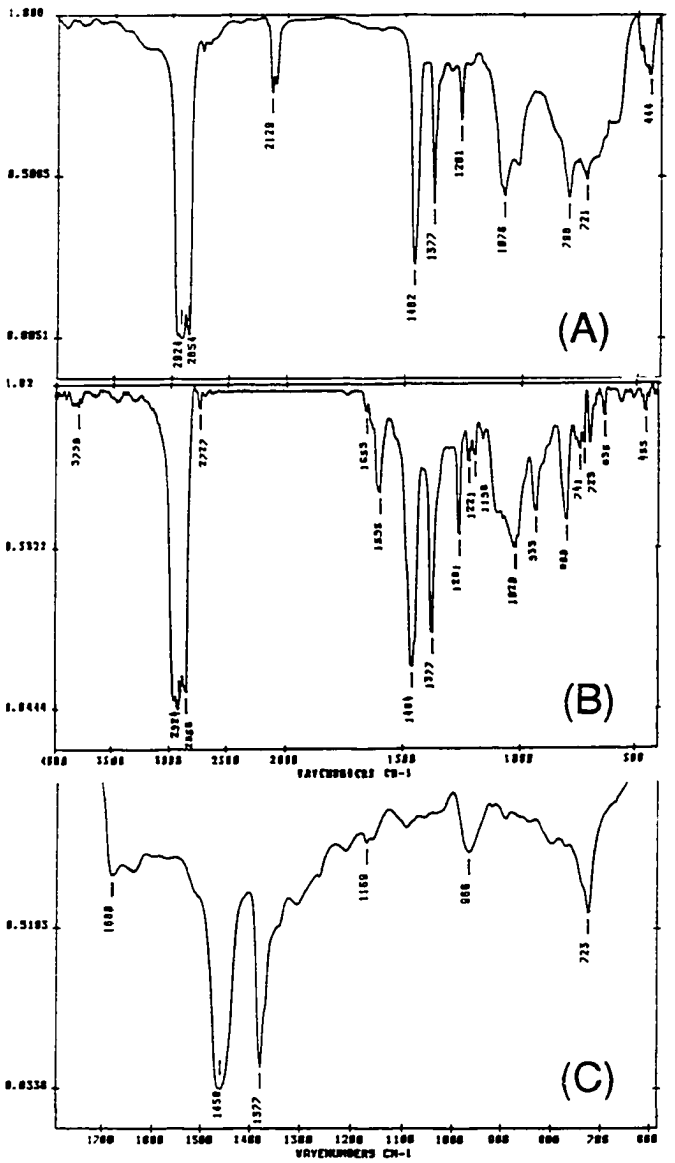

Figure II-7. Mid IR spectra (Nujol) of the products obtained from the reaction of $WNCl_3$ and TMSA in DCE (A), in pyridine/chlorobenzene (B) and butyronitrile (C). Although spectrum (C) does not cover the same range as (A) and (C), there is no additional functionality, besides Nujol, outside of the reported range. The azide peak at 2129 cm^{-1} does not appear in either (B) nor (C), indicating decomposition of the azide

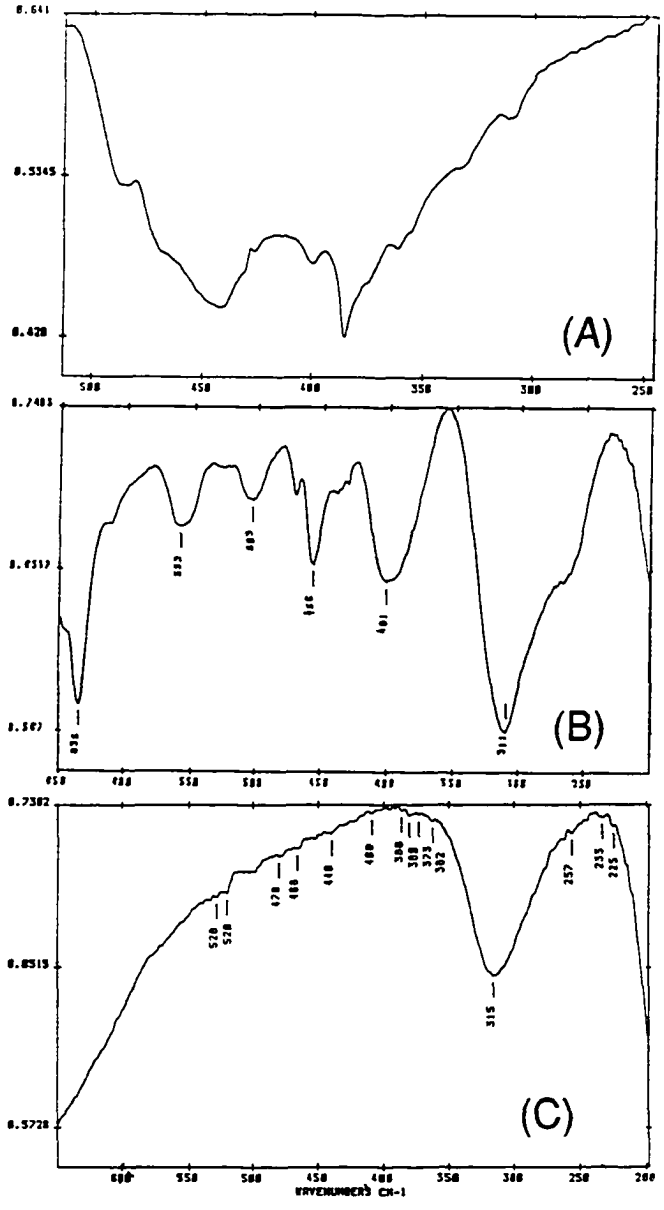

Figure II-8. Far IR spectra (Nujol) of the products obtained from the reaction of $WNCl_3$ and TMSA in DCE (A), in pyridine/chlorobenzene (B) and butyronitrile (C). The peaks in (A) centered at 450 and 380 cm^{-1} correspond to the W-N and W-Cl stretching frequencies, respectively while the peaks at 315 and 311 cm^{-1} in spectra (B) and (C) represent the stretching modes of the W-Cl bonds

after the addition of TMSA to the butyronitrile/$WNCl_3$ yellow - red solution, the reaction mixture became deeply red colored, similar to that observed in (2B). The reaction was conducted under refluxing conditions for four days and additionally at room temperature for two days. The material was isolated by filtering the insoluble portion of the product (2C) from the soluble fraction (2C'). The yield of the insoluble product was 496 mg. The solid was black, indicating a possible reduction of the metal. Anal. Found for 2C: W, 42.3; Cl, 13.35; N, 12.5; C, 24. IR (Nujol, cm^{-1}) for 2C: 1680 m, 966 m, 315 s (υ(W-Cl)). No asymmetric stretching mode was found for azide in the range 2000 - 2100 cm^{-1} nor was there a C≡N stretching frequency around 2200 cm^{-1} corresponding to the butyronitrile. The thermolytic decomposition was monitored by mass spectroscopy and is summarized in Figure II-9. A significant amount of the ion current in the mass spectrometer was due to acetonitrile, which is a very stable ion fragment of butyronitrile, indicating conclusively that butyronitrile was contained in compound 2C, even though the C≡N stretch was invisible in the IR spectrum. Additional mass fragments were associated with DCE and trimethylsilyl ions.

$WNCl_3$ + Li_3N --<DCE>--> (3A). Owing to a report of the exothermic, almost explosive nature of this reaction[15] producing (3A), Li_3N (110mg, 3.21 mmol) was loaded in a clean, dry 1 dram glass vial and placed in a 100 ml reaction flask containing $WNCl_3$ (976 mg, 3.21 mmol) in order to avoid mixing

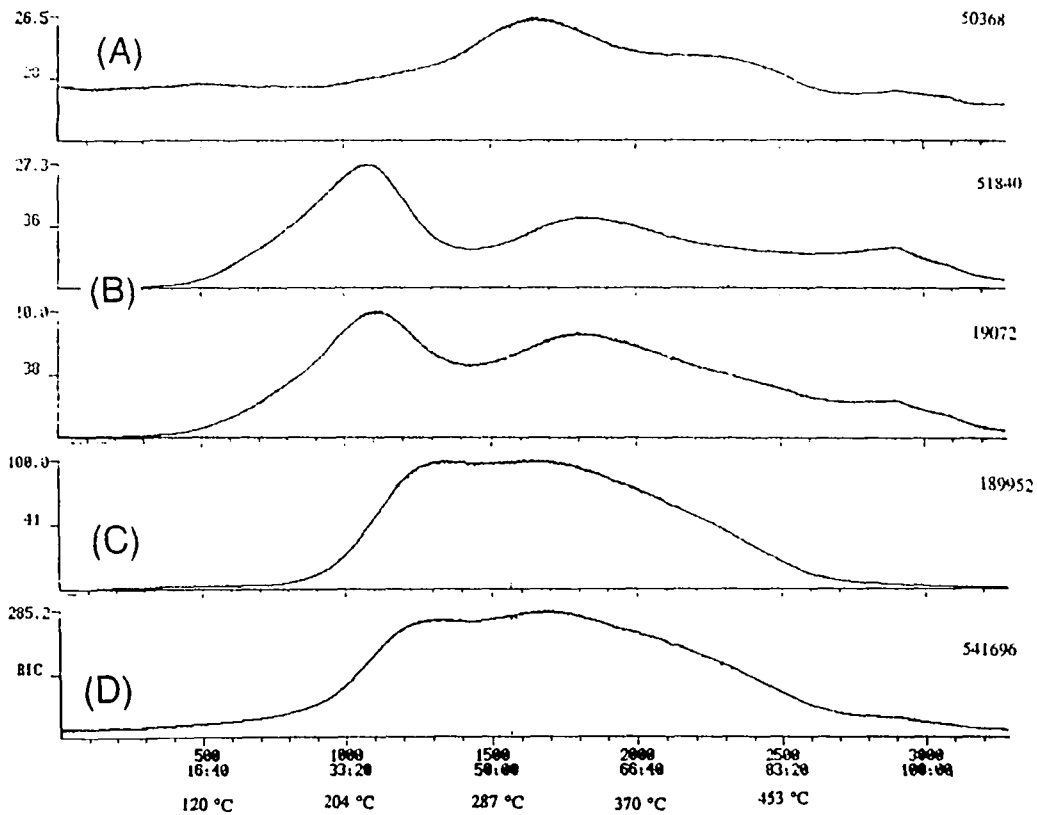

Figure II-9. Mass spectra correlation with the thermolysis of 3A in dynamic vacuum. The ion currents corresponding to molecular weights of 28 (A), 36 (B) and 41 (C) for N_2, $H^{35}Cl$, $H^{37}Cl$ and C_2H_3N ions, respectively. N_2 and Cl account for only a small part of the total ion current (D), whereas, the fragments of butyronitrile (including acetonitrile (C_2H_3N) account for the majority of the current

the two components directly as solids (it has since been shown that this solid mixture is not highly reactive in the drybox). Forty mL of DCE were vacuum transferred to the reaction flask containing $WNCl_3$ and Li_3N. The reaction was allowed to mix at ambient temperature for four days, under vacuum. The mixture changed color from orange to green to brown over the course of four days. The reaction proceeded at a slow rate because of the relative insolubility of both reactants in DCE. The product was insoluble in DCE and the filtrate was colorless. The solid was isolated on a filter frit and maintained under dynamic vacuum for 12 hours before recovery of ca. 1.0 g of (**3A**) in the dry box. The material was formulated as the addition product, $Li_3WN_2Cl_3$. A tungsten analysis was attempted on this material using the standard combustion gravimetric analysis but as the samples were placed into the furnance, flames were produced within the crucibles. IR (Nujol, cm^{-1}) for (**3A**): 1043 s (υ(W≡N)), 330 (υ(W-Cl)). In the IR spectrum there are no other assignable modes, aside from the Nujol peaks (see Fig II-10, 11). The X-ray powder data for (**3A**) indicate a slightly crystalline compound (see Fig. II-12). The diffraction peaks do not correspond to Li_3N, $WNCl_3$ or LiCl.

$WNCl_3$ + Li_3N ---<pyridine>---> (**3B, 3B'**). The Li_3N (119 mg, 3.42 mmol) and $WNCl_3$ (1.040 g, 3.42 mmol) were brought together in a 100 mL reaction flask as described for **3A**. The pyridine was vacuum transferred onto the two reactants and maintained at -25 °C while the two components were initially

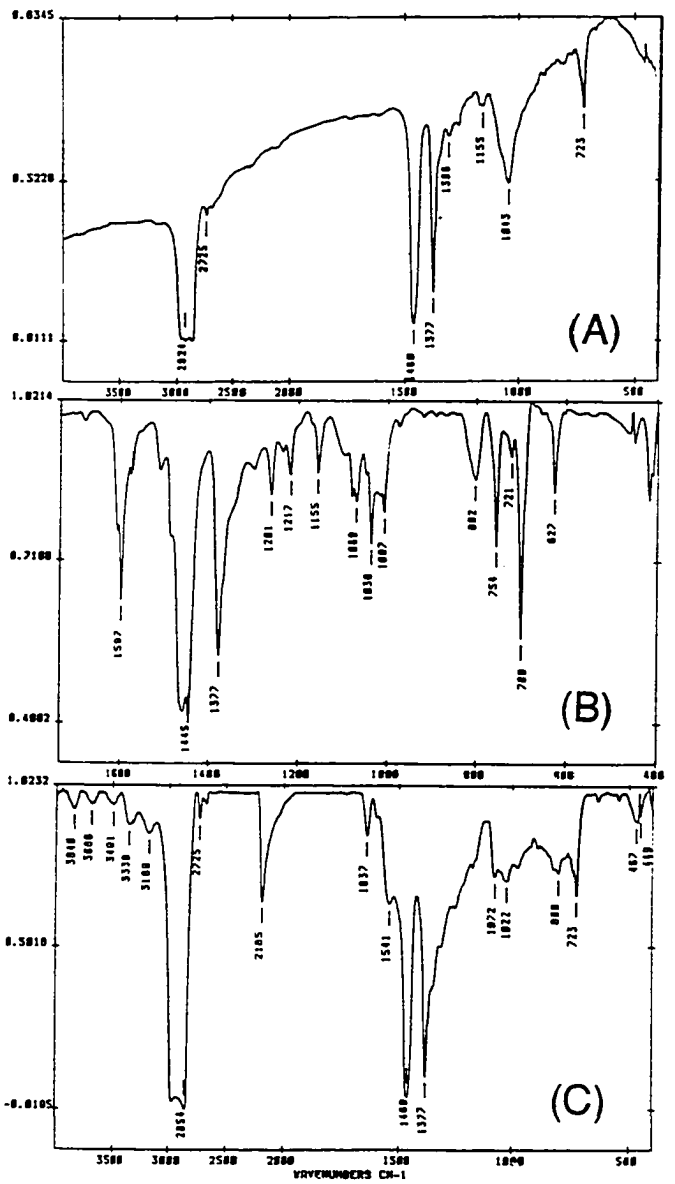

Figure II-10. Mid infrared spectra (Nujol) of the product formed when $WNCl_3$ and Li_3N were reacted in DCE (A), in pyridine (B) and in butyronitrile (C) corresponding to **3A**, **3B** and 3C respectively. The peak(s) in the range of 1100 to 1000 cm^{-1} correspond to the W-N multiple bond frequencies. In the case of (B), pyridine peaks are superimposed on the W-N mode(s)

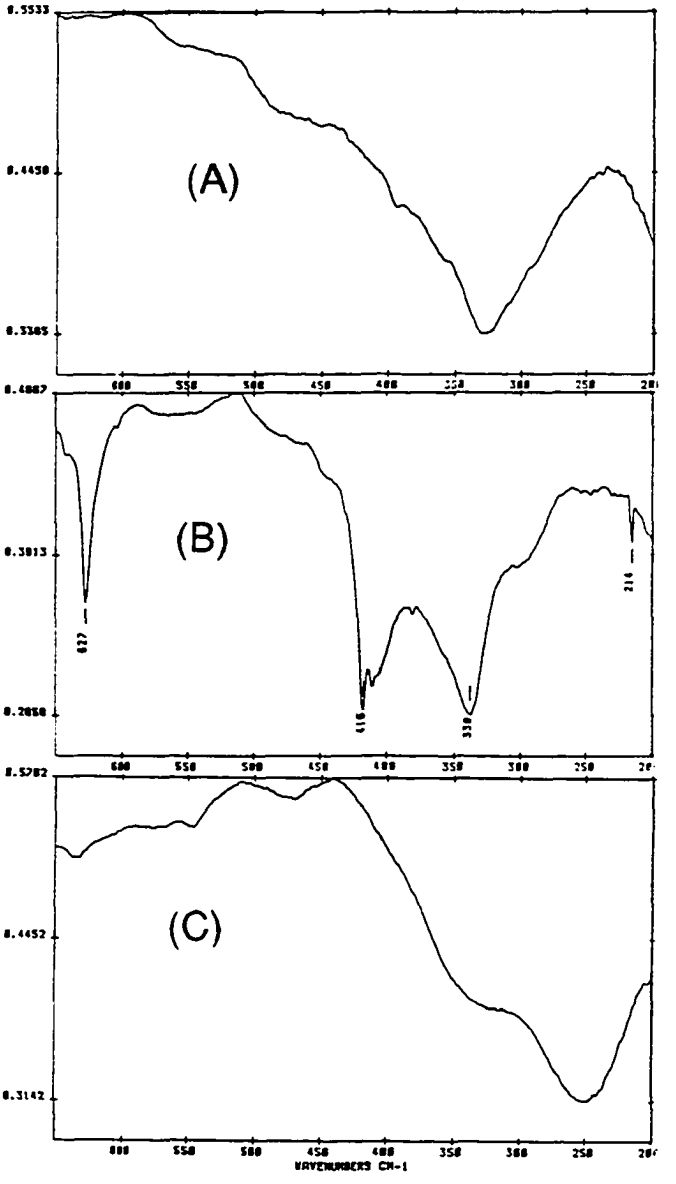

Figure II-11. Far infrared spectra (Nujol) of the product formed when $WNCl_3$ and Li_3N were reacted in DCE (A), in pyridine (B) and in butyronitrile (C) corresponding to **3A**, **3B** and **3C** respectively. The peaks at 338 cm^{-1} correspond to the stretching modes of W-Cl, while the bands at 416 and 250 in (B) and (C) respectively were assigned to a pyridine deformation mode for pyridine and υ(W-N) for butyronitrile, respectively

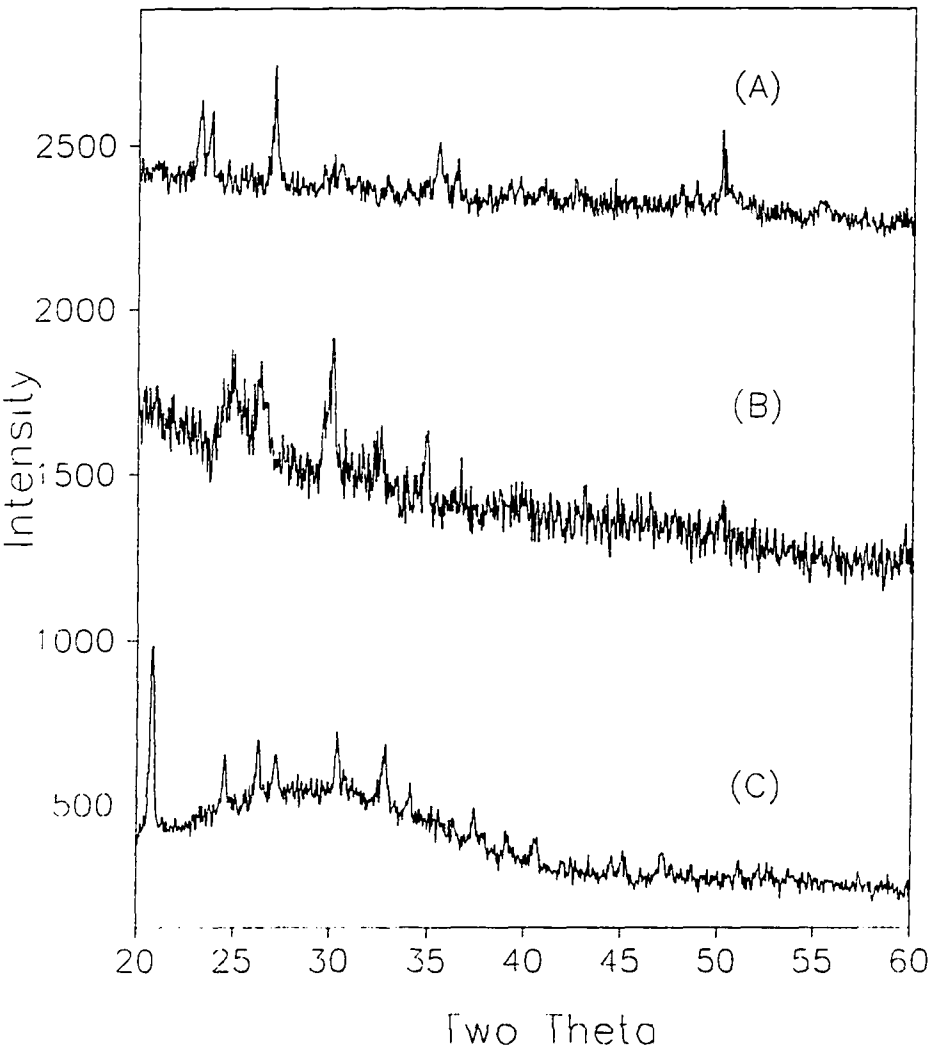

Figure II-12. A comparison of the X-ray powder data for **3A**, **3B** and **3C** corresponding to (A), (B) and (C) respectively. In each spectrum, the peaks are assigned to new compounds. Peaks corresponding to the starting reagents, $WNCl_3$ and Li_3N are not seen nor is LiCl which is a likely metathesis product

mixed to avoid a vigorous reaction, which did not occur. After two days of mixing at room temperature, under reduced pressure, the purple solution was filtered, which resulted in most of the material (1.6 g, 80%) passing through the frit as a soluble compound (**3B**) while 20% (0.4 g) of the material was isolated on the frit (**3B'**). The pyridine was distilled from the product, resulting in the formation of an oil for **3B**. DCE transferred onto the pyridine oil, resulted in ready precipitation of the solid, which allowed dry powders to be isolated for both **3B** and **3B'**. The difference between reactant and product mass was 0.841 g, which corresponds exactly to the mass of two moles of pyridine per mole of tungsten. A formulation of $Li_3WN_2Cl_3 \cdot 2py$ is consistent with this observation. The tungsten combustion analysis for **3B'** was not completed due to the presence of lithium, but the chloride composition was found to be 21.39% compared with the theoretical chloride percentage of 21.39%. IR (Nujol, cm^{-1}) for **2B'**: See Fig. II-10, 11. **3B** and **3B'** have the same X-ray powder pattern (see Fig. II-12). The bragg peaks cannot be assigned to a starting reactant or lithium chloride (a probable metathesis product).

$WNCl_3$ + Li_3N ---<butyronitrile>---> **(3C)**. $WNCl_3$ (1.026 g, 3.37 mmol) and Li_3N (114 mg, 3.37 mmol) were reacted under conditions that were the same as those used in the formation of **3B** and **3B'**. Over the two day reaction period, the mixture color changed from red to yellow-brown. The yellow-brown solid was isolated in two fractions; (**3C**), insoluble product isolated on the

ceramic frit (1.45 g) and 0.04 grams of product isolated in the receiver flask that was not characterized further. Based on the difference in reactant and product mass, the formulation for **3C** was $Li_3WN_2Cl_3 \cdot 1.5\ PrC{\equiv}N$. IR (Nujol, cm^{-1}) for (**3C**): 2185 ms ($\upsilon(C{\equiv}N)$), 1637 w, 1541 m, 1072 and 1022 m ($\upsilon(W{\equiv}N)$), 800 m, 338 s (υ(W-Cl)), 250 s (υ(W-N)). The X-ray spectrum for **3C** is shown in Figure II-12. In agreement with **3A** and **3B**, the X-ray powder diffraction data do not correspond to either of the two reactants or LiCl.

$WNCl_3 \cdot 3(C_5H_5N) + H_2O$ ---<pyridine>---> (4A, 4B). In one of the many attempts to grow single crystals of the pyridine adduct, $WNCl_3 \cdot 3py$, approximately 20 mg of $WNCl_3$ was placed in a test tube with 10 mL of pyridine and covered with a rubber septum. The test tube was in the lab environment for a period of 2.5 years! All the pyridine had diffused through the septum by this time and red cubic crystals (**4A**) surrounded by amorphous yellow material were identified in the tube in addition to blue-green laminar crystals (**4B**). In attempts to reproduce the result, diffracting blue crystals (**4B**) have been grown by inserting a small needle in the septum covering the $WNCl_3$/pyridine filled test tube and letting it sit for 2 weeks. The needle is used to facilitate the exchange of pyridine with O_2/water in the atmosphere. Single crystals of **4A** were isolated for SEM-EDS analysis and shown to contain tungsten, chloride and oxygen. A quantitative determination was not possible due to the morphology of the crystals. IR (Nujol, cm^{-1}) for (**4A**): 1734 mw, 1653 mw, 1084 m

(υ(W≡N)), 712, 638, 584 s (υ(W-O)), 442 s, 385 ms (υ(W-Cl)).

A single crystal X-ray data set was collected on the Siemans P4 rotating anode single crystal diffractometer for (**4A**). The crystal was found to be cubic and refinement was attempted in the space group $I\bar{4}3m$ with a = 13.421(2). There appears to be significant disorder in the system which has severely hampered the refinement. Currently the R factor is 0.2055. The largest Fourier peaks were found at 0, 0, 0 and 0, 0, 0.17 and assigned to tungsten based on their relative weights. The separation between these two positions is 2.2 Å. Since this is unreasonable for a W-W bond length, each position was refined with a 0.5 occupancy for W. The average structure appears to consist of an octahedron of tungsten atoms centered around the origin and tungsten atom at 0,0,0 surrounded by an octahedron of nonmetal atoms. There are Fourier peaks corresponding to edge-bridging and terminal positions of the tungsten octahedron (see Fig. II-13). Rotation photos of the blue laminar crystal (**4B**) showed intense diffraction but a single crystal data set has not been collected to date.

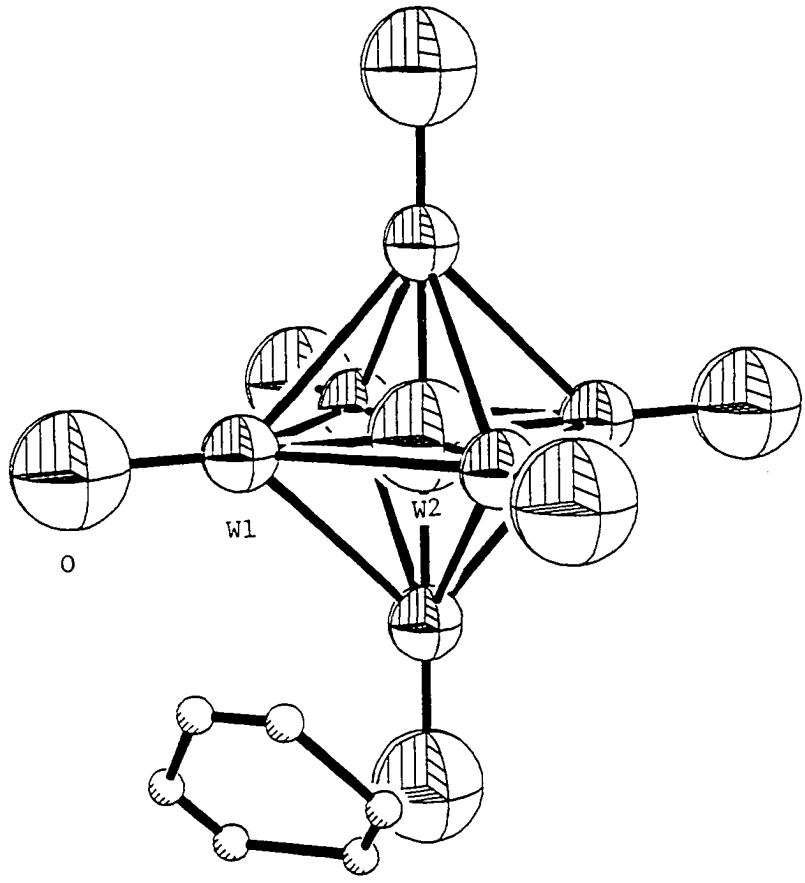

Figure II-13. Ball and stick representation showing the average structure of cubic **4A** produced from the gradual hydrolysis of $WNCl_3$ in pyridine. The positions for W1 and W2 are only 1/2 occupied. d(W1-W1) = 3.234(12), d(W1-W2) = 2.287(8), d(W1-O) = 2.04(9).

Physical Measurements

Infrared spectra were obtained from a IBM IR/90 or a Bomem MB-Series Fourier Transform infrared spectrometer. The samples were prepared as Nujol mulls and pressed between CsI plates. The spectra were recorded separately for the mid-IR (4000-600 cm^{-1}) and far IR (600-200 cm^{-1}) in the case of the IBM spectrometer and from 4000 to 185 cm^{-1} with the Bomem spectrometer. A Cambridge S-200 Scanning Electron Microscope (SEM) coupled to a Tracor Northern Micro Z II Energy Dispersive Spectrometer (EDS) with a Beryllium or ultra-thin carbon window was used to determine relative tungsten and chloride concentrations. A qualitative determination of the nitrogen composition could be obtained when the ultra-thin window was used. The X-ray diffraction data for finely ground powders of **1A** - **3C** were obtained from a Philips ADP3520 diffractometer using Cu $K\alpha_1$ and $K\alpha_2$ radiation. The samples were analyzed on zero-background quartz plates using the Philips environment cell reported in Section I of this work.

RESULTS AND DISCUSSION

Synthesis and Characterization

The coordination around W in $WNCl_3$ is pseudo octahedral with the position trans to the W-N multiple bond occupied by a chloride from an adjacent tetrameric unit. It is in this trans site that coordination by other ligands can readily occur by replacing the weakly bound chloride atom. This coordination should be considered to be the first step of a reaction involving a coordinating reactant. The following scheme of reactions summarizes the reactions in this work:

$$(1A)\quad WNCl_3 + 6NH_3(l) \xrightarrow[4\ hours]{-40^\circ C,\ NH_3(l)} WN(NH_2)_2Cl(NH_3)_2 + 2NH_4Cl$$

$$(1B)\quad WNCl_3(py)_3 + 3NH_3(g) \xrightarrow[5days,\ no\ mixing]{23^\circ C,\ pyridine} WN(NH_2)Cl_2(NH_3)_3 + NH_4Cl$$

$$(2A')\quad WNCl_3 + Me_3SiN_3 \xrightarrow[83^\circ C,\ 4days]{23^\circ C,\ DCE,\ 20hours} WN(N_3)Cl_2 + Me_3SiCl$$

$$(3A)\quad WNCl_3 + Li_3N \xrightarrow[4days]{23^\circ C,\ DCE} Li_3WN_2Cl_3$$

$$(3B)\quad WNCl_3 + Li_3N \xrightarrow[2days]{23^\circ C,\ pyridine} Li_3WN_2Cl_3(py)_2$$

$$(3C)\quad WNCl_3 + Li_3N \xrightarrow[2days]{23^\circ C,\ butyronitrile} Li_3WN_2Cl_3(prCN)_2$$

1A,1B. The ammonolysis in liquid ammonia of $WNCl_3$ (**1A**), as a first step to metathetically replacing chloride with amide, succeeded in removing two of the three chlorides, which is consistent with earlier work[15]. The ammonolyses of many metal chlorides show a similar retention of chloride. The ammonolysis of VCl_4 produces $VCl(NH_2)_3$ and $VCl(NH_2)_2$[16]. $MoCl_5$ ammonolyzes to yield $MoCl_4(NH_2)_2$ and $MoCl(NH)(NH_2)$[17]. For WF_6, reaction with liquid ammonia does not result in ammonolysis but rather reduces the tungsten to +4 with the formula $WF_4 \cdot 4NH_3$[18]. Part of the difficulty in completely removing the chloride is the insolubility of the ammonolyzed metal halides in ammonia. In the reaction yielding **1B**, gaseous ammonia was added to a pyridine/$WNCl_3$ solution, to induce gradual ammonolysis and replace all Cl atoms in $WNCl_3$. Nine moles of ammonia gas were added to replace completely the chloride and pyridine ligands. In agreement with the unobserved pyridine modes and observed ammonia modes in the IR for 1B (see Fig II-2), and the ammonium chloride observed in the X-ray powder diffraction, 1B represents partially ammonolyzed $WNCl_3$ where ammonia replaced all three pyridine ligands and reacted with the material to remove one of the chloride atoms. A chloride or tungsten analysis was not useful, due to the ammonium chloride present in 1B. It was discovered that even when the product **1A** is reacted with ammonia at 380 °C, the chloride is not completely removed[13].

2A-2C. When TMSA is reacted with $WNCl_3$, the product is dependent

on the solvent used. **2A'** represents the metathetic replacement of Cl with N_3 in $PWNCl_3$. In the reaction between WCl_6 and Me_3SiN_3, the azide intermediate, $W(N_3)Cl_5$, is formed and subsequently decomposes to $WNCl_3$ in an intramolecular oxidation-reduction reaction not involving a change in tungsten oxidation state. The detection of N_2^+ and HCl^+ is observed as this reaction proceeds. Cl^+ probably abstracts protons from any hydrocarbon present, resulting in HCl^+ detection. When **2A'** is decomposed thermally in dynamic vacuum, the mass spectra of the volatile components evolved in this heating process show a large amount of N_2^+ (mass 28) and HCl^+ (mass 36, 38) as seen in Figure II-6; in fact, N_2^+ and HCl^+ account for most of the ion current in the mass spectra for this decomposition. The azide appears to decompose (as evidenced by the nitrogen evolution in the mass spectra) before the HCl^+ is detected. This indicates that the azide is undergoing a net oxidation to dinitrogen while the tungsten is probably reduced in the process. One would expect a superposition of the nitrogen and HCl^+ peaks in Figure II-6 if the azide and chloride from $WN(N_3)Cl_2$ underwent reduction and oxidation respectively in a concerted manner, independent of the metal, as in the decomposition of WN_3Cl_5 to $WNCl_3$. It appears that WN_2 cannot be produced by the thermal decomposition of **2A'** in vacuo. The photolytic and thermal decomposition in inert or reactive gas atmospheres have yet to be investigated. By altering the atmosphere, the pathway of decomposition can also vary, which may allow for

the decomposition of the azide without reduction of the metal.

Both **2B** and **2C**, which were produced in pyridine/chlorobenzene and butyronitrile respectively, do not contain the azide ligand (based on the IR spectra, Fig. II-7,8). In the IR spectrum of **2B**, aside from the pyridine modes, there are two peaks corresponding to υ(W≡N) and υ(W-Cl) at 1080/1020 and 311cm,$^{-1}$ respectively. For **2C**, based on the C, N, W and Cl percentages of 24, 12.5, 42.0 and 13.35 respectively, the empirical formula is $WCl_{1.6}N_{2.4}(PrCN)_{2.2}$. The C≡N stretching mode was absent in the IR spectrum for **2C** but when the sample was decomposed thermally, butyronitrile and its ion fragments accounted for the majority of the total ion current (see Fig. II-8) with N_2 and HCl cations contributing about 1/4 of that produced by the nitrile. Masses 36 and 38 correspond to HCl for the two Cl isotopes. Ion current due to the HCl is seen beyond 500 °C which indicates that the solid produced by heating 2C in vacuo is contaminated by Cl.

3A-3C. Lithium nitride was used in these reactions in attempts to initiate a simple metathetic substitution of N^{3-} for 3 moles of Cl^- in $WNCl_3$. The resulting products from the three reactions of lithium nitride and $WNCl_3$ in DCE, pyridine and butyronitrile appear to represent addition compounds. The X-ray powder diffraction data for **3A-3C** (Fig. II-12) do not correspond to the reactants (Li_3N or $WNCl_3$) or potential product (LiCl) from a metathetic reaction, but illustrate three separate phases of moderate crystallinity . In each compound,

the W-Cl stretching frequencies have shifted from being centered at 385 cm^{-1} in $WNCl_3$ to 330-340 cm^{-1}. This shift is consistent with the shifts seen in anion formation from neutral compounds. The IR spectrum for **3A** is very simple, being comprised of two modes related to the tungsten compound. In $WNCl_3$ the IR stretching mode of triply bound W-N is centered at 1082 cm^{-1} while the corresponding mode for **3A** is found at 1043 cm^{-1} with a shoulder at approximately 1080 cm^{-1}. The possibility of a $WN_2Cl_3^{3-}$ anion, where tungsten is coordinated by two multiply bound nitrogen ligands must be considered based on the molecular formula and the perturbation of the W-N stretching frequency. In the far IR spectrum of **3C**, there are two modes at 338 and 250 cm^{-1}. The peak at 338 corresponds to W-Cl stretching mode while the other band is difficult to assign with certainty. Because of the variation in M-N assignments for nitrile compounds, 250 cm^{-1} is well within the accepted range for M-N(nitrile) stretching frequencies[19].

CONCLUSION

The ammonolyses of $WNCl_3$ in liquid ammonia or pyridine have yielded materials, whose compositions correspond to $WN(NH_{2)2}Cl(NH_3)_2$ and $WN(NH_2)Cl_2(NH_3)_2$, respectively. The reactions of $WNCl_3$ in non-coordinating and coordinating solvents with nitriding reactants, such as ammonia, TMSA and lithium nitride have not yielded higher binary tungsten nitrides, under the conditions specified. The thermolytic decomposition of WNN_3Cl_2 (**2A'**) resulted in azide decomposition at about 150 °C, followed by chloride evolution at 234 °C. The thermal decomposition of WN_3Cl_5 has been shown to evolve N_2 and Cl_2 in an intramolecular pathway in which the metal oxidation state remains constant. Heating $WNN_3Cl_2(DCE)_x$ in vacuo, results in N_3 and Cl decomposing at different temperatures. This indicates that the decomposition of $WNCl_3$ does not follow the same pathway as the WN_3Cl_5 decomposition. The dinitrogen anion, $WN_2Cl_3^{3-}$ has been identified by IR and compositional analyses. It was formed from the reaction of $WNCl_3$ and Li_3N in different solvents.

REFERENCES

1. Paccagnella, A.; Callegari, A. *IEEE Trans. Electronic Devices*, **1991**, 38(8), 1962.

2. Saito, Y.; Fukuda, K.; Washizuka, S.; Nozaki, C.; Yasumai, S.; Nishio, J.; Yashiro, S.; Watanabe, M.; Hirose, M. *Jpn. J. Appl. Phys.* **1991**, 30(10), 2432.

3. You-Xiang, Z.; Shou-An, H. *Solid State Commun.* **1983**, 45, 281.

4. Lyutaya, M. D. *Soviet Powder Met. Metal Ceram.* **1979**, 18, 190.

5. Hägg, G. *Z. Phys. Chem.* **1930**, B 7 339.

6. Kritrova, V. I. *Soviet Phys.- Crystall.* **1962**, 6(4), 439.

7. Walker, V. I.; Strähle, J.; Ruschke, P.; Dehnicke, K. *Z. Anorg. Allg. Chem.* **1982**, 487, 26.

8. Dehnicke, K.; Prinz, H.; Karitz, W.; Kujanek, R. *Liebigs Ann. Chem.* **1981**, 1, 20.

9. Goldmeyer, T.; Dehnicke, K.; Fluck, E. *Z. Anorg. Allg. Chem.* **1988**, 565, 41.

10. Lichtenhan, J. D.; Ziller, J. W.; Doherty, N. M. *Inorg. Chem.* **1992**, 31, 2893.

11. Musterle, W; Strähle, J.; Liebelt, W; Dehnicke, K. *Z. Naturforsch., B:* **1979**, 34B(7), 942.

12. Dehnicke, K.; Strähle, J. *Z. Anorg. Chem.* **1965**, 339, 171.

13. Close, M. R. Ph.D. Dissertation, Iowa State University, Ames, Iowa, 1992, Section I,III.

14. Bremner, J. M.; Mulvaney, C. S. *Methods of Soil Analysis, Part 2. Chemical and Microbiological Properties - Agronomy Monograph no. 9* 1982, 595.

15. Carlson, C. D. Ph.D. Dissertation, Iowa State University, 1989, section 1.

16. Fowles, G. W. A.; Nicholls, D. *J. Chem. Soc.*, **1958**, 1687

17. Edwards, D. A.; Fowles, G. W. A. *J. Less-Common Metals*, **1961**, 3, 181

18. Clark, H. C.; Emeléus, H. J. *J. Chem. Soc.* **1957**, 4778.

19. Nakamoto, K. "Infrared spectra of Inorganic Compounds"; John Wiley and Sons: New York, 1970

SECTION III. SYNTHESIS, NEUTRON POWDER DATA REFINEMENT, AMMONIUM CATION ORIENTATION AND PROPERTIES OF HEXAGONAL AMMONIUM TUNGSTEN BRONZES $(NH_4)_xWO_{3-y}(NH)_y$

INTRODUCTION

Ternary oxides with the general formula M_xWO_3 have been termed tungsten bronzes because of their similarity in metallic luster and electrical properties to copper-tin bronze. The tungsten oxide bronzes have been shown to form in triclinic, monoclinic, orthorhombic, tetragonal I, tetragonal II, hexagonal and cubic crystallographic systems. As the value of x is increased for a given M, the structure of the tungsten bronze changes to higher symmetry[1]. Some interesting properties are associated with these compounds.[1-3] The hexagonal bronzes are superconducting (Tc less than 8 K)$_4$, chemically inert and metallic[5] while the lower symmetry, low-x structures, such as tetragonal II and orthorhombic, are always semiconductors. The ionic mobility of some cations in these phases has lead to their use as non-polarizing electrodes in solid electrolytes.[6]

In the hexagonal bronze structure, hexagonal and trigonal channels are formed parallel to the c axis by interconnected tungsten-oxygen octahedra (Fig III-1). The cations are located in the center of the hexagonal channels. Most commonly, the mono-valent cations occupy the hexagonal chambers in a range of $0.16< x <0.33$[6-8] (0.33 is the maximum theoretical occupancy of M^+ in the hexagonal channels if it is assumed that one hexagonal cavity contains only one cation) although a value of x as high as 0.45 was reported by a group

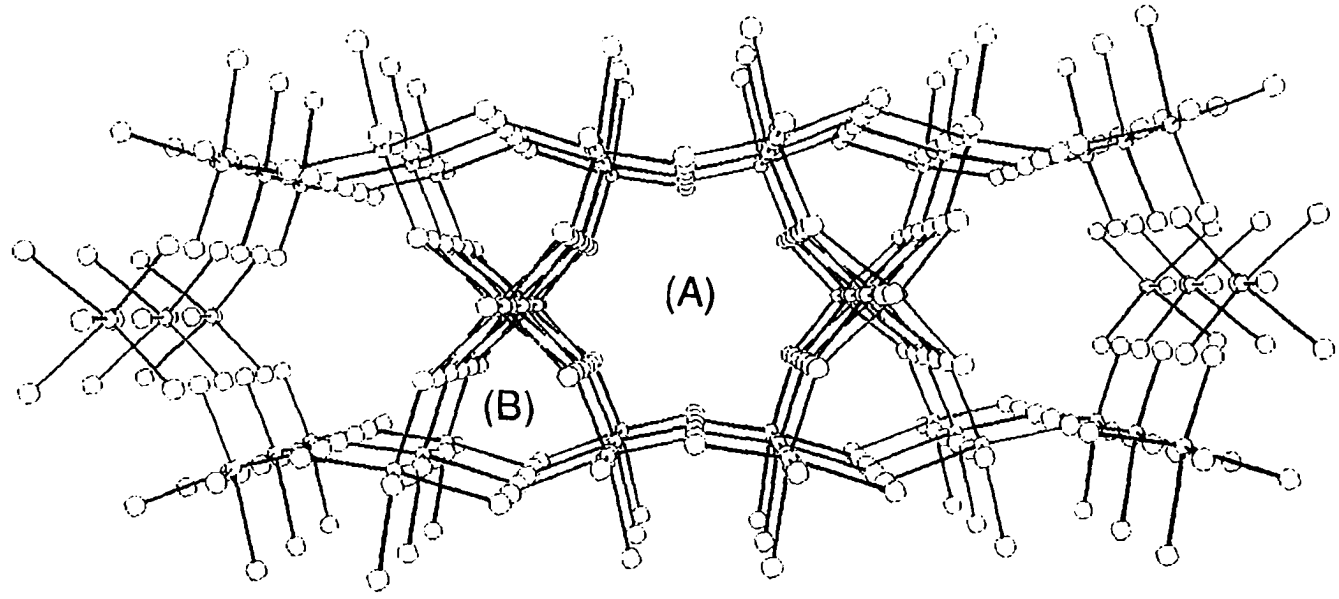

Figure III-1. View of the extended bonding arrangement in the hexagonal tungsten bronze M_xWO_3. The corner sharing tungsten-oxygen octahedra form hexagonal (A) and trigonal (B) channels parallel to the c axis. The monovalent cations occupy the hexagonal channels and are generally coplanar with the apical oxygens of the tungsten-oxygen octahedra

investigating differing routes to the ammonium tungsten bronze.[9] A recent paper[10] on hydrothermal synthesis of a fully oxidized hexagonal tungsten oxide reported that sodium resides in the constricted hexagonal window formed by the basal oxygens of the tungsten-oxygen octahedra. The conduction band of the tungsten bronze is formed by the π-bonding between the tungsten 5d (t_{2g}) and the oxygen 2p orbitals[11,12]. Variation of the electron density at the Fermi level by modulating cation type and stoichiometry account for most of the attempts to alter the electronic properties of the tungsten oxide bronzes. There has been no successful attempt to alter the anionic tungsten-oxygen framework by isoelectronic substitution for oxygen. Changes in the non-metal identity would also change the energy level of the p orbitals and consequently should alter the density of states at the Fermi level of the bronze.

The conventional syntheses of ammonium tungsten bronze utilize oxygenated reactants, thereby increasing the probability of a tungsten-oxygen anionic lattice. In this study the hexagonal ammonium tungsten bronze has been made from a new synthetic route with nitrogenated reactants which increases the probability of isoelectronic nitrogen substitution (in the form of imide-NH^{2-}) for oxygen in the anionic lattice. A slight excess of nitrogen was discovered in the ammonium bronze by elemental analysis and XPS spectra identified a small amount of imido-like nitrogen in the bronze phase. Because of the small difference in X-ray scattering length between oxygen and nitrogen,

a neutron powder diffraction study (the relative neutron scattering lengths of the atoms involved are: N = 0.93, O = 0.58, W = 0.48 and D = 0.67) was undertaken to determine the location of nitrogen, if any, in the anionic hexagonal lattice and determine the location and orientation of the ammonium cation in the hexagonal tunnels.

A report of a fully substituted imido bronze with the formula $(NH_4)_xW(NH)_3$ has been given recently[13]. In contrast to this report of an imido bronze, the results obtained from this study have shown that the imido ligand does not substitute to a significant degree in the oxide lattice of the ammonium bronze.

EXPERIMENTAL

General Considerations

The starting materials reported in this section are extremely reactive to air and water. Manipulations of air- and water-sensitive compounds were performed under inert atmosphere conditions using standard drybox, vacuum and Schlenk techniques.

Materials

Anhydrous ammonia (99.99% min) was obtained from Matheson Gas Products and was subsequently purified by dissolving sodium metal in the liquid ammonia to eliminate oxygen and water. The ammonia was distilled from the sodium for most of the reactions. Deuterated ammonia (ND_3) was obtained from Cambridge Isotope Laboratories (99% deuterated) and purified with sodium metal. 100 g. of Puratonic grade (99.999%) ammonium tungsten oxide ($(NH_4)_{10}W_{12}O_{41}\cdot 5H_2O$) was obtained from Johnson Matthey Chem. Ltd. and used as received. $WNCl_3$ was prepared according to the synthesis reported in Section I of this work. WCl_6 was obtained from Pressure Chemical and further purified by fractional sublimation to eliminate tungsten oxychloride impurities.

$WO_3 \cdot 2H_2O$ was prepared in this laboratory by a published method.[14]

Analytical Procedures

Potentiometric titrations with a standardized silver nitrate solution were used to determine total chloride content. Tungsten was determined gravimetrically, by conversion to tungsten trioxide. A LECO Model UO-14SP N Determinator (an automated Dumas combustion instrument) and Kjeldahl analyses were used for determination of total nitrogen[15]. In the Kjeldahl analysis, tungsten bronze samples were digested in boiling sulfuric acid for periods of 1-2 days. The relatively long digestion period (typical digestions of organic materials range from 30 minutes to two hours) was required to insure that the bronze completely decomposed to tungsten trioxide and liberated all of the nitrogen in the system. After the materials were fully digested, the appropriate amount of a sodium or potassium hydroxide solution was added to raise the pH above 7. The solution was then heated to boiling and the ammonia was distilled into a beaker containing a 5% aqueous solution of boric acid which was then titrated with .01 M sulfuric acid. Standards of $((NH_4)_{10}W_{12}O_{41} \cdot 5H_2O)$ were evaluated before and after the analyses and in each case the N percentages were those expected within the experimental error associated with the method.

Synthesis

Preparation of a tungsten imide ($W(NH)_{2.5}Cl_x$) (1A-1C). Two preparative schemes were employed to produce the tungsten imide.

Scheme I. In the first preparation, $WN(NH_2)_2Cl(NH_3)_2$ (reported in section II) was placed in a boat, made of either tungsten or pyrex, and inserted in a quartz reaction tube which was placed in a tube or split furnace and connected directly to a tank of anhydrous ammonia. The ammonia was admitted into the reaction tube at a rate not exceeding 10 cm^3/min and the temperature was increased to 380-400 °C over an hour period. The elevated temperature ammonolysis was allowed to continue for 12-24 hours depending on the experiment. Finely divided white powder was carried along in the ammonia stream which was subsequently identified as ammonium chloride by x-ray diffraction. The resulting product ranged in color from black to brown. The material was found to be hygroscopic and was isolated and stored in a drybox prior to characterization.

In order to prepare samples for a neutron diffraction experiment, a modified scheme was developed in which the amount of deuterated ammonia used in the preparation was minimized.

Scheme II: $WN(ND)_2Cl(ND_3)_2$ was prepared as outlined in section II of this dissertation for the hydrogen analog, except deuterated ammonia was

substituted for ammonia. The deuterated ammonia was also dried over sodium metal and frozen with liquid nitrogen. Figure III-2 gives the overall schematic for the imide preparation. Heating and ammonolysis was performed according to the following sequence:

1). $WN(ND_2)_2Cl \cdot ND_3$ was placed in a reaction tube and placed in a tube furnace at ambient temperature.
2). The sample compartment and the vacuum line were evacuated.
3). The system was backfilled with gaseous ammonia by allowing the solid ammonia to warm in a 2-propanol slush bath.
4). The sample was heated to 100 °C.
5). The sample was heated for two hours at 100 °C.
6). Repeat steps 2 and 3.
7). The sample was then heated to 200 °C.
8). The sample was heated for two hours at 200 °C.
9). Repeat steps 2 and 3.
10). The sample was then heated to 300 °C and reacted for 1/2 hour.
11). Then it was heated to 325 °C and reacted for 1 hour.
12). The system was evacuated at 325 °C to sublime ammonium chloride.
13). Then the sample was heated at 325 °C for 2 hours under static vacuum.
14). The sample was finally cooled to ambient temperature.

When the material was initially heated to 100 °C, a large quantity of gas was evolved. The evolution of gas did not occur to any significant degree after the material was heated beyond 100 °C. Ammonium chloride was produced in large quantities in this reaction and was isolated from the sample by breaking the reaction tube at the constriction.

Three samples of $WN(ND_2)_2Cl \cdot (ND_3)_2$ were reacted according to

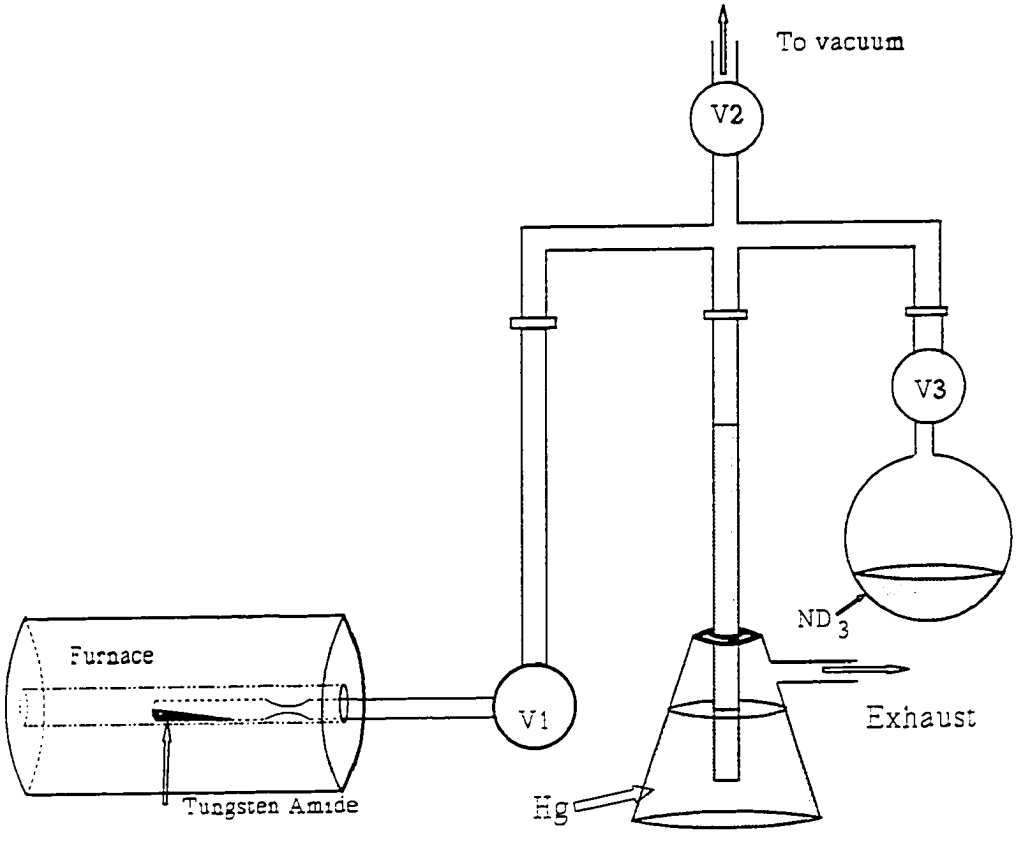

Figure III-2. Schematic of reactor for elevated temperature ammonolysis of $WN(ND_2)_2Cl{\cdot}(ND_3)_2$ which was used as a precursor to crystalline ATB (3E). The material was heated in increments of 100 °C to 300 °C. After each new temperature level was obtained, the system was evacuated and backfilled with dry deuterated ammonia

scheme II to produce products **1A, 1B** and **1C**. The starting amounts for each reaction were 11.00 g., 10.21 g. and 11.0 g., with yields of 5.2 g., 4.3 g. and 5.2 g. respectively for **1A, 1B** and **1C**. The X-ray powder diffraction patterns for **1A, 1B** and **1C** are shown in Figure III-3.

Preparation of $(NH_4)_xWO_3$ (2A) from nitrogen reactants. Reaction of the tungsten imide ($W(NH)_{2.5}Cl_x$) with varying amounts of water yields the ATB. The ATB in this study are synthesized according to the following general scheme:

1). $WCl_6 + Me_3SiN_3 \xrightarrow[80°C]{DCE} W(N)Cl_3 + N_2 + Cl_2$

2). $W(N)Cl_3 + xsNH_3(l) \xrightarrow[-40°C]{Neat} W(N)(NH_2)_2Cl{\cdot}2NH_3 + 2NH_4Cl$

3). $W(N)(NH_2)_2Cl{\cdot}2NH_3 \xrightarrow[340°C]{NH_3(g)} W(NH)_{2.5}Cl_x + (1-x)NH_4Cl + \frac{(1-x)}{6}N_2$

4). $W(NH)_{2.5}Cl_x + 3H_2O \xrightarrow[380°C]{2/3\ atm\ NH_3(g)} (NH_4)_{0.27}WO_{3-y}(NH)_y + xNH_4Cl + NH_3$

In the final step, the imide was added to a pyrex reaction tube which was connected to a vacuum line and evacuated. The desired amount of water was syringed into an adjacent glass tube which was being purged with argon. After the water was added, the valve to the water tube was closed and the water was frozen with liquid nitrogen and then evacuated. The water was then vacuum transferred to the imido material, frozen with liquid nitrogen and backfilled with

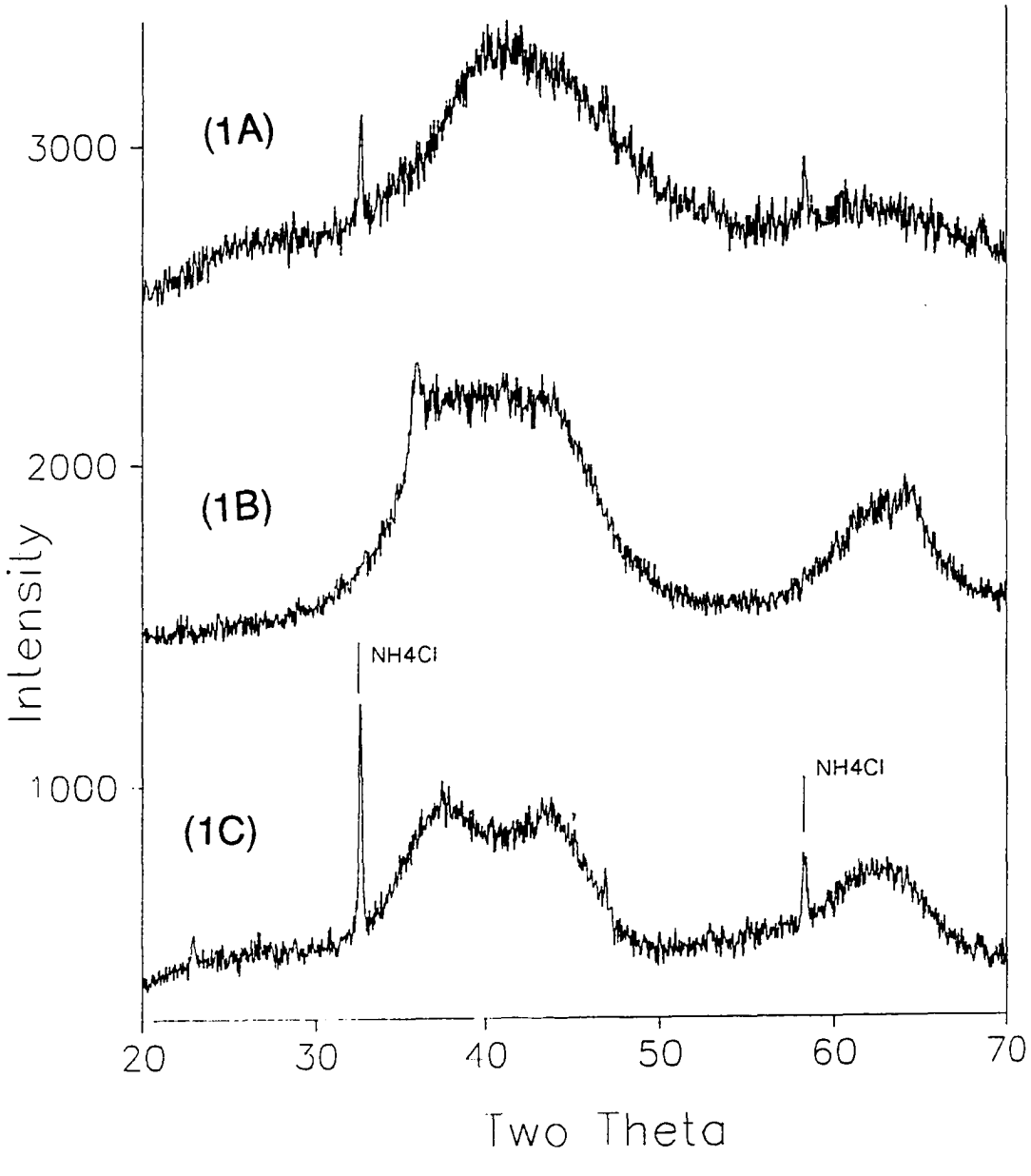

Figure III-3. X-ray powder diffraction of the products of three separate elevated temperature ammonolyses, **1A**, **1B** and **1C** conducted according to Scheme II. The narrow peaks in the spectra are due to ammonium chloride and the broad peaks are due to the amorphous tungsten imide

approximately 2/3 atmosphere of ammonia. The tube containing the imide, water and ammonia was then melt sealed and placed in a tube furnace at 380-400 °C for three to ten days, depending upon the experiment. If less than 2 moles ofwater is added to the imide, the material does not convert fully to the crystalline bronze. The X-ray diffraction patterns in Figure III-4 illustrate the dramatic influence of water on crystalline bronze formation. The imide has been shown to be hygroscopic and can be left in air for several days and it absorbs enough water to convert the imide to the bronze when heated in a sealed pyrex tube for several days in static ammonia at 380 °C.

Conventional preparation of $(NH_4)_xWO_3$ (2B). Ammonium paratungstate (APT) with the formula $(NH_4)_{10}W_{12}O_{41}\cdot 5H_2O$ was reacted with ammonia at 380 °C in two separate experiments under flowing and static ammonia. In the flowing ammonia reaction the APT was loaded in a pyrex boat and placed in a reaction tube and allowed to react for 18 hours (**2B**). The static reaction was performed as recorded in Scheme II in the preparation of a tungsten imide ($W(NH)_{2.5}Cl_x$) in this section.

New preparation of $(NH_4)_xWO_3$ (2C) with an oxygenated reactant. When $WO_3\cdot 2H_2O$ was allowed to react with flowing ammonia at 380 °C for 17 hours a material was produced that corresponded to the hexagonal tungsten bronze phase with small particle size (see Fig. III-5). Comparative X-ray powder data for **2A-2C** are given in Figure III-6.

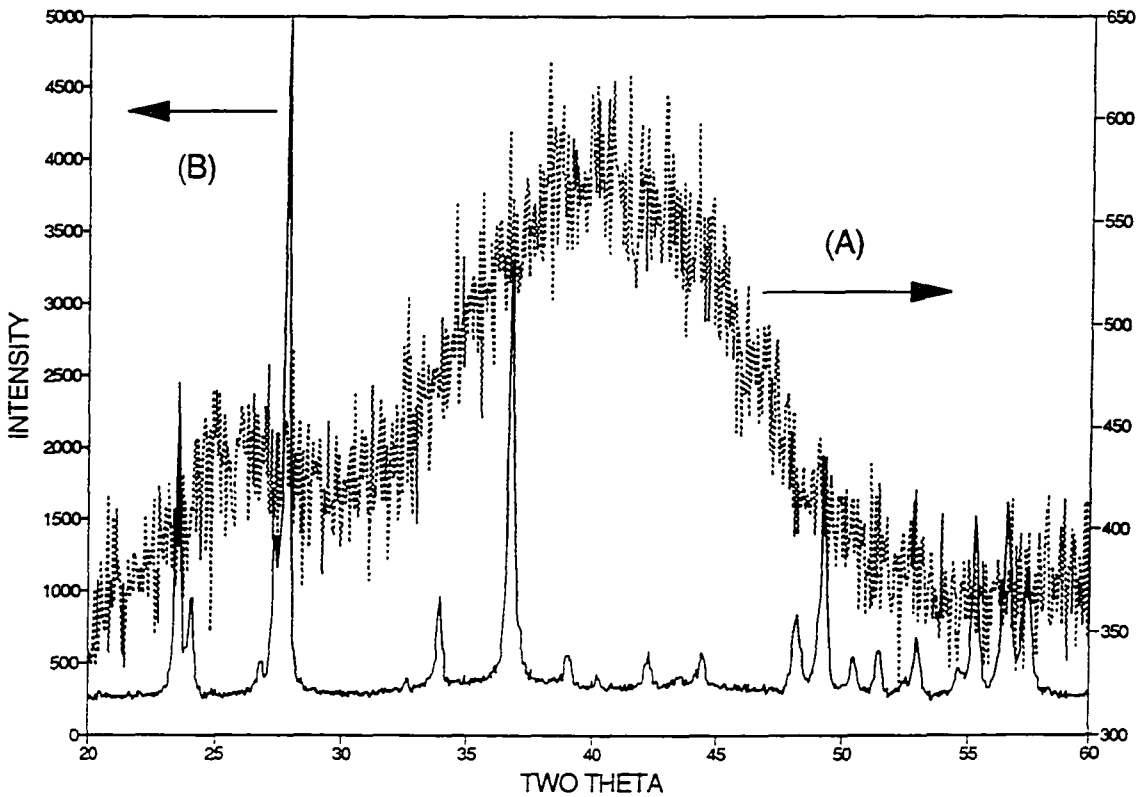

Figure III-4. X-ray powder diffraction of the amorphous tungsten imide made according to Scheme I (A) and the hexagonal bronze (2A) formed by the reaction between amorphous tungsten imide and 3 moles of water per mole of tungsten at 380 °C for 3 days under reduced ammonia pressure (B)

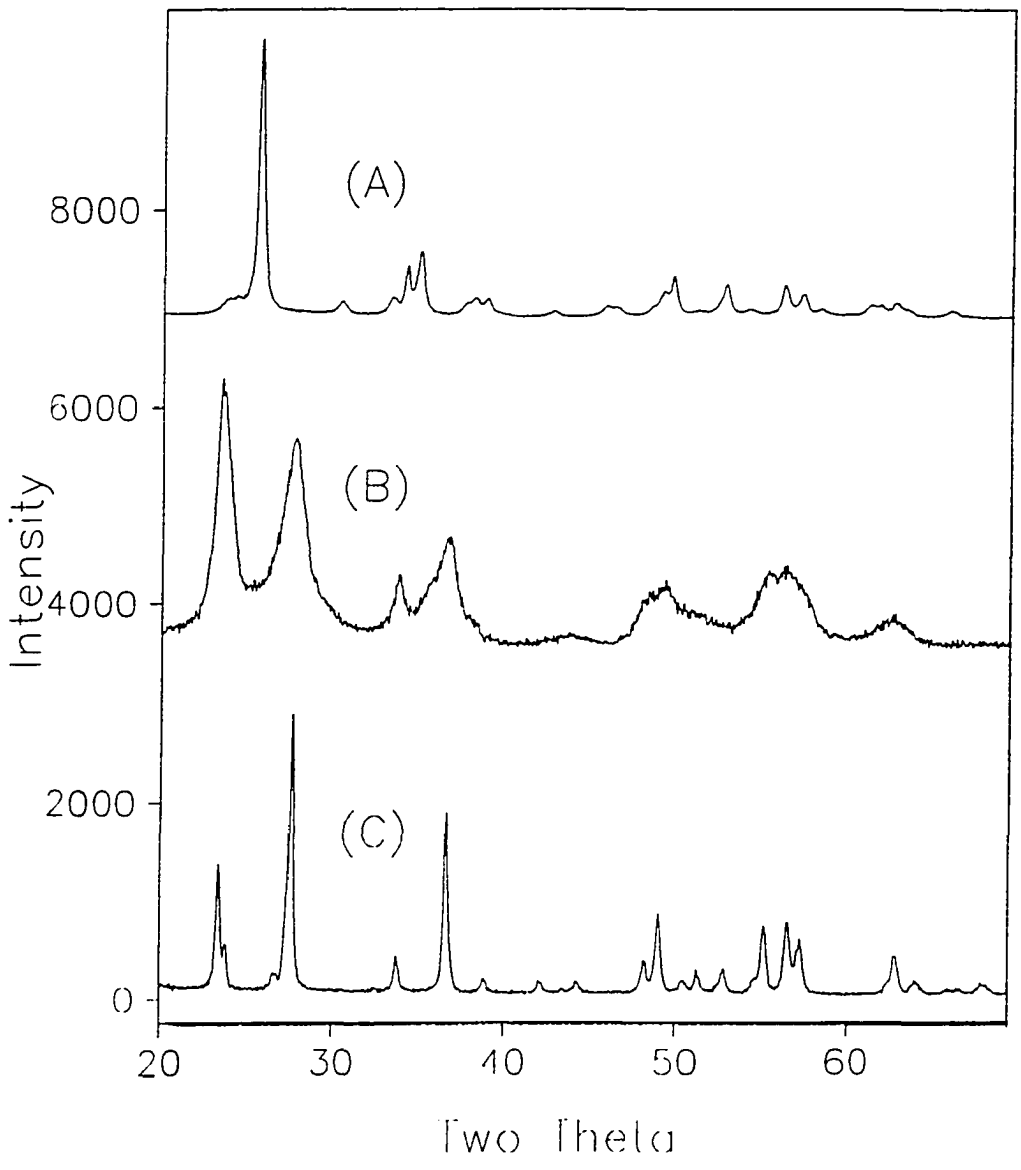

Figure III-5. X-ray powder diffraction of $WO_3 \cdot 2H_2O$ (A), the product of the reaction between $WO_3 \cdot 2H_2O$ and flowing ammonia at 380 °C (B) and **2A** - crystalline hexagonal ammonium tungsten bronze (C)

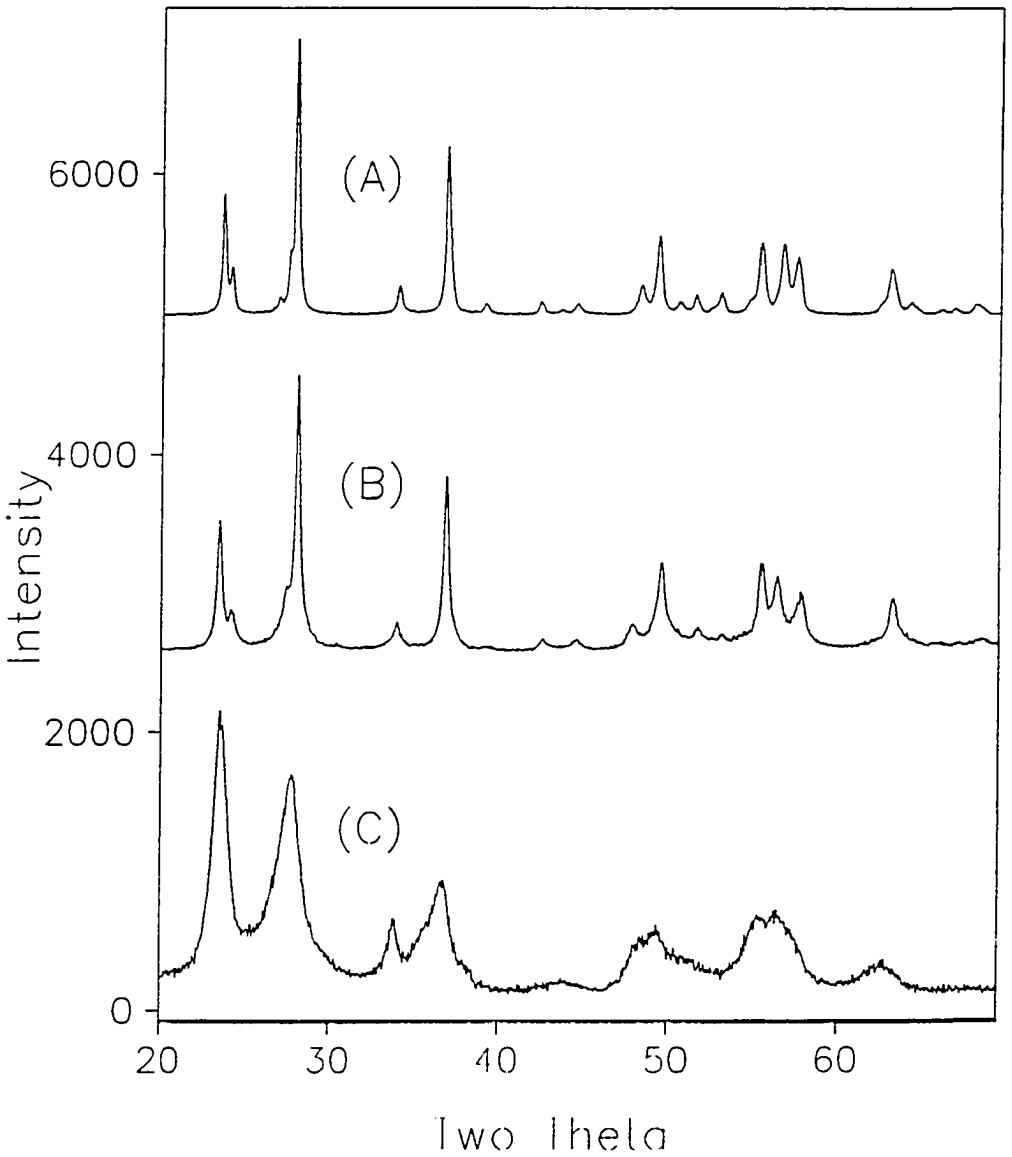

Figure III-6. X-ray powder diffraction of hexagonal bronze **2A** made by the reaction of tungsten imide with 3 moles of water at 380 °C (A), **2B** made by the reaction of ammonium paratungstate and ammonia at 380 °C (B) and **2C** made by a reaction between $WO_3 \cdot 2H_2O$ and ammonia, at 380 °C (C)

Preparation of deuterated ATB samples for neutron powder diffraction studies. Six samples were taken to Los Alamos National Laboratories for neutrondiffraction studies. The tungsten imido compounds, **1A-1C**, were reacted with differing amounts of D_2O to yield compounds **3A-3E** as described in the preparation of **2A**. The water was added on the basis of a water to metal mole ratio e.g., 0.5 moles of water added to a compound means 0.5 moles of water per 1 mole of metal in $W(NH)_{2.5}Cl_x$. **3A** was obtained by the reaction of **1A** and 0.5 moles of D_2O, **3B-3D** were obtained by the reaction of **1B** and 1.5 moles of water(**3B** was doped with 25 % NH_4Cl, **3C** was doped with 50 % NH_4Cl and **3D** was doped with 75 % NH_4Cl) and **3E** was obtained by the reaction of **1C** and 3.0 moles of water. **3E** was annealed twice in sealed pyrex tubes at 380 °C for 4-5 days to induce further crystallization and sublime ammonium chloride, produced by the hydrolysis, from the bronze (see Fig. III-7 and Fig. III-8 for the neutron powder diffraction spectra for **3A**, **3B** and **3E**, **3F** respectively). **3F** was prepared according to scheme II but ammonium paratungstate was used instead of $WN(NH_2)_2Cl{\cdot}NH_3$ as the starting tungsten reagent. Based on elemental analyses of **3E**, the weight percent of N is 2.60 and that of Cl (from NH_4Cl) is 1.40. The nitrogen percentage in the tungsten bronze is 2.05 after the nitrogen that arises from ammonium chloride is taken into account. In the formulation $(ND_4)_xWO_{3-y}(NH)_y$, if x = 0.25 then y = 0.09, and if x = 0.28 then y = 0.06.

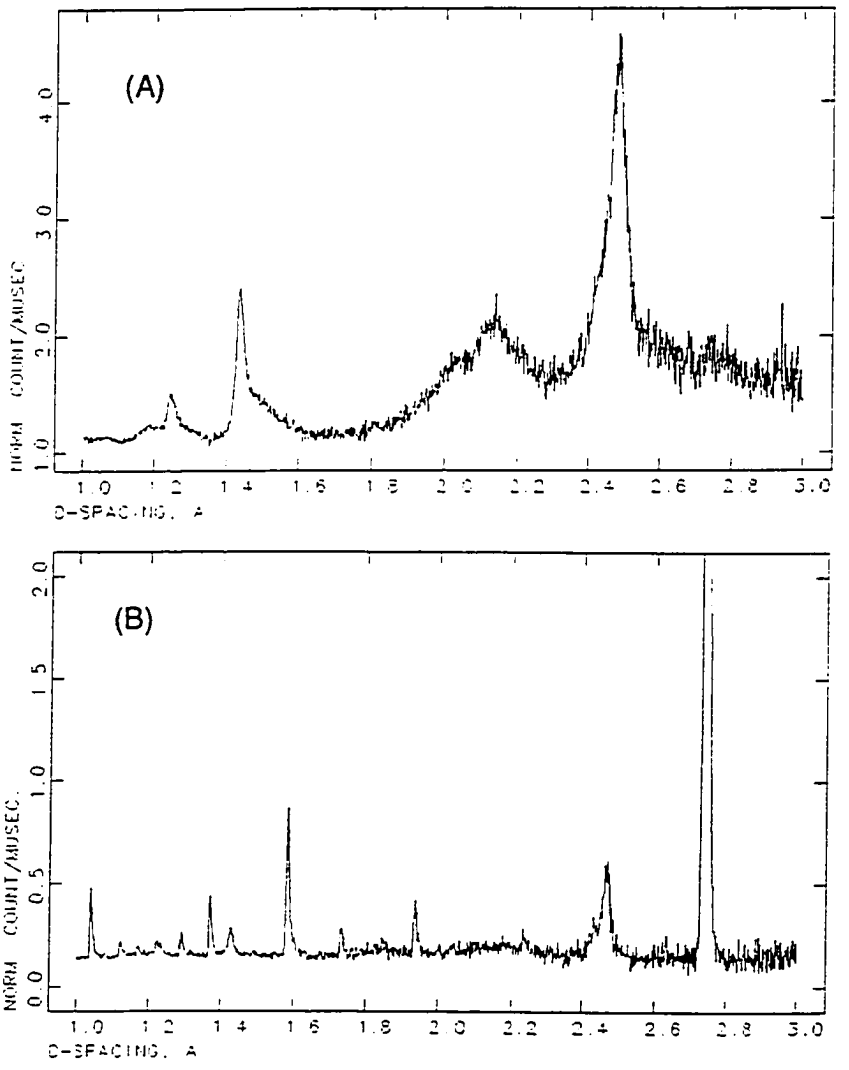

Figure III-7. Neutron powder diffraction of tungsten imido/bronze compounds **3A** (A) and **3B** (B) prepared by the addition of 0.5 and 1.5 moles of D_2O to **1A** and **1B** respectively. The narrow peaks in (b) are due to ammonium chloride. The spectra are scaled independently and illustrate the increase in crystallinity resulting from the addition of increasing amounts of water to the imide

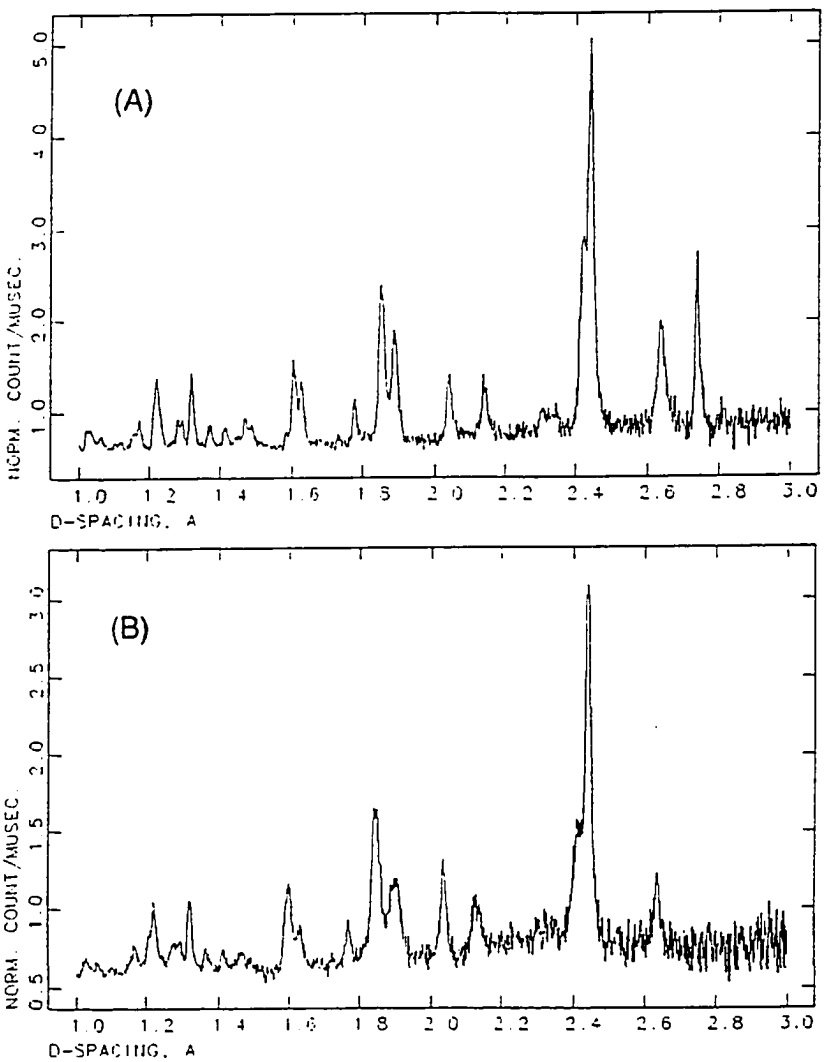

Figure III-8. Neutron powder diffraction of crystalline hexagonal tungsten bronze compounds **3E** and **3F** prepared from the elevated temperature hydrolysis of tungsten imide (A) and elevated temperature ammonolysis of ammonium paratungstate (B)

Physical Measurements

A Cambridge S-200 Scanning Electron Microscope (SEM) coupled to a Tracor Northern Micro Z II Energy Dispersive Spectrometer (EDS) with a Beryllium or ultra-thin carbon window was used to determine relative tungsten and chloride concentrations. A qualitative determination of the nitrogen composition could be obtained when the ultra-thin window was used. X-ray photoelectron spectra were obtained from a Perkin Elmer model 5500 Multi-Technique system by James Anderegg at Ames Laboratory. Magic angle spinning and static solid state NMR spectra were obtained by Vinko Rutar in the Iowa State Instrument Services Group on a Bruker MSL-300 Solid State NMR spectrometer. Variable temperature magnetic susceptibility was measured on powdered samples with a Quantum Design Squid magnetosusceptometer. Variable temperature electrical resistivity was measured on square pellets of ATB which were annealed at 380 °C under 2/3 atmosphere of ammonia for 6 days. The measurement was based on the Van der Pauw four-probe method[16] using the system developed by the David Johnston group at Ames Laboratory.

X-ray Powder Diffraction Data

The X-ray data for finely ground powders of **2A** and **2B** were obtained from a Scintag θ-θ powder diffractometer while X-ray data for powdered **2C** were obtained from a Philips ADP3520 diffractometer using Cu $K\alpha_1$ and $K\alpha_2$ radiation. The samples were analyzed on zero-background quartz plates (obtained from Gem Dugout[17]) which had been sandblasted using a square template to create a depression for the samples.

Neutron Powder Diffraction Data

Six deuterated samples of the ATB of varying degrees of crystallinity, **3A-3F**, were prepared and powder neutron diffraction data sets were collected on the hexagonal bronzes using the HIPD (High Intensity Powder Diffractometer) at the LANSCE facility of Los Alamos National Laboratory. LANSCE uses a proton accelerator and synchrotron to produce high-energy neutrons by bombardment of a tungsten target. The neutrons are moderated to lower energies before they are used for diffraction by a filter containing heavy water. The HIPD is equipped with 10 time-off-flight detectors at angles of ± 153.4, ± 90.0, ± 39.8, ± 14.0
and ± 5 degrees. The time-of-flight data were collected on 4-5 gram samples

loaded into thin-walled quartz tubes at 300 K. **3A-3D** and **3F** were collected for 2 hours each while data for **3E** (representing the most crystalline ammonium bronze prepared from the tungsten imide) was collected for 12 hours.

Rietveld Refinement

The neutron data were fit to a hexagonal unit cell with lattice parameters: a = 7.3958(3), c = 7.5446(5). The high-resolution data obtained from the + 153.4° bank for **3E** were used in three separate Rietveld refinements. The diffractometer and Rietveld refinement procedures are found in Ref. 18-22. The first refinement covered the range from 0.3 Å to 2.273 Å. It was discovered that the data contained a broad peak at low d spacing which was difficult to fit when the background parameters are obtained by direct refinement, therefore a radial distribution (RD) function was determined from the + 153.4° data obtained for **3A** (the least crystalline sample) and selected coefficients of this RD function were used in the 12 variable background function for the refinement. The final result was a reasonable fit of the overall data (R_{wp} = 0.034, R_p = 0.025, χ^2 = 3.728) but the Bragg residual based on F^2_{obs}, R_b, was 0.214. The information for this report will not include the first refinement from 0.3 Å to 2.273 Å but contains two refinements covering the d space range 1.0 Å - 3.33 Å (to focus more on fitting the bragg intensities). The structural model used for

the Rietveld refinements was the hexagonal tungsten bronze of rubidium $Rb_{0.27}WO_3$[3] and refinements were made in the space groups $P6_3/mcm$ (no. 193) and $P6_322$ (no. 182) for Rietveld refinements 1 and 2 (RR1 and RR2), respectively. Atomic parameters are reported in Table III-1 and Table III-2 for refinements 1 and 2 respectively, while pertinent experimental data for refinement 1 and 2 are given in Table III-3. Selected bond distances and angles for refinement 1 are given in Table III-4. Neutron difference spectra from refinement 1 and 2 are reported in Figure III-9 and III-10 respectively.

Ammonium chloride was observed in the neutron diffraction data for 3E and was refined using the atomic parameters from reported crystallographic determinations of NH_4Cl.[23] The phase fraction variable for the ammonium chloride in 3E was refined to 0.18(7) but potentiometric chloride analyses determined a 2.26 % weight ratio. The ammonium cation in the hexagonal bronze channels was modeled as a rigid body in two orientations (Fig. III-11). In model I, one N-D vector is parallel to the c axis and the other three deuterium atoms lie on planes bisecting the crystallographic mirror planes. The 4 D atoms are disordered over 14 positions. Model II represents a precession of the cation about the c axis with the four D atoms disordered over 48 positions. Model II can be generated from model I by rotating model I 30° about $\vec{c}$ and then 30° about $\vec{a}$. The torsional angle about $\vec{c}$ was refined initially but the angle in those refinements increased to values over 3000 degrees and

Table III-1. Positional Parameters for $(NH_4)_{0.28}WO_3$ from Refinement #1 using Space Group $P6_3/mcm$ (no. 193)

atom	site	x	y	z	$100*U_{iso}$	Occup.
W	6g	0.4717(8)	0	0.25	.5(2)	1.0
O(1)	6f	0.5	0	0	[a]	1.0
O(2)	12j	0.4221(3)	0.2120(3)	0.25	1.6(2)	1.0
N(1)	2b	0	0	0	[a]	0.844
D(1)	24l	-0.041(1)	-0.080(3)	-.115(2)	7.6	0.070
D(2)	24l	0.0939(8)	-0.037(2)	0.0706(6)	7.6	0.070
D(3)	24l	0.0773(4)	0.1546(8)	-0.026(3)	7.6	0.070
D(4)	24l	-0.1300(9)	-0.37(2)	0.0706(6)	7.6	0.070

[a] O(2) and N(1) refined anisotropically:
O(2): U11 = 3.1; U22 = 0.6; U33 = 0.9; U12 = 0.3; U13 = 3.0; U23 = 0
N(1): U11 = 5.1; U22 = 5.1; U33 = 1.7; U12 = 2.6; U13 = 0; U23 = 0

Table III-2. Positional Parameters for $(NH_4)_{0.28}WO_3$ from Refinement #2 using Space Group $P6_322$ (no. 182)

atom	site	x	y	z	$100*U_{iso}$	Occup.
W	6g	0.4739(7)	0	0	1.4	1.0
O(1)	6h	0.4989(7)	-0.002(1)	0.25	1.7	1.0
O(2)	12i	0.4214(3)	0.2116(7)	0.0177(4)	2.1	1.0
N(1)	4e	0	0	0.234(3)	5.5	0.420
D(1)	12i	-0.0734(6)	-0.147(1)	-0.185(5)	10.0	0.21
D(2)	12i	0.1224(9)	0.021(2)	0.309(2)	10.0	0.21
D(3)	12i	0.052(1)	0.103(3)	0.132(2)	10.0	0.21
D(4)	12i	-0.1007(9)	0.022(2)	0.309(2)	10.0	0.21

Table III-3. Crystallographic and Experimental File Data for $(ND_4)_{.28}WO_3$,

Crystal system:	Hexagonal
Space group:	$P6_3/mcm$ (n. 193)
Volume of cell:	357.43 (3)Å^3
Form. units/cell:	6
d(calcd):	6.616 g/cm^3
Diffractometer:	HIPD
No. of data points:	3143
No. of reflections:	105
D space region:	1.0 Å ≤ d ≤ 3.3 Å

Histogram Refinement Parameters	Refinement 1. ($P6_3/mcm$; no. 193)	Refinement 2. ($P6_322$; no. 182)
a	7.3951(3)	7.3958(3)
c	7.5448(4)	7.5446(5)
Scale factor	7.6(4)	8.8(1)
Sig(1)[a]	216(9)	190(8)
Sig(2)[a]	16(2)	21(2)
Cation angle (X)	30(1)	69(1)
Absorption	-0.047(5)	-0.039(2)
R_p[b]	0.0549	0.0536
R_{wp}[c]	0.0386	0.0380
χ^2[d]	2.504	2.285

[a] Isotropic strain (σ1) and particle size (σ2) broadening of profile function.

$$^b R_p = \frac{\Sigma |I_{(obs)} - I_{(calc)}|}{\Sigma I_{(obs)}} \qquad ^c R_{wp} = \sqrt{\frac{\Sigma w [I_{(obs)} - I_{(calc)}]^2}{\Sigma [w I^2_{(obs)}]}}$$

$$^d \chi^2 = \frac{\Sigma w |I_{(obs)} - I_{(calc)}|^2}{(N_{(obs)} - N_{(var)})}$$

$N_{(obs)}$ = number of independent observations, $N_{(var)}$ = number of refined parameters, I = integrated Bragg intensities, w = weights.

Table III-4. Interatomic Bond Distances (Å) and Selected Angles for $(ND_4)_{.28}WO_3$, from Refinement 1

W(1) - O(1)	1.8976(6)	O(1) - W(1) - O(1)	167.45(30)
W(1) - O(2)	1.780(4)	O(1) - W(1) - O(2)	94.06(9)
W(1) - O(2)	2.061(5)	O(1) - W(1) - O(2)	85.25(12)
O(1) - N(1)	3.69757(16)	O(2) - W(1) - O(2)	89.55(12)
O(2) - N(1)	3.29262(11)	O(2) - W(1) - O(2)	171.11(21)

caused the refinements to diverge, indicating that the ammonium cation was spinning around the c axis. The angle about $\vec{a}$ (i.e, the angle between a N-D vector and the c axis in the $\vec{c}\vec{b}$ plane) was allowed to vary in the refinement and in each refinement the angle converged to values between 27 and 33 degrees from the c axis.

There was no significant indication of reflections that violated extinction conditions of the c glide operation ($hoh\bar{l}$ reflections absent), although there was a small peak corresponding to the $(10\bar{1}3)$ reflection (d = 2.296 Å), not accounted for in refinement 1.

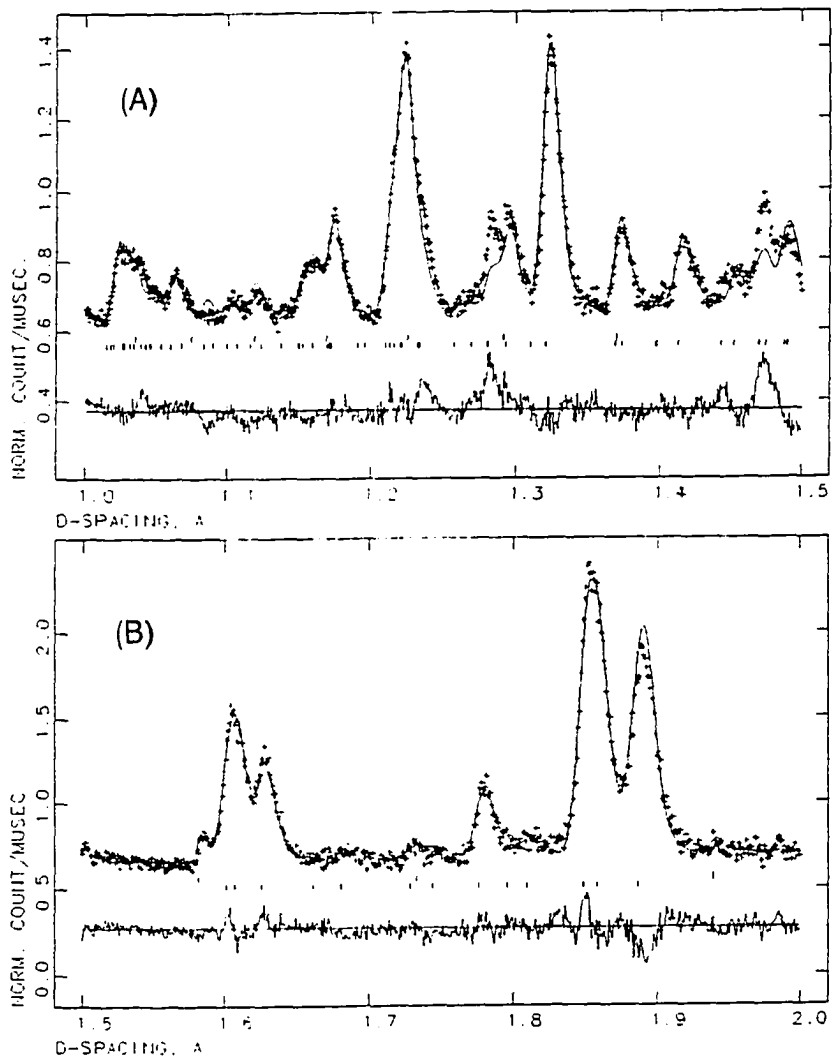

Figure III-9. Plot of the neutron experimental data (+), calculated spectra (line through the experimental points) and the difference curve at the bottom of the graph for refinement 1 ($P6_3/mcm$) of hexagonal ammonium bronze (3E) made from nitrogenated reactants

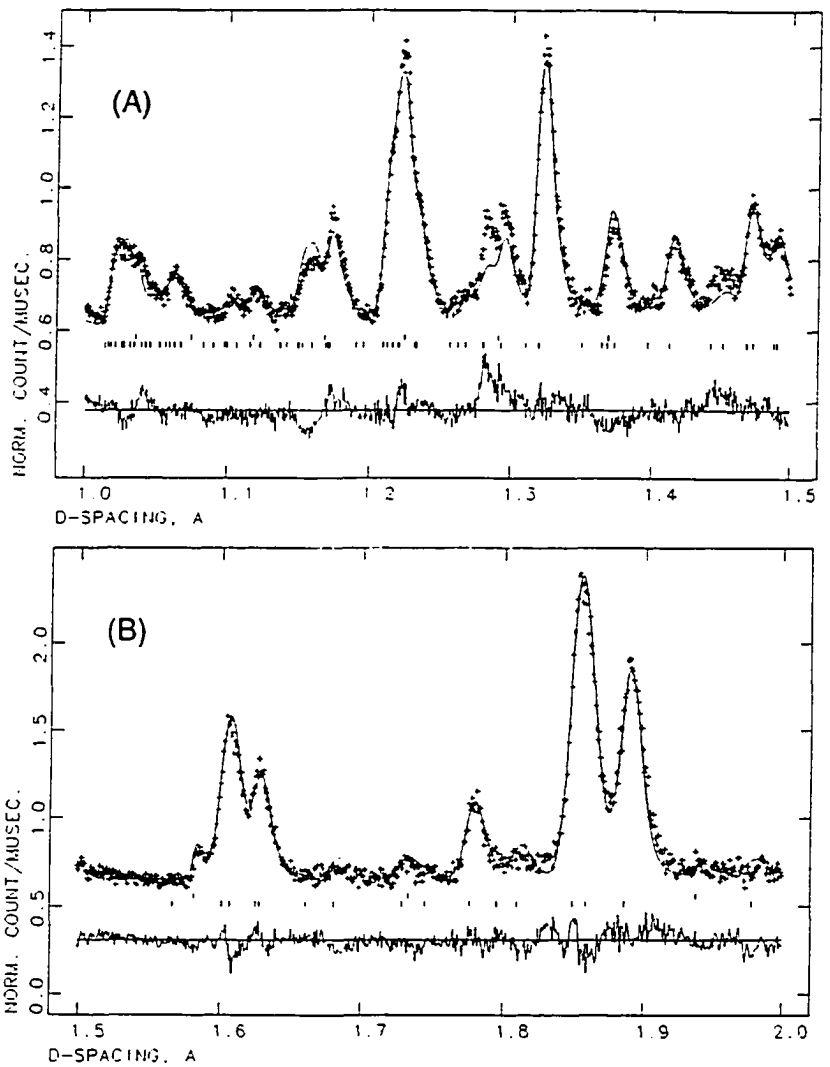

Figure III-10. Plot of the neutron experimental data (+), calculated spectra (line through the experimental points) and the difference curve at the bottom of the graph for refinement 2 ($P6_322$) of the crystalline hexagonal ammonium bronze (3E) made from nitrogenated reactants

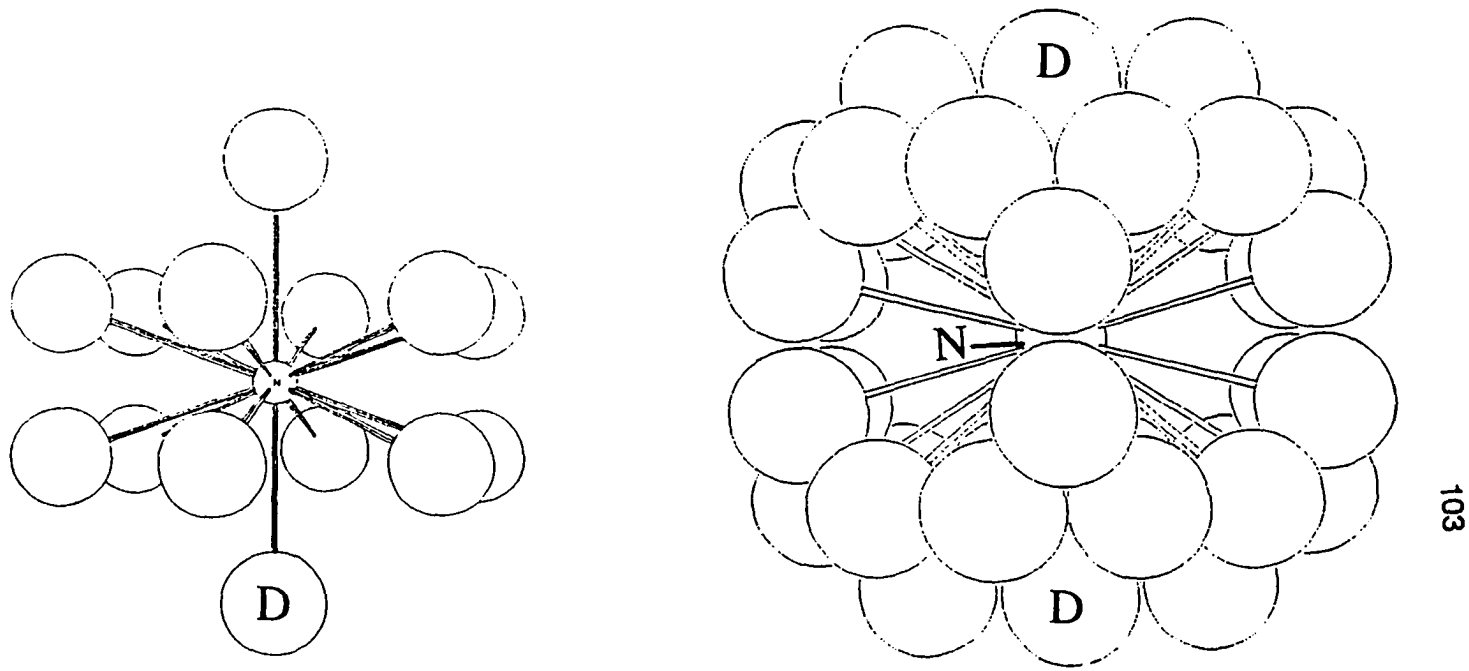

Model I *Model II*

Figure III-11. Model I: Ortep drawing of ammonium cations in which the vertical N-D vector is parallel to c and the four D atoms are disordered over 14 positions. Model II: Ortep drawing of an ammonium cation model representing precession about the c axis at an angle of 30°. The four D atoms are disordered over 48 positions. Model II represents the best fit for the Rietveld refinement

RESULTS AND DISCUSSION

Synthesis of ATB with Nitrogenated and Oxygenated Reactants

The conversion of $WNCl_3$ to crystalline ATB is illustrated in Figure III-12. The initial low-temperature ammonolysis of $W(N)Cl_3$ produces tungsten (VI) (see reaction 2). Subsequently, the tungsten is reduced to an average oxidation state of 5.72 (based on a 0.28 NH_4Cl:W ratio) during the ammonolysis and hydrolysis at elevated temperatures (see reactions 3 and 4) to yield crystalline ATB. After the hydrolysis of the tungsten imide (reaction 3), the sealed reaction tubes explode when opened and evolve ammonia gas. Based on this, water appears to react metathetically with the imide in reaction 3 to form the oxide and liberate ammonia. This observation is consistent with the higher affinity of tungsten for oxygen relative to nitrogen.

Based on both the conventional and this new synthetic approach to the ammonium bronze, it appears that four conditions are necessary for the production of the bronze. First, there must be a source of tungsten in an oxidation state near +6 due to the inherently reducing atmospheres used in the syntheses (NH_3, H_2O and H_2). Second, there must be a source of oxygen, either as part of the metal or a secondary reactant. Third, nitrogen must be present in the -3 oxidation state and converted ultimately to ammonium.

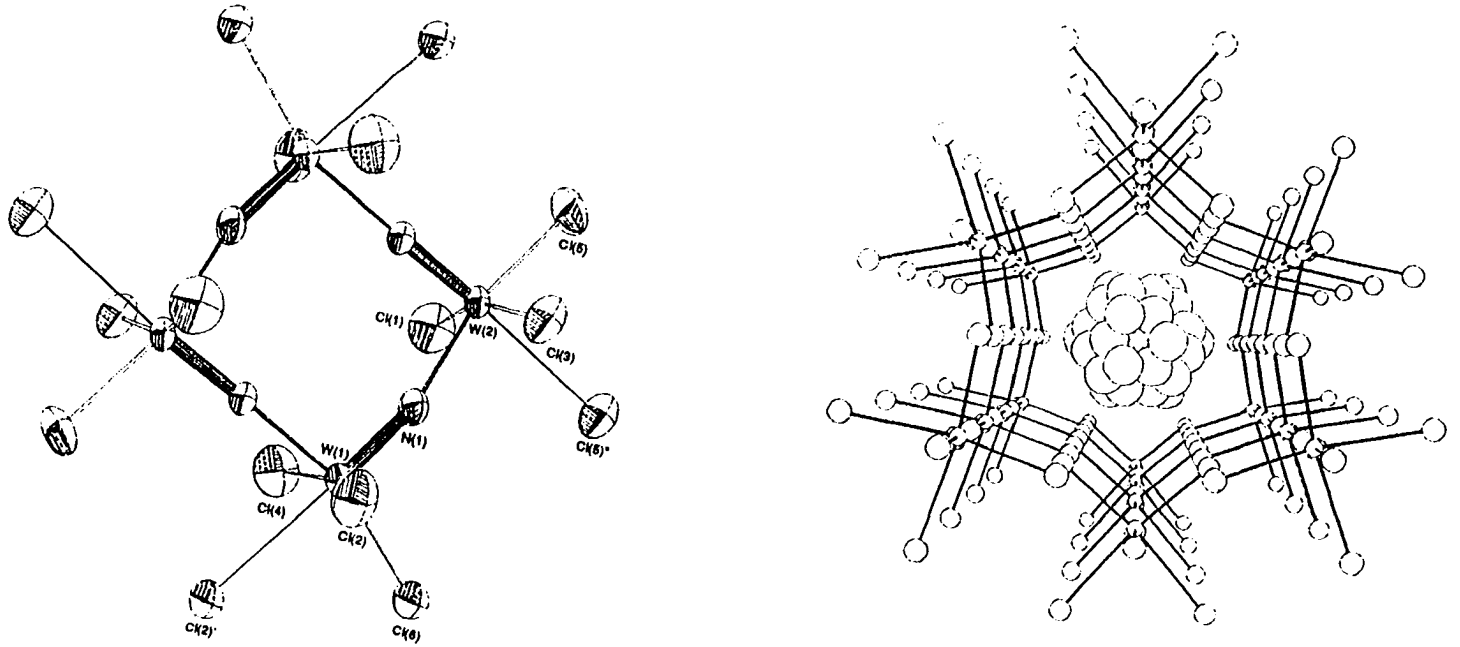

(A) $\xrightarrow[-40°C]{NH_3(l)}$ $\xrightarrow[340\text{-}380°C]{NH_3(g)}$ $\xrightarrow[380°C]{3H_2O(g)}$ (B)

Figure III-12. Illustration and reactions showing the conversion of $WNCl_3$ (A) to $(NH_4)_{.28}WO_3$ (B). The bronze is shown with the model II cation occupying 0,0,0 positions within the hexagonal channels

Fourth, any compounds containing elements other than W, O or N, must be removable from the product, either by vaporization or washing and filtration technique. Preceding the synthesis of (2C), yellow WO_3 (anhydrous) was reacted in flowing ammonia at 400 °C for 3 days and yielded, according to the X-ray powder pattern (Fig. III-13), a blue tungsten oxide of unknown composition and structure. It has been shown that tungsten trioxide can be converted into the subnitride W_2N[24]. In contrast to these results, the dihydrate of WO_3 was reacted in flowing ammonia to produce a product (2C) whose X-ray powder spectrum matched the hexagonal bronze phase (Fig. III-5) although the peaks were much broader due to particle size broadening. Subsequent annealing of (2C) for 5 days in 2/3 atm of ammonia at 380 °C did not change the peak widths in the X-ray spectrum. This indicates that the fundamental anionic tungsten-oxygen hexagonal framework is being formed on a submicron level but due to a shortage of cations in the reaction, further grain growth does not occur.

Rietveld Refinement and Structure of Crystalline ATB (3E)

Although single crystal diffraction studies have not been accomplished on the ATB, a detailed study of the structural analog $K_{0.26}WO_3$ using neutron and X-ray single crystal diffraction techniques was recently accomplished by Schultz

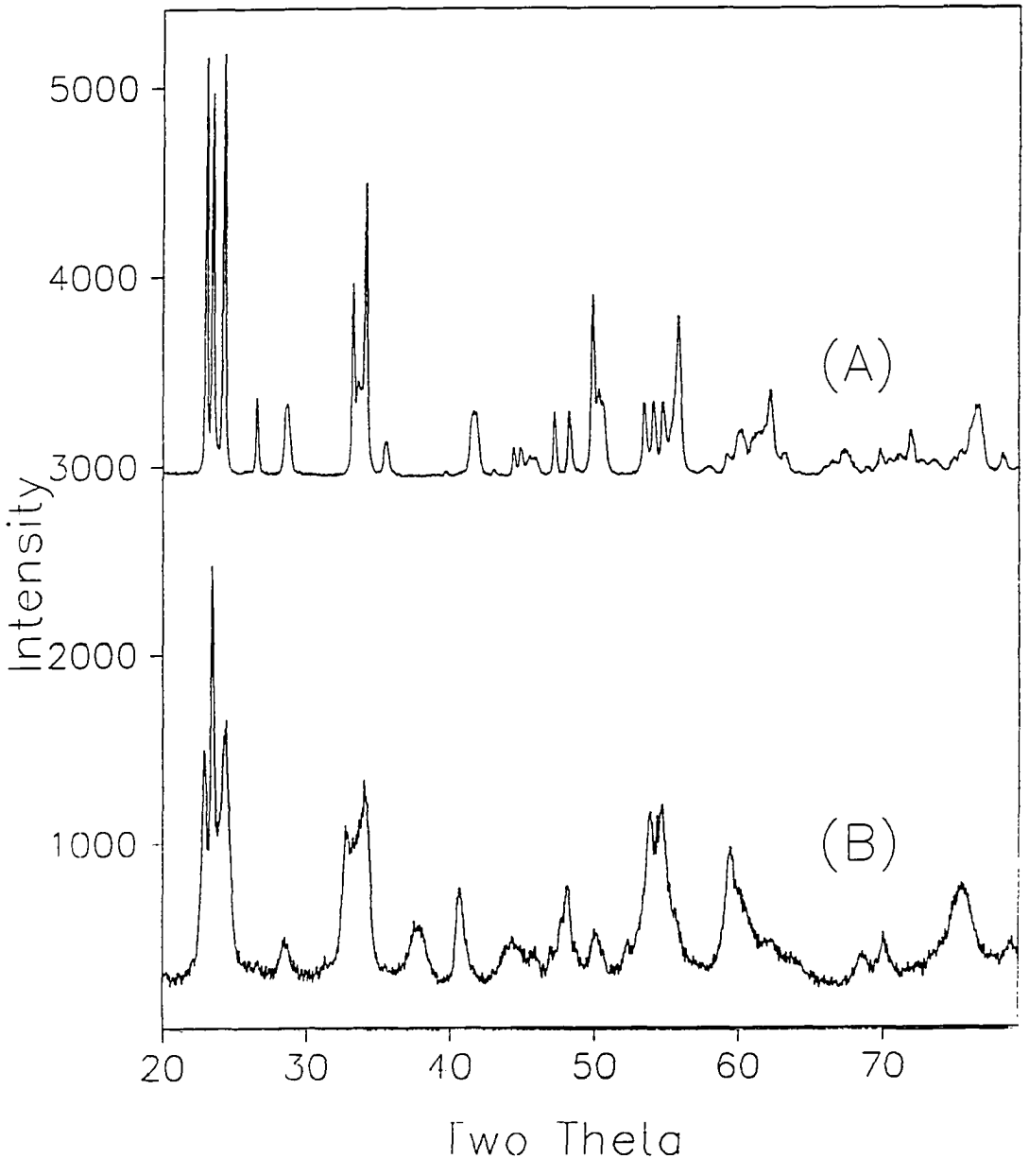

Figure III-13. X-ray powder diffraction pattern of anhydrous WO_3 (A) and corresponding pattern of the product resulting from the reaction of anhydrous WO_3 and flowing ammonia at 400 °C for 4 days (B)

and coworkers[25]. They reported a very complicated superstructuring involving the cations which they modeled with the $P6_3$ space group and used only the l-even reflections because of the poor correlation with l-odd reflection intensities. Pye and Dickens[26] reported the single crystal X-ray solution for $Rb_{0.27}WO_3$, solved in the space group $P6_322$, instead of $P6_3/mcm$ reported by Magneli,[3] because of c glide extinction violations observed in neutron diffraction data.

The bronze in this work was refined initially in the space group $P6_3/mcm$ (refinement 1) because the only noticeable extinction violation for the c glide was a very small peak at 2.296 Å corresponding to the $10\bar{1}3$ reflection. A refinement in the space group $P6_322$ (refinement 2) that was attempted subsequently showed an improvement in certain parts of the refinement. Because of the differing space groups, the atomic coordinates are not comparable. The utility of using the lower symmetry space group is that it allows for the oxygen position to vary from z = 0 and fit more closely the puckered W-O rings found in single crystal studies of the hexagonal bronze, as well as providing an additional degree of freedom for the position of N along z (see Table III-1 and Table III-2). Although the isotropic temperature factors are closer to conventional values in RR2, RR1 allowed for refinement of anisotropic temperature factors for all non-deuterium atoms (although W and O(2) refined to negative U values) with convergence whereas RR2 diverged when any non-nitrogen temperature factor was refined anisotropically. Only N and O(1) from

RR1 gave non-negative anisotropic temperature values; therefore N and O(1) were the only atoms in the two refinements with refined anisotropic factors. RR2 gave a slightly better fit (with only 22 parameters refined) of the intensity data with R_{wp}, R_p and χ values of 0.0536, 0.038 and 2.285 respectively compared to 0.0549 0.0386 and 2.504 for RR1 (with 26 parameters refined). Part of the reason for this improvement can be seen in a comparison of the Bragg R factors listed in hkl classes based on F^2_{obs} for the two refinements in Table III-5. The most obvious improvements of RR2 relative to RR1 are seen in classes -EO, OEO and EEO, in fact, most of the l = odd classes show an lower R factor for RR2.

Nitrogen substitution

This synthesis attempts to optimize the possibility of imido substitution for oxygen in the bronze. From Kjeldahl analyses of nitrogen in the bronze, y is 0.06 in the formulation $(NH_4)_{.28}WO_{3-y}(NH)_y$. In the XPS spectrum (Fig. III-14) for **3A** and **3E**, two distinct types of nitrogen were observed. In the ammonium bronze (A), the N-1s peaks correspond to a small amount of metal bound nitrogen and a large percentage of ammonium nitrogen, while the XPS data for the tungsten imide (B), identifies primarily metal bound nitrogen. In contrast to the **3E** spectrum, the XPS spectrum of ATB made from conventional

Table III-5. Comparison of Bragg Residuals Based on Selected hkl Classes for Refinement # 1 and Refinement # 2 using Space Groups 193 and 182

	$P6_3/mcm$ (no.193)			$P6_322$ (no. 182)		
hkl class	Count[a]	F^2_{obs}	R	Count[a]	F^2_{obs}	R
- - -	82	114	0.103	98	96	0.106
E - -	40	162	0.062	48	133	0.083
O - -	42	69	0.195	50	60	0.154
- E -	42	187	0.090	58	137	0.093
- O -	40	38	0.172	40	38	0.173
- - E	55	165	0.096	55	162	0.099
- - O	27	10	0.324	43	13	0.221
E E -	24	252	0.054	32	187	0.078
E O -	16	26	0.178	16	27	0.155
O E -	18	99	0.211	26	75	0.139
O O -	24	46	0.170	24	45	0.180
E - E	28	229	0.058	28	223	0.077
E - O	12	5	0.464	20	8	0.321
O - E	27	99	0.188	27	98	0.150
O - O	15	14	0.282	23	18	0.183
- E E	33	237	0.089	33	230	0.091
- E O	9	2	0.435	25	14	0.151
- O E	22	58	0.143	22	59	0.146
- O O	18	14	0.316	18	12	0.338

Table III-4 continued:

(no.193)		$P6_3/mcm$		$P6_322$ (no. 182)		
hkl class	Count	F^2_{obs}	R^*	Count	F^2_{obs}	R^*
E E E	19	319	0.054	19	309	0.0739
E E O	5	0.136	0.689	13	7	0.331
E O E	9	39	0.125	9	40	0.129
E O O	7	9	0.461	7	9	0.306
O E E	14	126	0.209	14	122	0.148
O E O	4	5	0.426	12	21	0.084
O O E	13	71	0.149	13	72	0.153
O O O	11	18	0.268	11	14	0.35
L = 3N	33	116	0.139	38	97	0.122
L=3N+1	26	155	0.073	33	120	0.090
L=3N+2	23	67	0.092	27	67	0.108
H H L	23	167	0.083	23	166	0.106

[a] Refers to the number of reflections used in calculations.

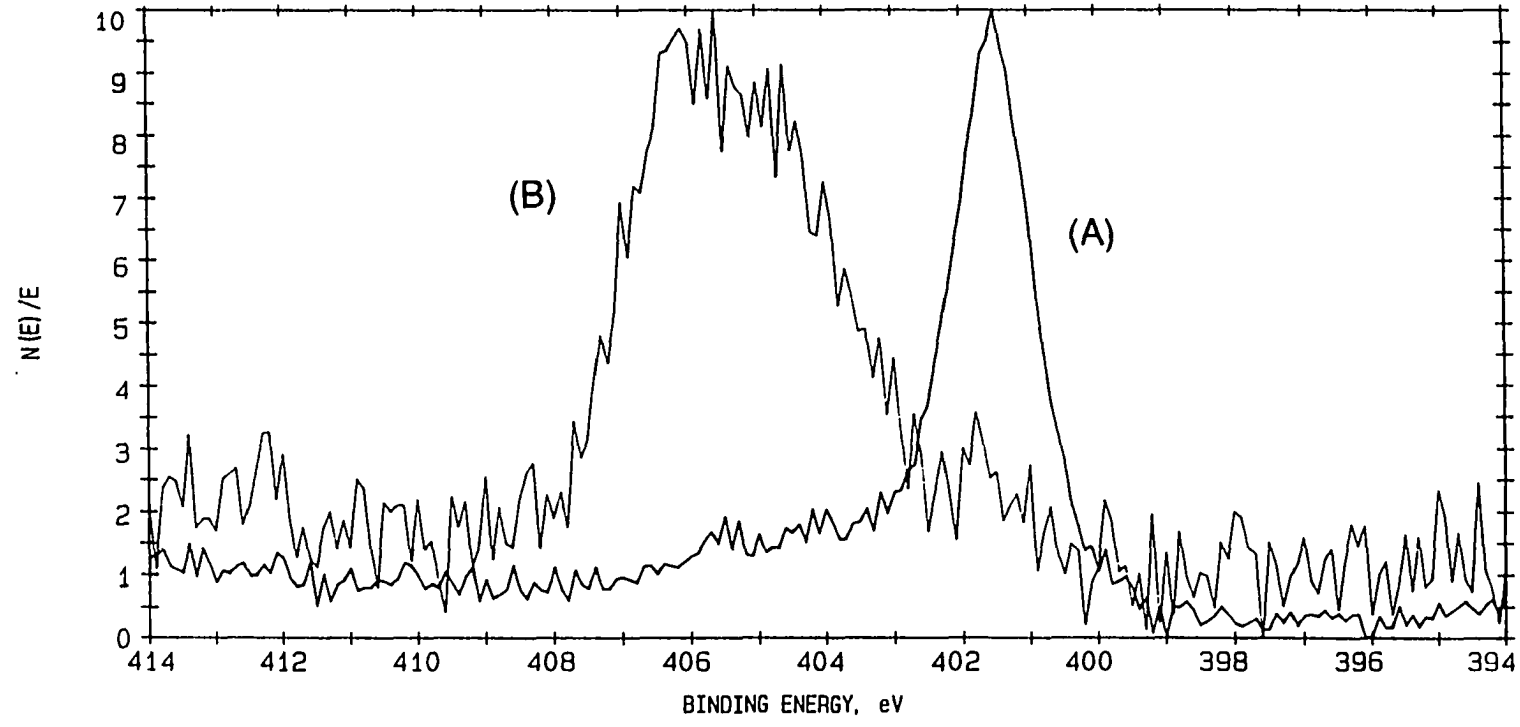

Figure III-14. XPS spectra of the N-1s emission from $W(NH)_{2.5}Cl_x$ (A) and the crystalline tungsten bronze (B). The tungsten imide has mostly metal-bound nitrogen while the bronze has mostly ammonium nitrogen. There is a small shoulder on the bronze peak which indicates that there is a small amount of metal-bound nitrogen present in the bronze

ammonium paratungstate identifies only the ammonium nitrogen. The result that there was excess nitrogen in **3E** and that, according to the XPS spectra, there was a small amount of metal-bound nitrogen present in the system provided the stimulus for the neutron study. The extent of nitrogen substitution was determined by allowing the fraction of nitrogen to be related inversely to that of oxygen in the final phase of refinement 1. The resulting substitution gave a refined nitrogen occupancy of 0.0074 and 0.0013 corresponding to O(1) and O(2) respectively, which translates to a y value of 0.01, which is within the error of the experiment. Unreacted amorphous tungsten imido impurities in the bronze phase appear to account for the excess nitrogen found by Kjeldahl analyses, the metal-bound nitrogen seen in the XPS spectra, the undulating baseline in the neutron powder spectra and the low level of nitrogen substitution for oxygen from the Rietveld refinement. It has also been observed that there is an inverse correlation between crystallinity and nitrogen percentage. Crystallization of the bronze from the imide requires an oxygen source, such as water. Without an oxygen source, temperature, ammonia pressure and time variations have not been shown to induce crystallization in the amorphous tungsten imide. This is a strong indication that imido substitution has not occurred in the oxide bronze and that imide will not readily substitute for oxide in this bronze system.

Cation model

Temperature dependent ^{1}H NMR studies of the ATB[27] have concluded that motion of the ammonium cation is due to rearrangement, localized hopping of the cations along the c axis and dissociative proton diffusion at room temperature. In order to model the cation three orientation models for the bronze were developed, of which, two allowed for temperature factor refinement of the D atoms (Fig. III-11) without divergence. Model II produced the lowest residuals in bronze RR1 and yielded reasonable temperature factors for D. More significantly, the center area of the neutron difference map for the refinement using model II in Figure III-15 shows zero neutron density for space corresponding to the D atom 1.1 Å away from N(1) along [001], while the neutron difference map for the refinement of the bronze containing model I showed negative neutron density at the same location. In RR2, the orientation angle of the cation refined to 69° which substantiates the precession model. The observation that there is no D along the c axis is reasonable when the interactions between the ammonium deuterium and the oxygen atoms forming the hexagonal channel are considered. The distances from the nitrogen at 0,0,0 to the apical and basal oxygens of the tungsten-oxygen octahedra are 3.69757(16) Å and 3.29262(11) Å, respectively. Based on van der Waals radii for H and O, the van der Waals distance for the N-D···O vector is 3.70 Å while

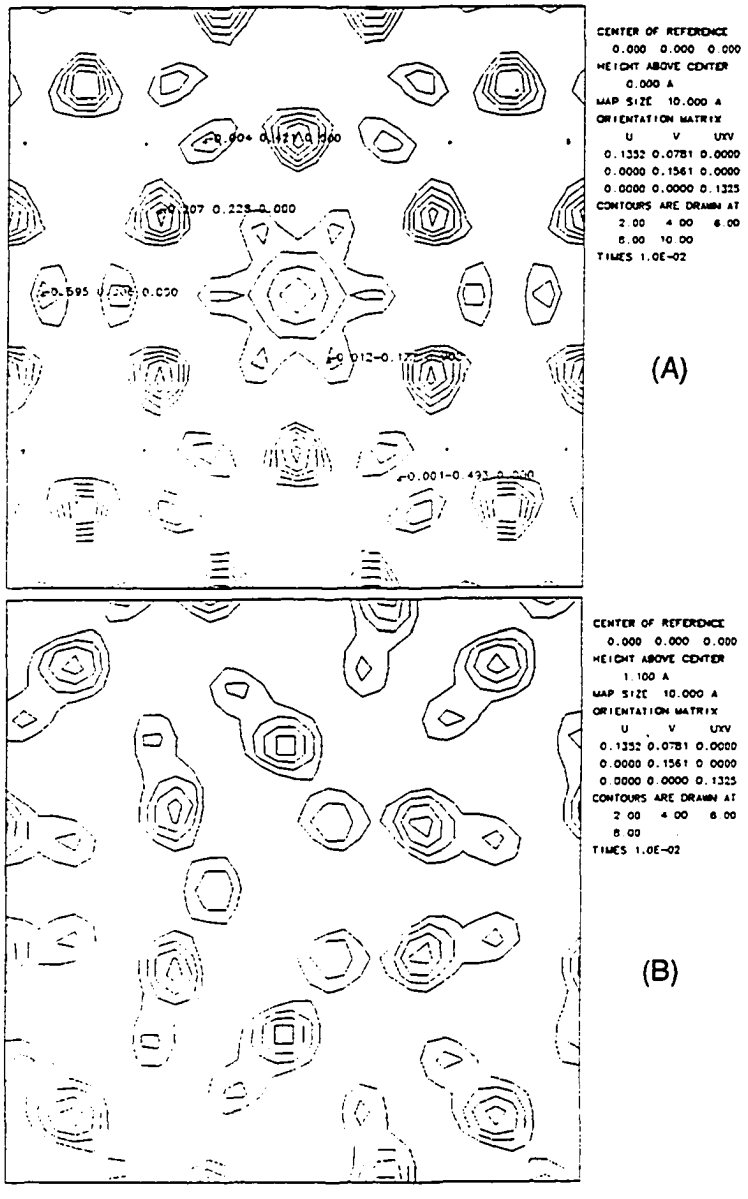

Figure III-15. Neutron scattering density difference maps for refinement 1, using the precession cation model I, illustrating the region of space parallel to the a b plane. The center of (A) is the 0,0,0 N position while the center of (B) defines the theoretical location of D if model II were used. Zero neutron scattering density at the center of (B) supports the precession model I over model II with D along the z axis

the hydrogen bonding distance for the same vector is 2.90 Å. Based on these distances there is certainly some interaction between D and the basal oxygen atoms and a slight interaction with the apical oxygen atoms. Because of this stabilizing interaction, it appears to be more favorable for all four deuterium atoms to be directed toward the oxygen atoms than three as shown in model I. A slight amount of excess neutron density was detected in the difference map at 0,0,0.25. When N was placed in this position and allowed to refine inversely with the N at 0,0,0, the amount present at 0,0,0.25 refined to 1 percent of the total N, which indicates that essentially all of the N is located at 0,0,0 in refinement 1.

Physical Properties

Solid state ^{1}H NMR spectra were obtained on static samples of the bronze material prepared from scheme I at three levels of crystallinity (Fig. III-16). As the bronze material, **2A**, becomes more crystalline the full-width at half-height (FWHH) dimension narrowed, which indicated that the ^{1}H NMR active protons were in varying environments. There appear to be at least two proton environments contributing to the peak shape for the amorphous bronze NMR spectrum. The peak shape for the amorphous material can be understood in terms of a superposition of a relatively narrow resonance (arising from the

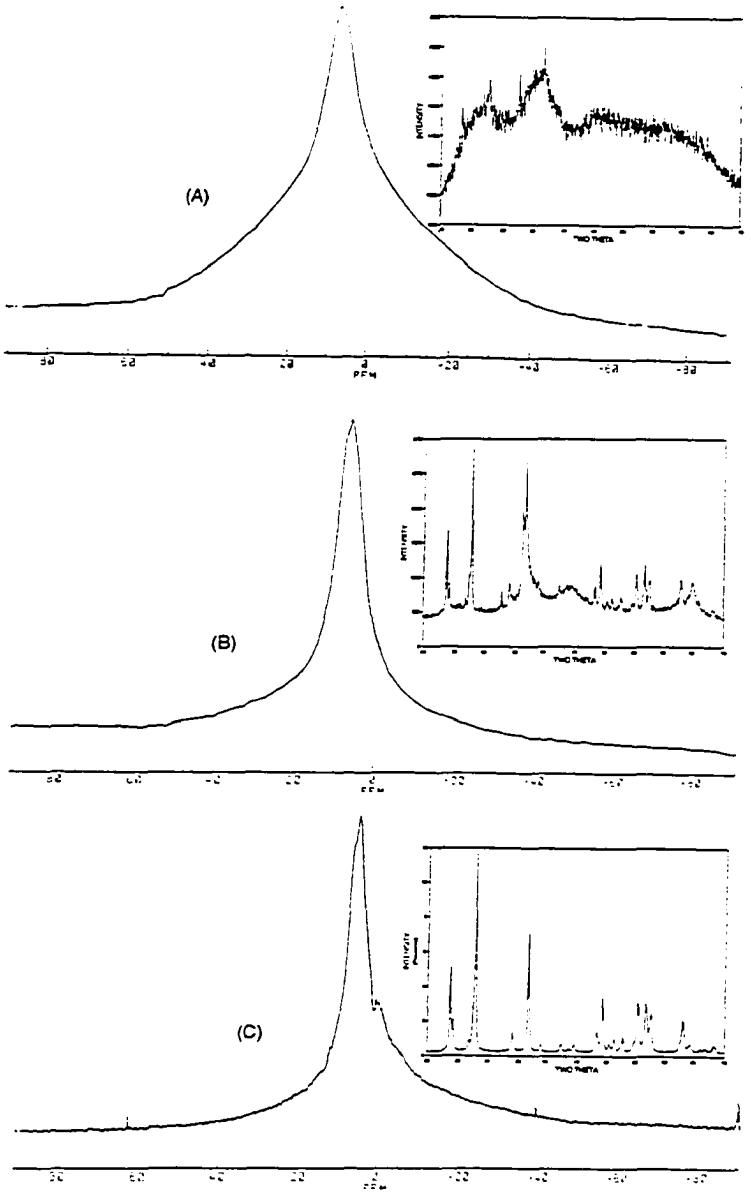

Figure III-16. Solid state ^{1}H NMR spectra correlation with X-ray diffraction patterns for amorphous tungsten imide (A), a tungsten bronze phase of intermediate crystallinity (B) and crystalline ATB (C). The width of the spectral peak decreases with increasing crystallinity, reflecting a higher percentage of mobile ammonium protons

ammonium in the system) and a broadened peak (due to the limited mobility of the imido hydrogens). As the material becomes more crystalline the imido groups are replaced with oxide, thereby decreasing the number of low mobility protons in the system. The crystalline material (C in Fig. II-16) then, has very few imido protons (as substantiated by XPS in Fig. III-14) resulting in a peak width essentially reflecting only the mobile ammonium protons.

Three separate electrical resistivity studies were accomplished on annealed pressed pellets of the ATB made from $WNCl_3$. In each case, the electrical resistance decreased with increasing temperature (see Fig. III-17), in contrast to a study which determined ATB to possess temperature dependent metallic properties.[3] The resistivity of **3E** at 293 K was 6×10^{-2} ohm-cm which is comparable to the results of powder experiments on $K_{0.27}WO_3$ (5×10^{-2}) and $Rb_{0.29}WO_3$ (3×10^{-2}).[3] Based on the electrical resistivity data (Fig. III-18), **3E** appears to be a low band gap semiconductor (E_a = 4.76 mev) that goes through a semiconductor/metal transition near room temperature. Impurities at the grain boundaries could also lower the conductivity to that of a semiconductor. Based on the metallic conductivity of other hexagonal tungsten bronze compounds, it is likely that the apparent semiconducting behavior in this ammonium bronze is due to impurities at the grain boundaries.

The magnetic susceptibility of the crystalline bronze (**2A**) was measured at 1 Tesla over the range 6 K to 296 K (Fig. III-19). The material was found to

be diamagnetic with a paramagnetic impurity accounting for the sharp increase in susceptibility at low temperatures.

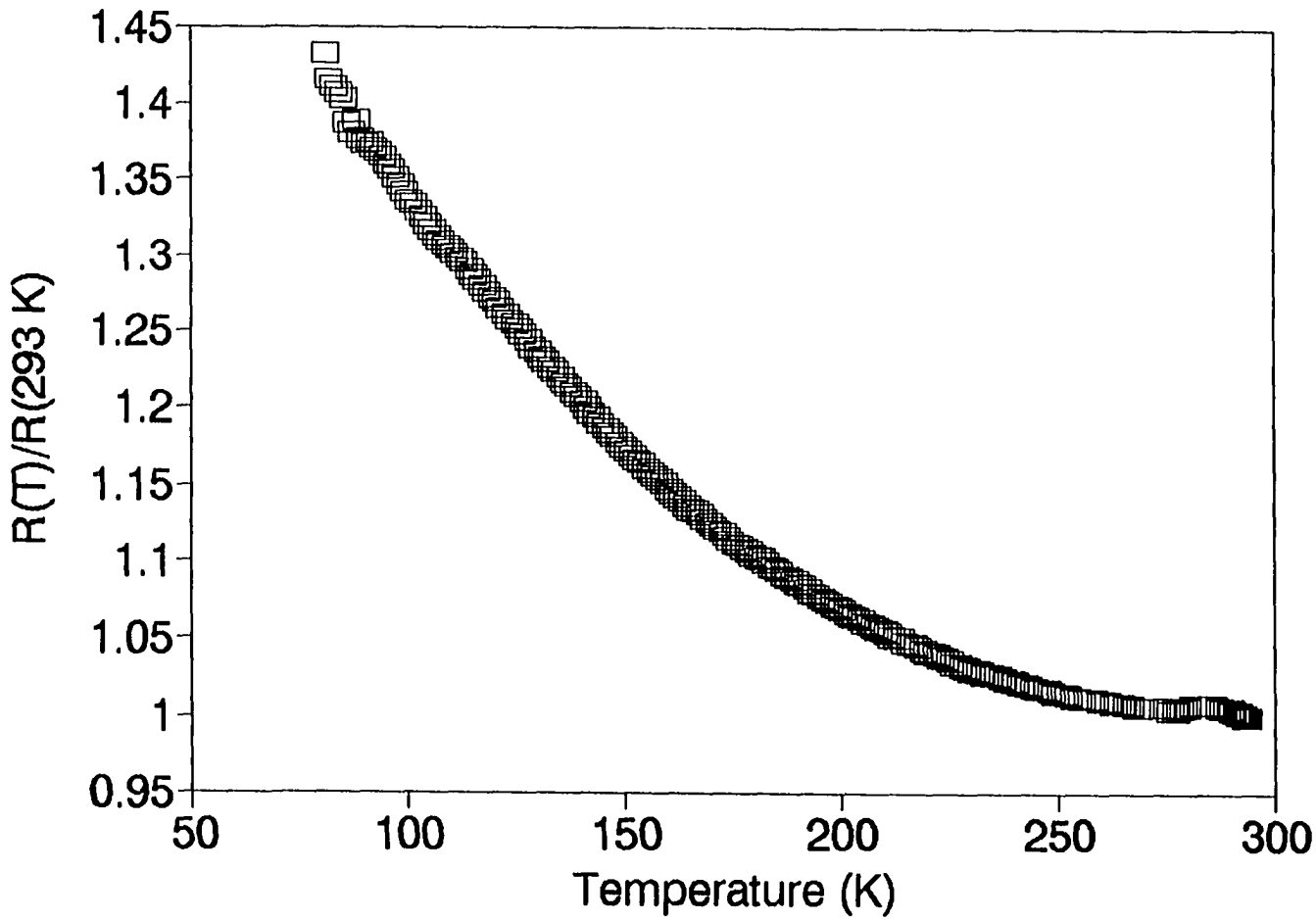

Figure III-17. Temperature dependent electrical resistivity measurement of ATB. The measurements were conducted using a four probe DC technique on pressed pellets, annealed in 2/3 atm. of ammonia at 400 °C for 5 days

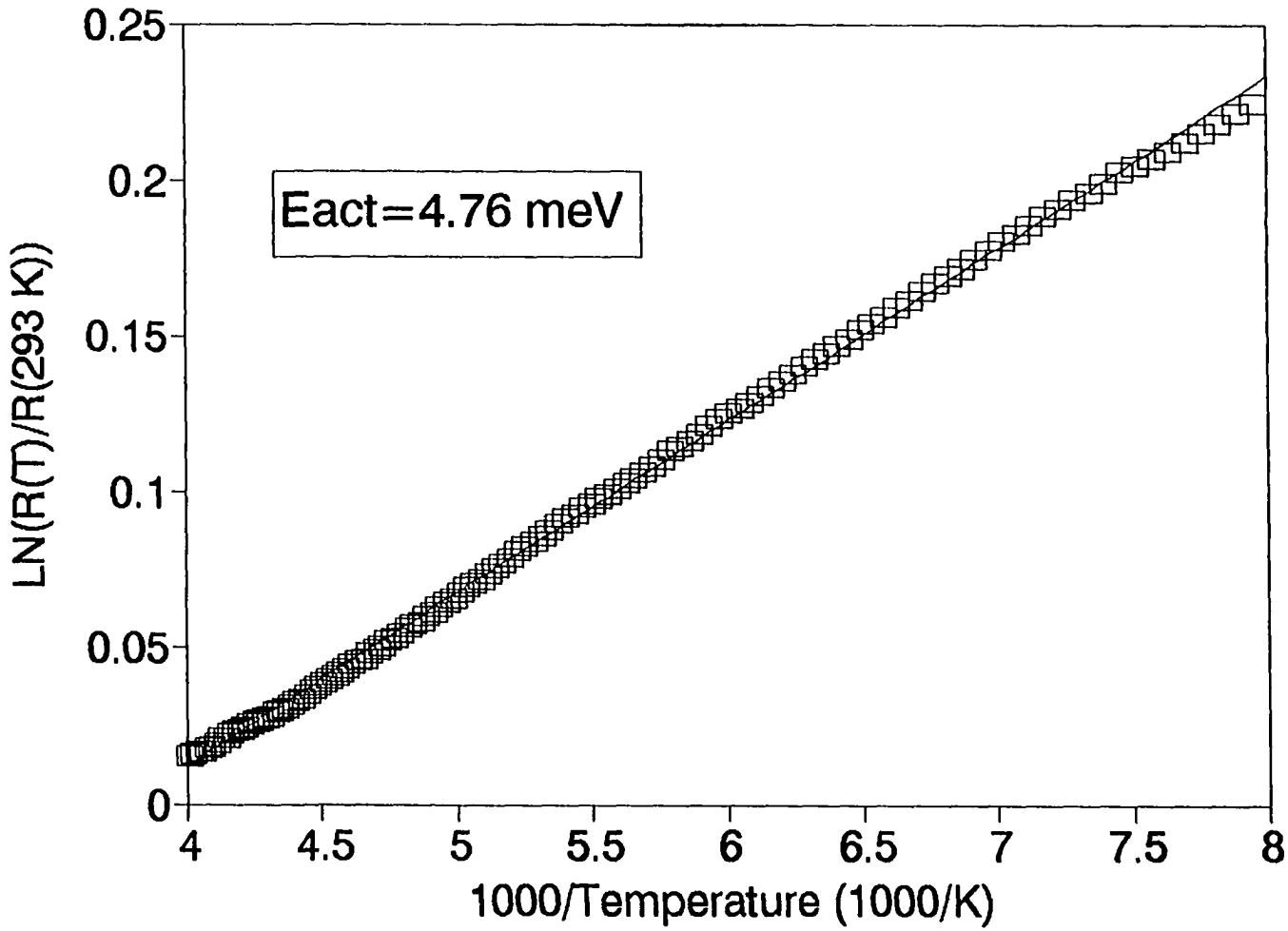

Figure III-18. $Ln((R_T)/R_{293\ K}))$ vs. (1/T) x 1000 plot for **3E** over the temperature range 250 - 125 K

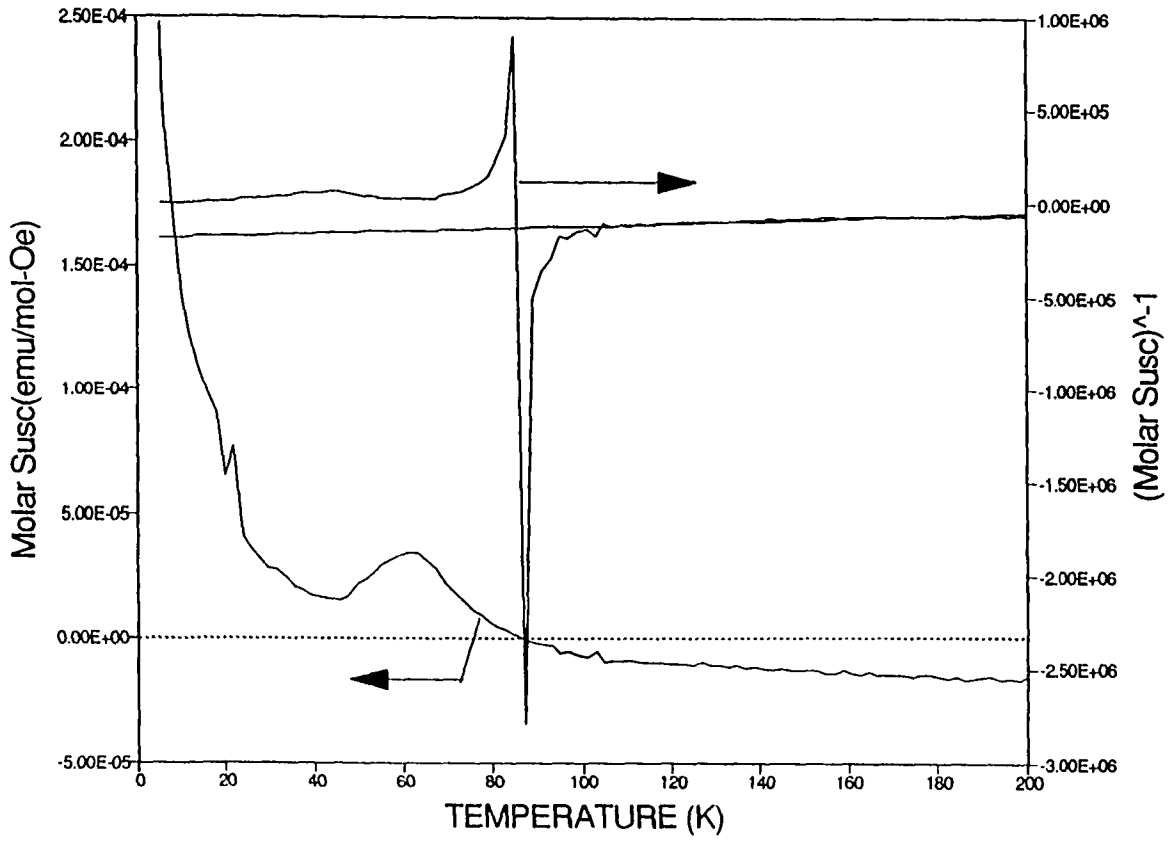

Figure III-19. Magnetic susceptibility vs. temperature plot for crystalline ATB (2A). The peak in the molar susceptibility curve at 60 K is due to paramagnetic dioxygen. The reciprocal molar susceptibility plot identifies the bronze as diamagnetic with paramagnetic impurities accounting for the increase in susceptibility at low temperature

CONCLUSION

Two new routes to the hexagonal bronze phase have been discovered. By the use of oxygenated reactants, $WO_3 \cdot 2H_2O$ can be converted to the hexagonal bronze phase by reaction with flowing ammonia at 380 °C. More unique, is the new synthesis in which nitrogenated reactants have been used for the first time to synthesize an ammonium tungsten bronze $(NH_4)_{0.28}WO_3$. This pathway significantly improves the probability of imido substitution for oxygen in the anionic W-O lattice. The model for the ATB obtained from the Rietveld refinement of neutron powder diffraction data, XPS spectra of the bronze and the undulating background in the neutron data indicate strongly that nitrogen, in the form of imide, does not substitute to a measurable degree for oxygen in the anionic lattice of ATB. Space group $P6_322$ more closely models the Bragg and histogram intensities relative to $P6_3/mcm$. A c glide does not appear to be present in this structure, consistent with other structural studies of hexagonal bronzes. Over 99 percent of the ammonium nitrogen resides at 0,0,0 while a small amount (<1 percent) is found disordered at 0,0,0.25. The N-D vectors of the ammonium cation are directed toward the oxygen atoms forming the hexagonal channels and not along [001]. A precession model of the ammonium cation, Model II, represents the best fit to the Rietveld refinement of the three orientations tested.

REFERENCES

1. Kienzle, W. E. Ph.D Dissertation, Iowa State University, **1973.**

2. Ranninger, J; Sinha, K.P. *Proc. Indian. Acad. Sci (Chem. Sci.)*, **1985**, 95, 101.

3. Magneli, A. *Acta Chem. Scand.* **1953**, 7, 315.

4. Whittingham, M.S.; Huggins, R.A. *J. Chem. Phys.* **1971**, 54, 414.

5. Dickens, P.G.; Whittingham, M.S. *Quart. Rev. Chem. Soc.* **1968**, 22, 30.

6. Hagenmuller, P. *Progr. Solid State Chem.* **1971**, 5, 71.

7. Kihlborg, L; Sharma, R. *J. Microsc. Spectrosc. Electron.* **1982**, 7, 387

8. Kihlborg, L. in *Solid State Chemistry, Preoceedings of the Second European Conference,* Veldhoven, The Netherlands, 7-9 June 1982.

9. Volkov, V.L. *Inorg. Mat.* **1990**, 26, 101.

10. Reis, K. P.; Prince, E.; Whittingham, M. S. *Chem. Mater.* **1992**, 4, 307.

11 Goodenough, J. B. *J. Appl. Phys.* **1966**, 37, 1415

12. Wertheim, G. K.; Campagna, M.; Chazalviel, J.-N.; Buchanan, D. N. E.; Shanks, H. R. *Appl. Phys.* **1977**, 13, 225

13. Carlson, C. D. Ph.D Dissertation, Iowa State University, **1990.**

14. Schumb, W. C.; Hartford, W. H.; *J. Am. Chem. Soc.*, **1934**, 56, 2613.

15. Bremner, J. M.; Mulvaney, C. S. *Methods of Soil Analysis, Part 2. Chemical and Microbiological Properties - Agronomy Monograph no. 9* 1982, 595.

16. Van der Pauw, L. J. *Phillips Research Reports*, **1958**, 13, 1.

17. Gem Dugout, c/o Deane Smith, 1652 Princeton Dr., State College, PA 16803

18. Rietveld, H. M. *J. Appl. Crystallogr.* **1969**, 2, 65.

19. Larson, A. C.; Von Dreele, R. B. *GSAS (General Structural Analysis System)*, Los Alamos National Laboratory, Los Alamos, NM.

20. Von Dreele, R. B.; Jorgensen, J. D.; Windsor, C. G. *J. Appl. Crystallogr.* **1982**, 15, 581.

21. Jorgensen, J. D.; Rotella, F. J. *J. Appl. Crystallogr.* **1982**, 15, 2.

22. Howard, S. A.; Preston, K. D.; Post, J. E.; Bish, D. L.; Finger, L. W.; Von Dreele, R. B. *Rev. Mineral. (Modern Powder Diffraction)*, **1989**, 20, 217-367.

23. Levy, H. A.; Peterson, S. W. *Phys. Rev.* **1952**, 86(5), 766

24. Volpe, L.; Boudart, M. *J. Solid State Chem.* **1985**, 59, 332

25. Schultz, A. J.; Horiuchi, H.; Kraise, H. B. *Acta Cryst.* **1986**, C42, 641

26. Pye, M. F.; Dickens, P. G. *Mater, Res. Bull.* **1979**, 14, 1397.

27. (a) Clark, L. D.; Whittingham, M. S.; Huggins, R. A. *J. Solid State Chem.* **1972**, 5, 487 13. (b) Slade, R.C.T.; Dickens, P.G.; Claridge, D.A.; Murphy, D.J.; Halstead, T.K. *Solid St. Ion.* **1990**, 38, 201.

SECTION IV. SYNTHESIS AND CHARACTERIZATION OF MOLYBDENUM AZIDO COMPOUNDS AND THEIR THERMOLYTIC DECOMPOSITION TO YIELD MOLYBDENUM NITRIDES

INTRODUCTION

Much of the work in molecular nitrido molybdenum compounds has been motivated by the discovery of the iron-molybdenum cofactor in nitrogenase[1]. The utility of converting molecular nitrogen into ammonia has far reaching economic significance. Perhaps the most investigated solid state molybdenum nitride is the cubic compound MoN (B1 structure type) which was initially predicted to be a high temperature superconductor[2]. Experimental results[3] have shown that the B1 phase of MoN has a T_c as high as 14.9 K or as low as 3 K, depending on the method of preparation. Attempts have been made to convert the hexagonal δ-MoN to B1 MoN (1800 K and 6 Gpa) with no success[4]. In the case of lower nitrides, γ-Mo_2N and β-Mo_2N, they represent the cubic high-temperature phase and the tetragonal low-temperature phase, respectively. These lower nitrides have been formed by direct reaction of the elements above 1000 °C at N_2 pressures above 1 atmosphere[5]. As the reaction temperature is increased, the nitrogen pressure must also be elevated above the dissociation temperature of the nitride, which is 10 atm at 1020°C and 100 atm at 1380 °C for γ-Mo_2N. The formation of δ-MoN has not been observed in the reactions of Mo and N_2 at temperatures between 600 and 1400 °C and pressures of 1 to 300 atm[6] which is an illustration of the decreased thermodynamic stability of MoN relative to Mo_2N. The nitrides are formed under less severe conditions

when ammonia or other more active nitriding agents are reacted with the metal or more reactive molybdenum oxides or chlorides. Elevated temperature reactions of ammonia and finely divided molybdenum metal have led to the formation of δ-MoN ultimately in a reaction of the two components at 800 °C for a few hours and slowly cooling to 300 °C over a period of four weeks[7]. The reaction of ammonia and MoO_3 at elevated temperatures has been shown to yield the lower nitride, Mo_2N[8]. Recently, the conversion of MoO_3 and ammonium molybdates to fcc Mo_2N and hexagonal MoN, respectively, by the reaction of the oxides with ammonia at temperatures up to 625 °C, has been reported[9]. Through the use of inorganic synthetic procedures, highly reactive molybdenum compounds can be made and ideally converted to the known higher molybdenum nitrides at lower temperatures[10] or can facilitate the synthesis of new nitrogen rich metal nitrides[11], such as a molybdenum nitride with the empirical formula, Mo_2N_3. This higher nitride was formed by chemical vapor deposition from the reaction of tetrakis(dimethylamido)molybdenum (IV) in an ammonia stream at temperatures ranging from 200 - 400 °C.

MoN_2 represents the final frontier in higher molybdenum nitrides and due to the inherent thermodynamic instability of this material, it may only be accessible as a low temperature, kinetically stabilized compound. In Section II of this work, WN_2 synthesis was attempted by starting with a tungsten compound in the +6 state and replacing all non-hydrogen ligands with nitrogen

by ammonolysis, intramolecular oxidation-reduction and metathetic approaches. Although evidence for the formation of the anion $WN_2Cl_3^{3-}$ was found in that work, binary WN_2 was not made. Instead of starting with the metal in a high oxidation state and chemically altering its coordination sphere, this work focuses on the synthesis of new molybdenum azido compounds, and their thermal decomposition to yield higher metal nitrides at temperatures below 300 °C. Since the highest oxidation states of molybdenum are less stable with respect to reduction, relative to the tungsten analogs, lower oxidation state molybdenum azido compounds that can be internally oxidized have been prepared.

EXPERIMENTAL

Materials

The organic solvents, pyridine and butyronitrile, were dried according to procedures given in Section II of this report. Anhydrous ammonia (99.9%) was obtained from Matheson Gas Products. The ammonia was dried by passing the ammonia through finely divided CaH_2 prior to use in gas flow reactions. Trimethylsilylazide (TMSA) was obtained from Hüls Petrarch Systems, Inc. and transferred to a solvent flask and stored in the dark, under vacuum, to avoid hydrolytic and photolytic decomposition of the azide. Dimolybdenum tetraacetate $Mo_2(C_2H_3O_2)_4$ was synthesized in this laboratory according to literature methods.[12] $Mo_2Cl_4py_4$ was also made in this laboratory, according to the following reaction:

(1) $Mo_2(O_2CCH_3)_4 + 4(CH_3)_3SiCl + 4py \Rightarrow Mo_2Cl_4py_4 + 4(CH_3)_3SiO_2CCH_3$

A typical large scale reaction was completed by adding $Mo_2(O_2CCH_3)_4$ (4.00g, 9.34 mmol) to a 250 mL reaction flask. Pyridine was syringed onto the acetate under a stream of inert gas. An excess of trimethylsilylchloride (8.56 g, 78.8 mmol) was then added, by syringe, to the pyridine mixture. The compounds were allowed to react for 20 hours in refluxing pyridine. The red molybdenum chloride complex was then filtered and dried under dynamic vacuum for 24 hours.

Analytical Procedures

Molybdenum content was determined by two methods. In the first, Mo was analyzed by the precipitation of the 8-hydroxyquinolate, $MoO_2(ONC_9H_6)_2$[13]. The samples were initially transferred to screw-top vials and weighed under argon. The samples were then poured into 250 mL beakers in the dry-box and covered with parafilm. The sample vials were reweighed and the sample mass was determined by difference. Dilute base (KOH) was then added to the beakers to initiate decomposition into the soluble molybdate ions. The solutions were heated to boiling and hydrogen peroxide was added to insure complete conversion to the molybdate. After complete conversion to MoO_4^{2-}, the solutions were acidified with dilute sulfuric acid to a pH of 6-8 and then buffered with an acetic acid/ammonium acetate mixture. The analyte was precipitated by the addition of 8-hydroxyquinoline solution. The solid was filtered through tared fritted filters, washed with hot water and dried at 140 °C to constant weight. In the second method for molybdenum analysis, the samples were weighed by difference from the dry-box and used to prepare acidic solutions for analyses on the ICP maintained by Ames Laboratory. The solutions were prepared in this lab, within the range of pre-made standards, and analyzed by Ames Laboratory staff. Nitrogen and carbon analyses were performed using the Dumas combustion method[14] on a Carlo

Erba Instruments NA1500 Nitrogen/Carbon/Sulfur Analyzer at the National Soil Tilth Laboratory, under the supervision of Richard Fifer. In this method 10-15 mg. samples were weighed by difference in tin crucibles and placed in the instrument. The samples would first drop into an argon purged compartment and subsequently drop into a furnace, heated to 1021 °C, that was purged with pure oxygen. The nitrogen and carbon in the samples would first be converted to the corresponding oxides, by the high temperatures and oxygen atmosphere. The eluent was then passed over a bed of finely divided copper metal which would reduce the nitrogen oxides to N_2. The carrier stream was then passed through a chromatography column, separating out the N_2 and CO_2 components for subsequent determinations of C and N. Standards of acid aniline were run every seven samples for C and N comparisons. The standards were within 0.3 percent of calculated value for N, while C values were low by 10 percent of the calculated amount. The carbon values obtained from this procedure were reported for comparative purposes only.

Synthesis

The following set of reactions involve the synthesis of molybdenum azido compounds. Because of their unknown sensitivity to heat, shock and friction, each new reaction in which a metal azide was the predicted product, was

placed in a vented hood and surrounded by blast shields consisting of 3/8" polycarbonate sheets. All synthesized azido materials were evaluated for their sensitivity. Frictional sensitivity was determined by grinding 1-2 mg quantities with a mortar and pestal in the dry-box. Shock sensitivity was evaluated by allowing a hammer to drop on metal sheet containing a 1-2 mg sample of the azide. The thermal stability of the azides was determined by heating the material in small quantities and observing thermal events visually or through thermal analyses (TGA/DTA).

The X-ray powder diffraction data for the following materials were recorded using a specially designed sample holder for air reactive samples. The results of these diffraction tests show that the azide compounds **1A-2C**, and the materials formed from the decomposition of molybdenum azide compounds, **3A-3C**, are amorphous. Some of the X-ray diffraction data show broad peaks due to extremely small crystallites, but in each case the X-ray data are of little value in determining the identity of the compounds.

Attempts have been made to grow crystals of **1B** and **1C** by dissolving small amounts of the compounds in pyridine and layering ether on the top. Although, some solid was deposited in these experiments, the formation of crystals was not observed.

$Mo_2(O_2CCH_3)_4$ + X $SiMe_3N_3$ --<pyridine>--> (1A, 1B, 1C). This reaction can be considered analogous to the synthesis of $Mo_2Cl_4py_4$, where

azide (considered a pseudo-halide in terms of its chemical reactivity) replaces chloride. The initial reaction conditions parallel those reported for the formation of the tetrachloro molybdenum dimer. Four moles and 8 moles of TMSA per mole of acetate dimer were used in separate reactions to form **1A** and **1B**, **1C**, respectively. In the first reaction, $Mo_2(O_2CCH_3)_4$ (0.525 g, 1.23 mmol) was added to a 100 mL reaction flask (X=4 in reaction above). TMSA (3.23 mL, 4.91 mmol) and pyridine were added to the acetate by syringe, with the pyridine preceding the TMSA addition by 5 minutes. The mixture was allowed to react under a stream of argon at refluxing temperature for two days. The solution became deeply colored upon the addition of TMSA. The black product (**1A**) was extremely soluble in pyridine. Most of the product passed through the filter frit, and thus was isolated by distilling the volatile components from the filtrate under reduced pressure. Based on the IR spectrum of **1A** (Fig. IV-1), it was clear that the reaction had not gone to completion, in contrast with the 20 hour reaction time required for the formation of $Mo_2Cl_4py_4$. The difference in solubility between $Mo_2Cl_4py_4$ and **1A** in pyridine was dramatic. This was the first indication that the product, **1A**, did not ultimately form the desired product, $Mo_2(N_3)_4py_4$. It was envisioned that the reaction may go to completion if TMSA was added in excess and the reaction time was increased. Therefore, in the second reaction, $Mo_2(O_2CCH_3)_4$ (1.00g, 2.34 mmol) was reacted

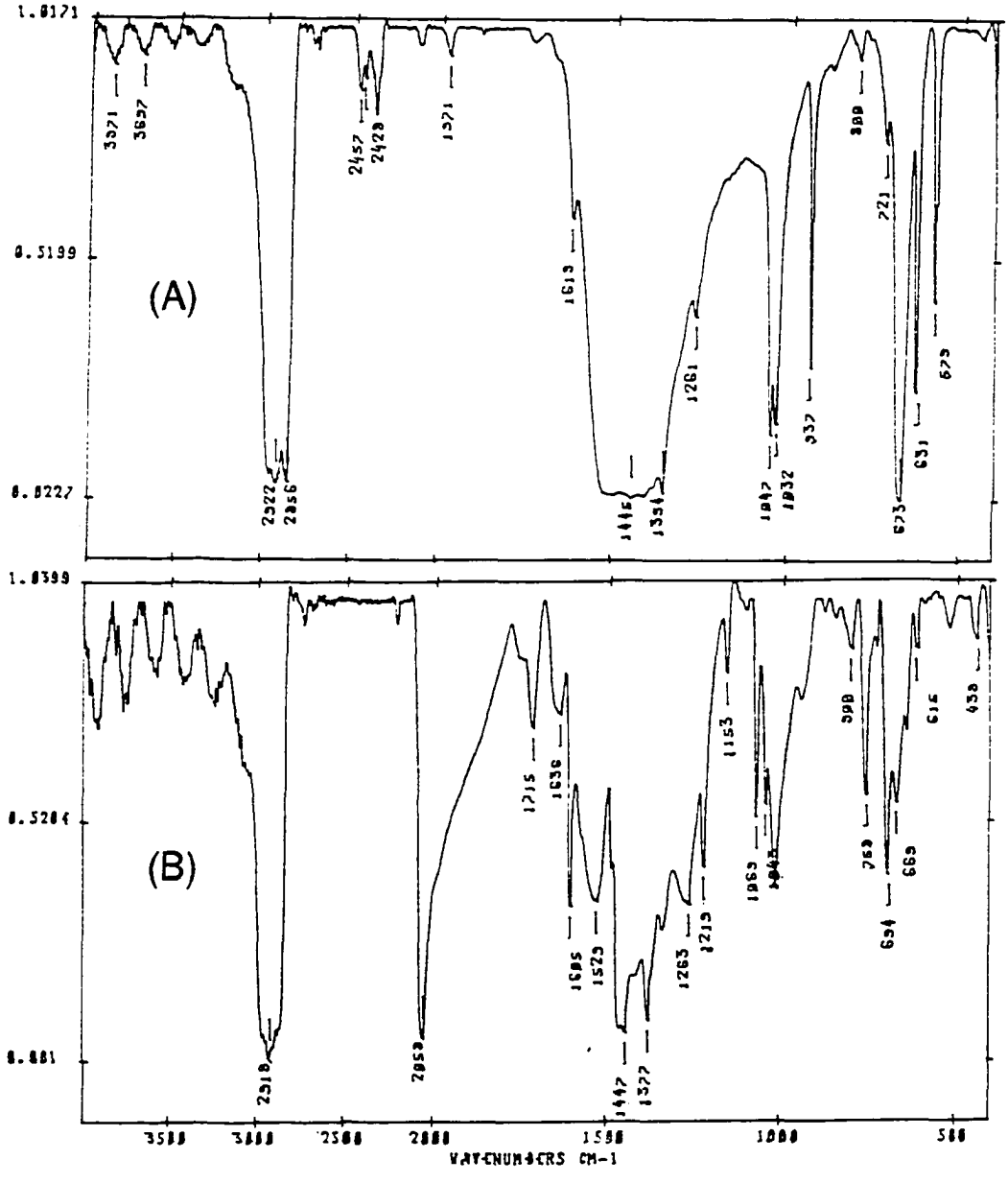

Figure IV-1. Comparative mid IR spectra (Nujol) of $Mo_2(O_2CCH_3)_4$ (A) and **1A**, the product of the incomplete reaction of $Mo_2(O_2CCH_3)_4$ with 4 moles of TMSA in pyridine (B). The peak at 2058 cm^{-1} in (B) is the asymmetric stretching mode of azide

in a manner analogous to the preceding scheme, with TMSA (2.46 ml, 18.7 mmol) in approximately 40 mL of pyridine, for 7 days in refluxing pyridine. The solution was filtered and two components were isolated; one material, with apparent low pyridine solubility (**1B**), on the ceramic filter and a second fraction which had a higher pyridine solubility (**1C**), in the receiver flask. A comparison of the IR spectra for **1B** and **1C** is given in Figure IV-2. The empirical formulation for products **1B** and **1C** is $MoN(N_3)py_1$. Anal. Calc. for $MoN(N_3)py_1$: Mo, 41.54; N, 24.57; Mo:N, 1:4 (not including the N from pyridine). Found for **1B**: Mo, 39.6; N, 21; Mo:N, 1:3.6 (accounting for only the azide and nitride nitrogen). Found for **1C**: Mo, 39.3; N, 22; Mo:N, 1:3.8 (accounting for only the azide and nitride nitrogen).

$Mo_2Cl_4py_4$ + $8Me_3SiN_3$ --<pyridine, butyronitrile>--> (2A, 2B, 2C, 2D). $Mo_2Cl_4py_4$ (1.490 g, 2.3 mmol) was loaded into a 100 mL reaction flask. Approximately 35 mL of pyridine was syringed onto $Mo_2Cl_4py_4$, followed by TMSA (2.41 mL 18.4 mmol). The resulting solution was not deeply colored, even after the azide addition. $Mo_2Cl_4py_4$ is relatively insoluble in pyridine so the reaction is less facile than the corresponding reaction of TMSA and $Mo_2(O_2CCH_3)_4$. The reactants were mixed at ambient temperature for four days, at which time there appeared to be remaining $Mo_2Cl_4py_4$ in the flask; therefore the reaction was heated to reflux and allowed to mix for an additional

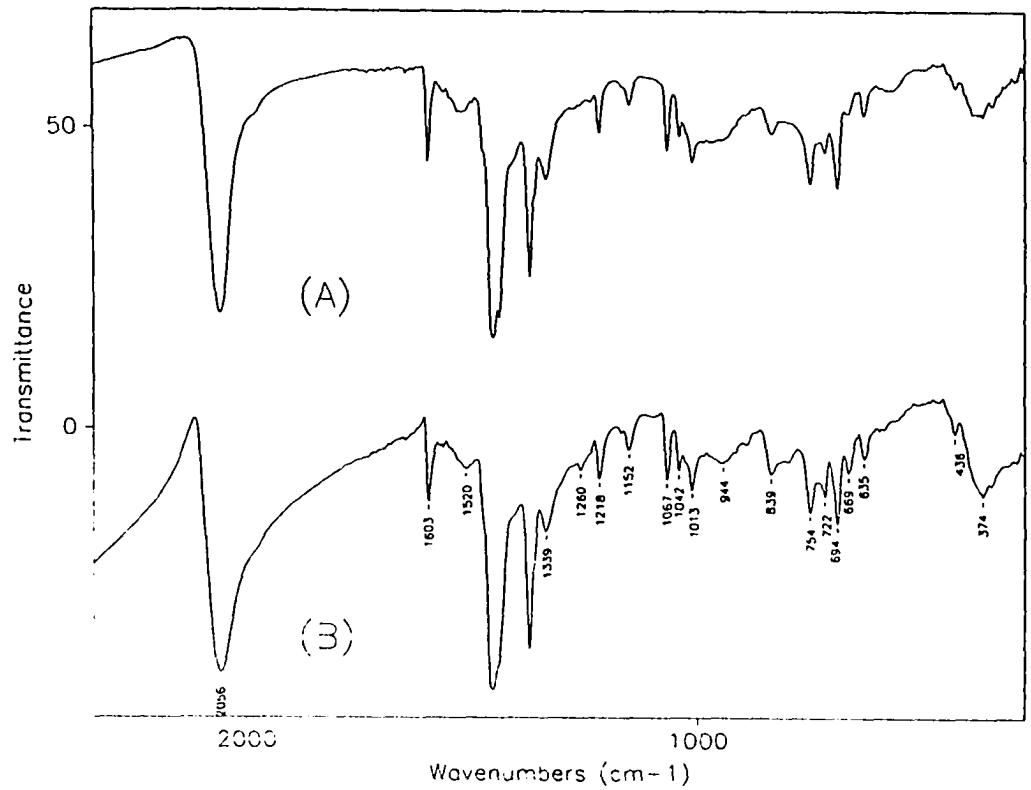

Figure IV-2. Comparison of the IR spectra (Nujol) of **1B** (A) and **1C** (B) which are the insoluble and soluble products of a $Mo_2(O_2CCH_3)_4$/TMSA (1:8 mole fraction) reaction in pyridine, respectively. Most of the narrow bands are attributed to pyridine modes while the peaks at 2056 and 944 cm^{-1} are attributed to the asymmetric azide vibration mode and the multiple Mo-N bond vibrations, respectively

2 1/2 days. The material was filtered and two components were isolated. The insoluble fraction (**2A**) was isolated on a ceramic frit, while the soluble fraction (**2B**) was isolated by solvent removal from the filtrate under reduced pressure. The yields for **2A** and **2B** were 0.160 and 0.710, respectively. For a comparison of the IR spectra for **2A** and **2B**, see Figure IV-3. Anal. Calc. for $MoN(N_3)py$: Mo, 41.54. Found for **2A**: Mo, 40.6.

Due to the apparent insolubility of $Mo_2Cl_4py_4$ in pyridine, butyronitrile was substituted for pyridine in one experiment, in an effort to increase the solubility of the chloride. $Mo_2Cl_4py_4$ was solubilized more quickly in butyronitrile than pyridine. $Mo_2Cl_4py_4$ (2.230 g, 3.43 mmol) was reacted with TMSA (2.71 mL, 20.61 mmol) in 40 mL of butyronitrile utilizing similar procedures as those used in the synthesis of **2A** and **2B**. The reaction was conducted under reflux for 7 days. After filtration, one solid was isolated on the frit (**2C**) and the other was isolated from the filtrate (**2D**) after the volatile components were removed under reduced pressure. A comparison of the IR spectra for **2C** and **2D** is shown in Figure IV-4.

^{1}H NMR study of $Mo_2(O_2CCH_3)_4$, $Mo_2Cl_4py_4$ reactivity with TMSA. $Mo_2(O_2CCH_3)_4$ (20.4 mg, 0.048 mmol) was added to a 5 mm NMR tube. TMSA (0.05 mL, 0.38 mmol) and 4 mL of deuterated pyridine were syringed and distilled, respectively, onto the acetate and the tube was sealed by fusing the end. Immediately afterwards, TMSA (0.05 mL, 0.38 mmol) and 4 mL of

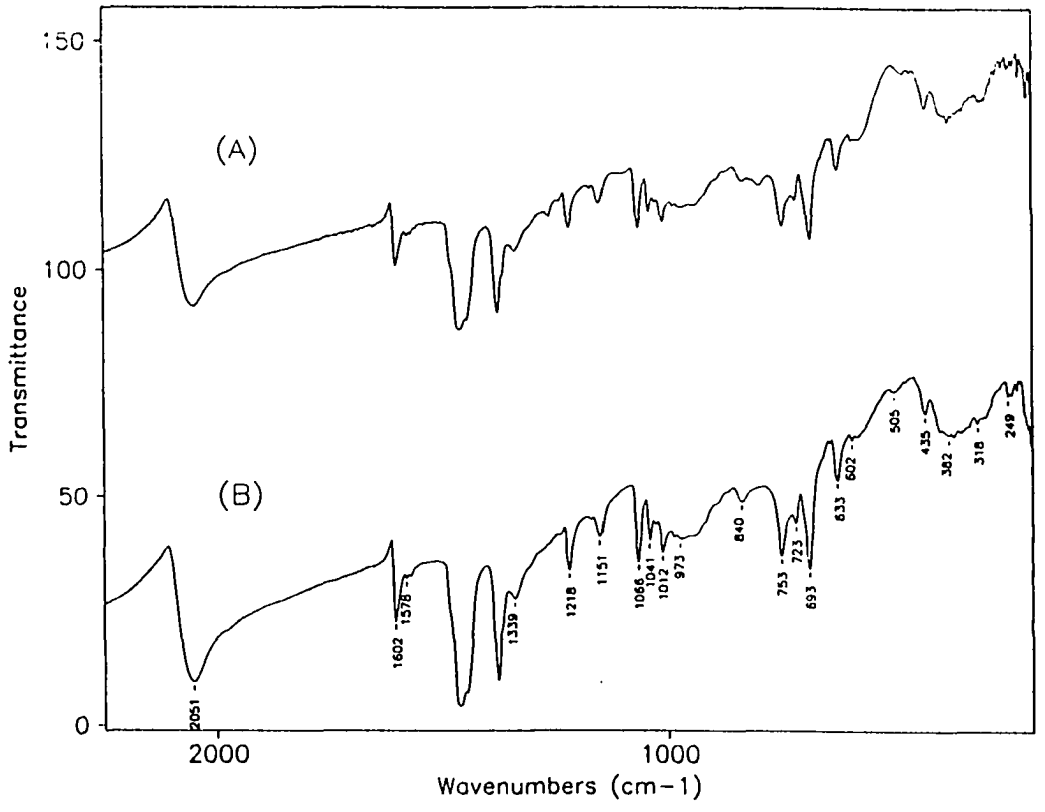

Figure IV-3. IR spectra comparison (Nujol) of **2A** (A) and **2B** (B). The two samples were obtained from the same reaction of $Mo_2Cl_4py_4$ and excess TMSA in pyridine and differ in their pyridine solubilities. The two spectra are essentially identical. Aside from the pyridine peaks, the peaks at 2051 and 930-973 cm^{-1} identify an azide stretching mode and υ(Mo≡N), respectively

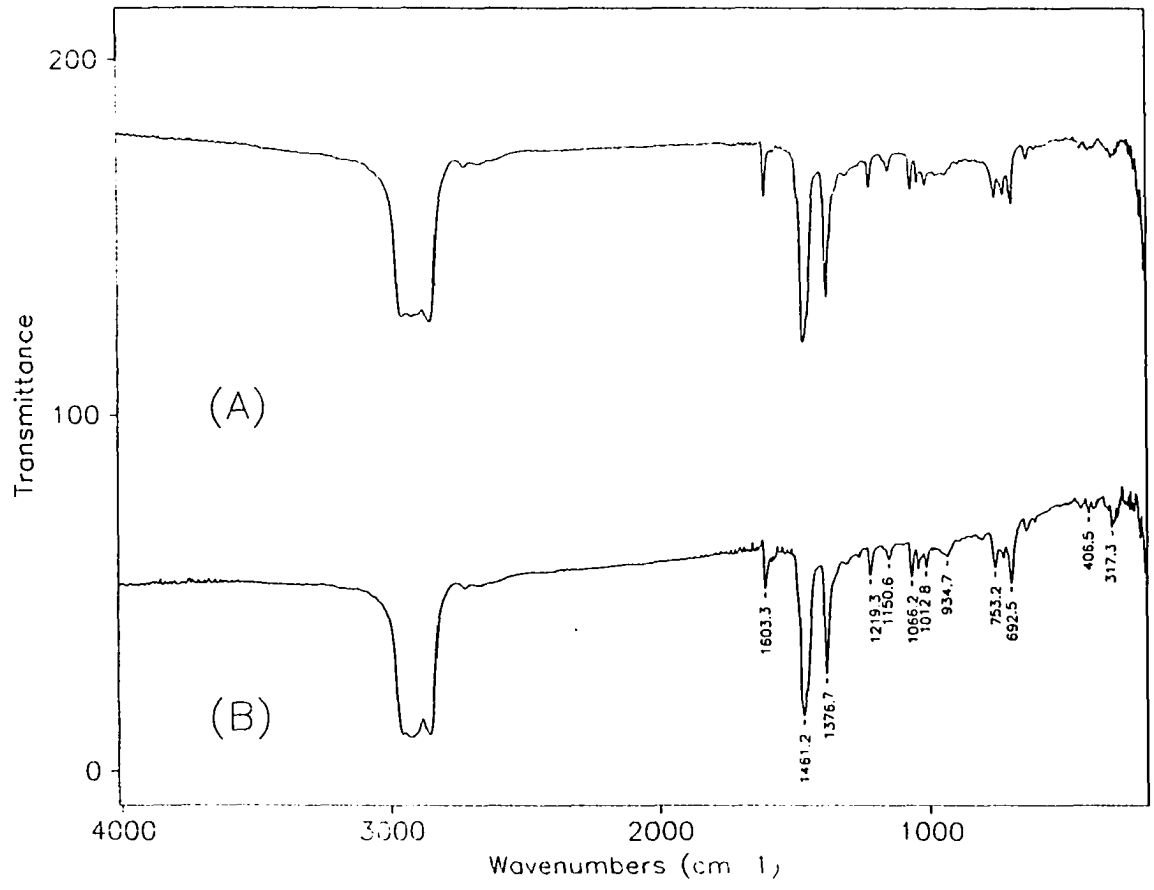

Figure IV-4. IR spectra comparison (Nujol) of **2C** (A) and **2D** (B). The two samples were obtained from the same reaction of $Mo_2Cl_4py_4$ and excess TMSA in butyronitrile

deuterated pyridine were added to an NMR tube containing $Mo_2Cl_4py_4$, (30.9 mg, 0.048 mmol). Four spectra were taken for each tube at different time intervals (see Fig. IV-5, 6). For the first 15 days, of the 18 day reaction, the two NMR tubes were left at ambient temperature. For the last three days, the tubes were placed into a oil bath at 90 °C to complete the reactions.

Thermal decomposition of $MoN(N_3)py$ (1B) in flowing Ar (3A). Initial thermal decomposition studies were performed on a vacuum line for samples of **1B**. The material was heated under dynamic vacuum and a correlation between sample temperature and line pressure was determined. The vacuum line traps were cooled with liquid N_2, therefore any nitrogen given off in the thermal decomposition of the azide increased the total pressure in the line. All volatile organics were condensed in the N_2 traps. Sample **1B**, heated in this manner, showed a pressure maximum at 240 °C. The reaction was then repeated in an argon environment. **1B** (50 mg) was placed in a dried pyrex tube which was inserted into a sand bath for heating. An atmosphere of argon was maintained by flowing the gas through the upper joint of the reaction tube. Under these conditions, **1B** was heated for 18 hours at 250 °C to yield **3A**. IR spectra contrasting **1B** with the thermolyzed product, **3A**, is reported in Figure IV-7. The nitrogen and carbon percentages for **3A** were: N, 16; C, 24, rswpectively. Thermal gravimetric and differential thermal data were obtained for **3A** (see Fig. IV-8).

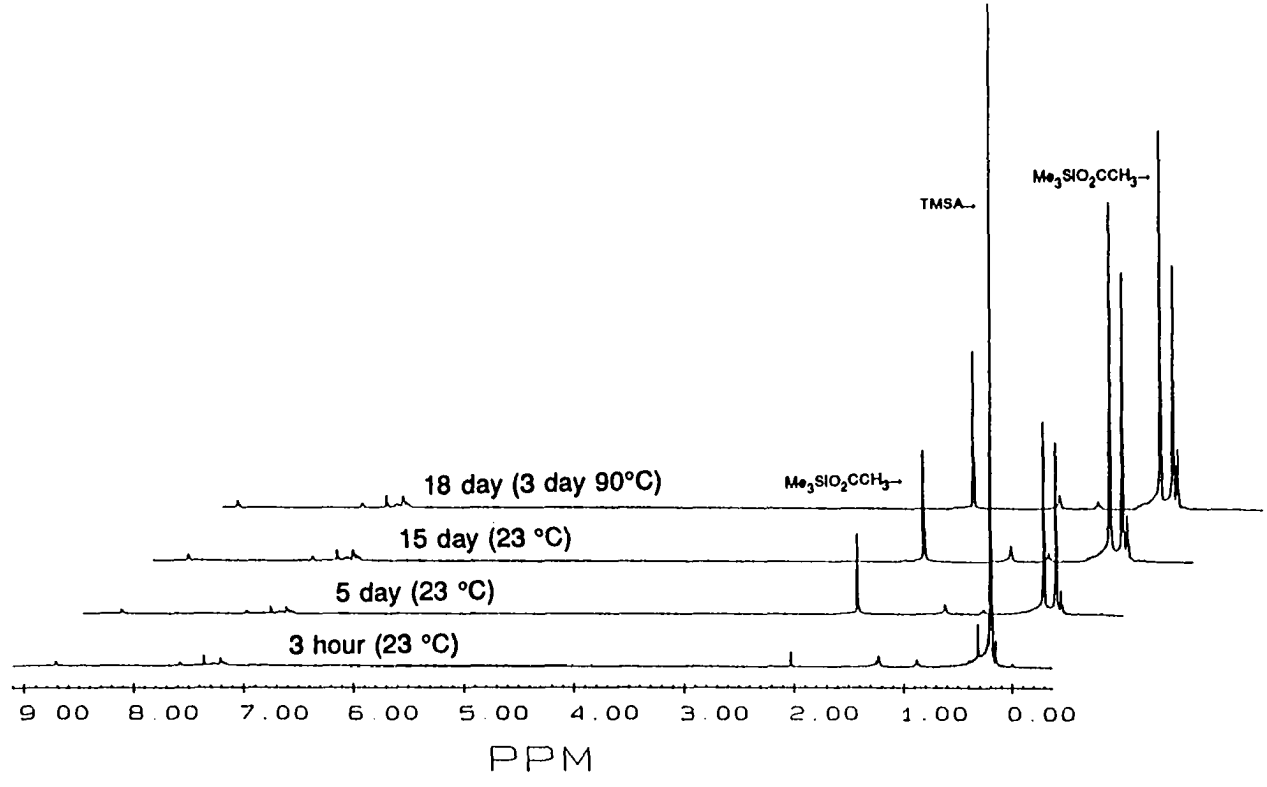

Figure IV-5. ^1H NMR spectra for the reaction of $Mo_2(O_2CCH_3)_4$ with TMSA (1:8 mole ratio) in deuterated pyridine. The peak attributed to TMSA decreases with time by reacting to form the acetate compound. The facile nature of the acetate in this reaction is demonstrated

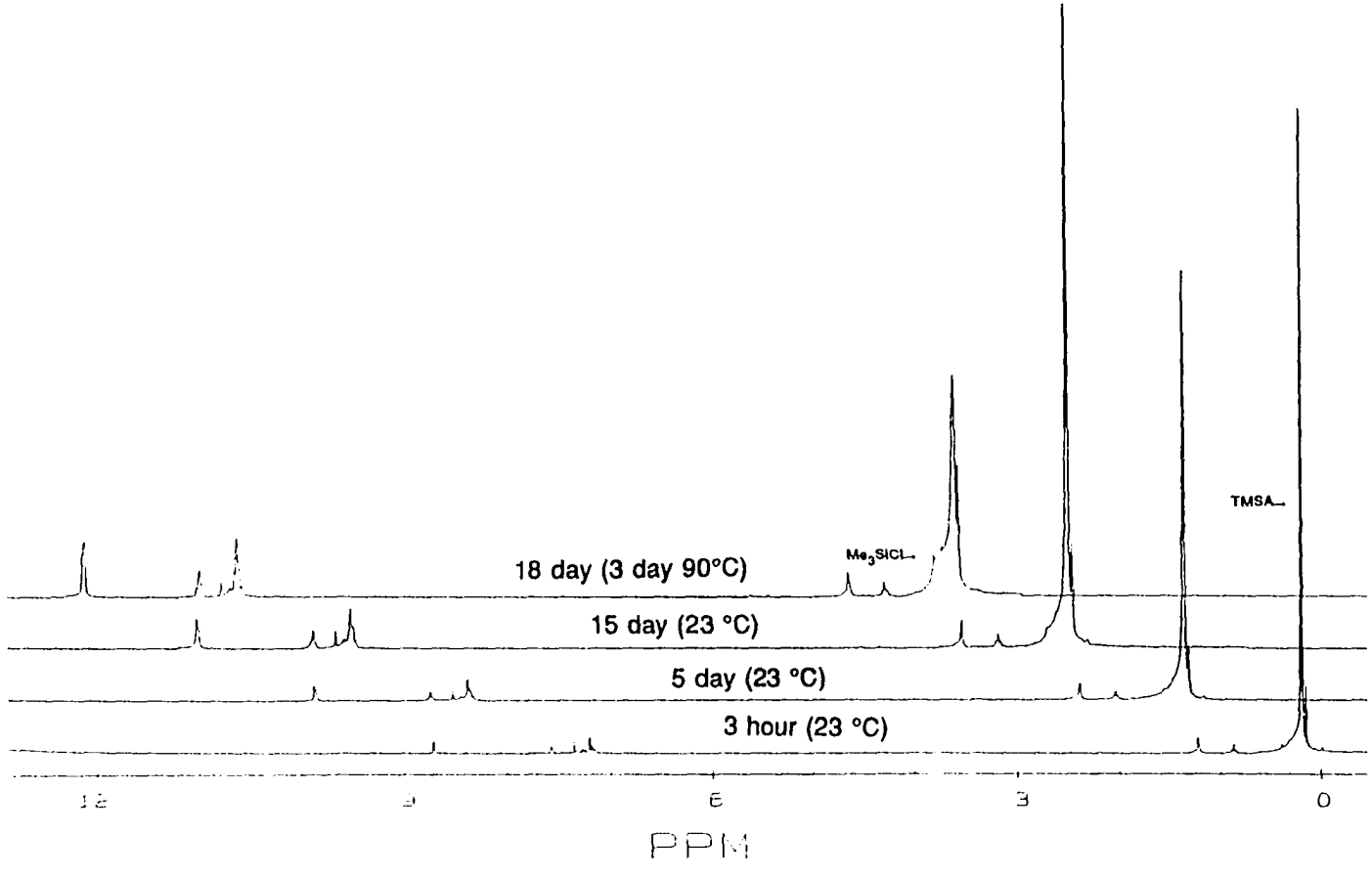

Figure IV-6 ^1H NMR spectra for the reaction of $Mo_2Cl_4py_4$ with TMSA (1:8 mole ratio) in deuterated pyridine. Only a small amount of the chloride has reacted after 15 days and it is not until refluxing is employed that any significant amount reacts

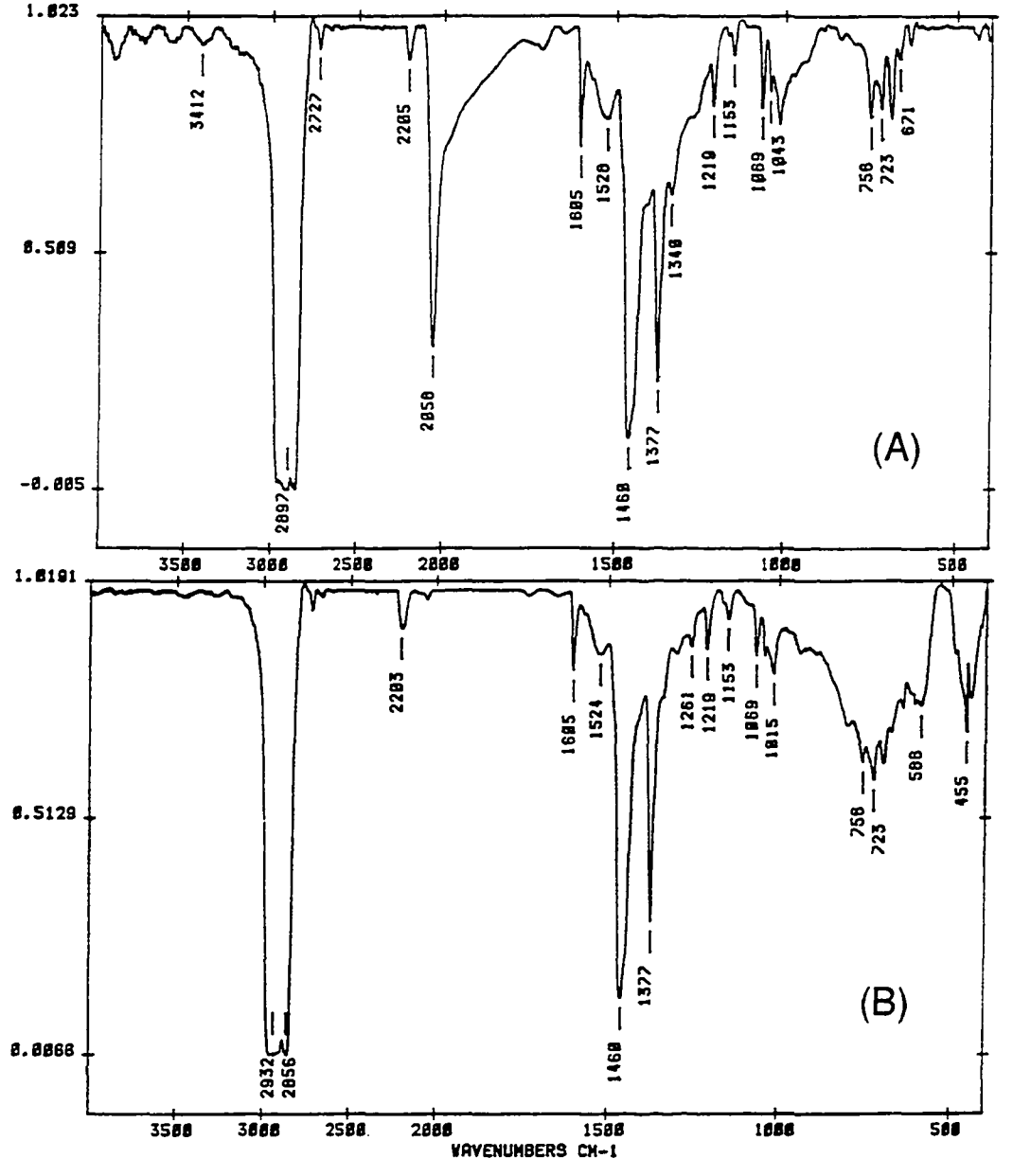

Figure IV-7. Mid IR spectra (Nujol) of $MoN(N_3)py$ (**1B**) and the product of heating **1B** at 200 °C in flowing argon (**3A**) corresponding to (A) and (B), respectively. Note that there is still significant functionality in (B) indicating probable inclusion of carbon compounds

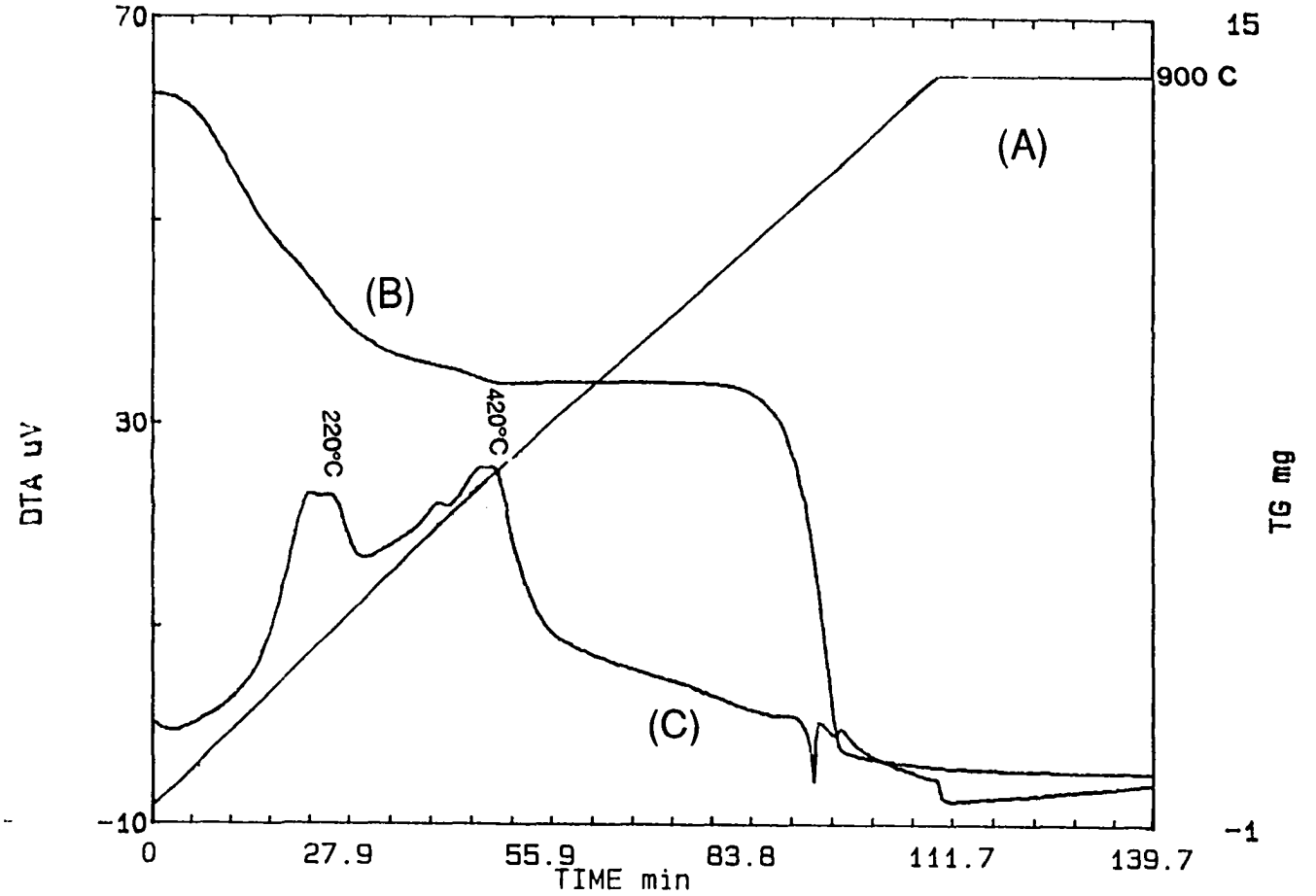

Figure IV-8. TG\DTA of $MoN(N_3)py$ (**1B**) in flowing argon. The line (A) represents the temperature, while (B) accounts for the weight variation (TGA) and (C) is the DTA curve in which heat capacity changes are recorded

Thermal decomposition of $MoN(N_3)py$ (1B, 1C) in flowing ammonia.

Due to the high carbon content determined for **3A**, a variation of environment was considered. Ammonia was used to replace the pyridine ligands and lower the amount of carbon included in the pyrolysis product. A special reaction tube was built, which consisted of 14 inches of 12 mm (OD) pyrex tube capped on the ends by an inner or outer 24/40 ground glass joint and a ceramic filtering frit centered between the ends. In the reaction, a powdered sample was placed in the glass tube, on the course ceramic fritted disk to maximize exposure of the powder to ammonia flowing through the tube. **1B** (0.261 g) was placed on the frit in the reaction tube and in a flowing ammonia environment, heated at 130°C for 3 hours, producing (**3B**). 0.161 grams of **3B** were recovered. Peaks corresponding to pyridine vibrational modes were observed in the IR spectrum of **3B** (see Fig. IV-9), thus the reaction of **3B** was pursued at higher temperatures in an atmosphere of flowing ammonia. **3B** was heated to 180 °C in an atmosphere of flowing ammonia. At 180 °C the flow of ammonia was stopped and the reaction vessel, which was connected to a mercury bubbler, was allowed to heat further to 280 °C. At 223 °C rapid bubbling was observed from the bubbler, which indicated azide decomposition. The temperature was lowered to 200 °C and the ammonia flow was resumed. The reaction was continued at 200 °C under flowing ammonia for 12 hours, which resulted in the isolation of 0.076 grams of a low density black powder (**3C**) with no IR active

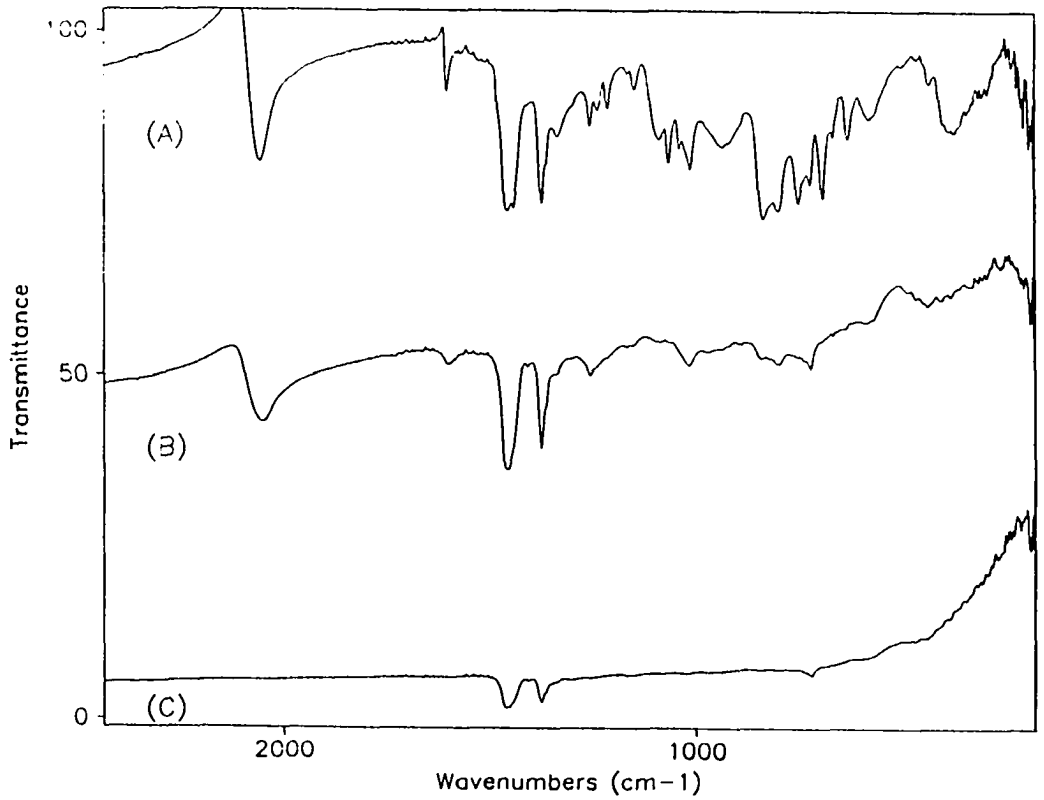

Figure IV-9. IR spectra (Nujol) illustrating the influence of heat and ammonia atmospheres on ammonia substitution for pyridine and thermal decomposition of $MoN(N_3)py$ (**1B**). Spectra (A), (B) and (C) correspond to **1B**, **3B** and **3C**, which were reacted at successively higher temperatures

bands (see Fig. IV-9). The nitrogen and carbon percentages for **3C** are 18 and 5, respectively. In a related experiment, **1C** (0.200 g) was placed in the reaction tube described previously and heated in flowing ammonia for 1 hour at 150 °C. Then the temperature was increased to 280 °C and held there for two hours. As the material was heating, an explosion was heard at a temperature of 241 °C. Finely divided black powder was scattered throughout the tube as a result of the azide decomposition. The black powder was heated for an additional two hours in flowing ammonia at 280 °C and isolated as a low density powder in the drybox (**3C**). Anal. Found for **3C**: Mo, 70.0,; N, 18; C, 5; Mo:N, 1.0:1.8. IR spectra illustrating the differences between the starting material, **1C**, and the final molybdenum nitride, **3C**, is found in Figure IV-10.

Physical Measurements

The X-ray diffraction data for finely ground powders of **1A** - **3C** were obtained from a Philips ADP3520 diffractometer using Cu $K\alpha_1$ and $K\alpha_2$ radiation. The samples were analyzed on zero-background quartz plates using the Philips environment cell reported in Section I of this work. X-ray photoelectron spectra were obtained from a Perkin Elmer model 5500 Multi-Technique system by James Anderegg at Ames Laboratory. Solution ^1H NMR was obtained from a Nicolet MS-300, maintained by the Instrument Services

Group at ISU. Analysis of the volatile components produced during thermolysis of **1B** was performed by using a Finnigan mass spectrometer (maintained and operated by Chemistry Instrument Services) coupled to a reaction tube through thick-walled glass capillary tubing. Infrared spectra were obtained from a IBM IR/90 or a Bomem MB-Series Fourier transform infrared spectrometer. The samples were prepared as Nujol mulls and pressed between CsI plates.

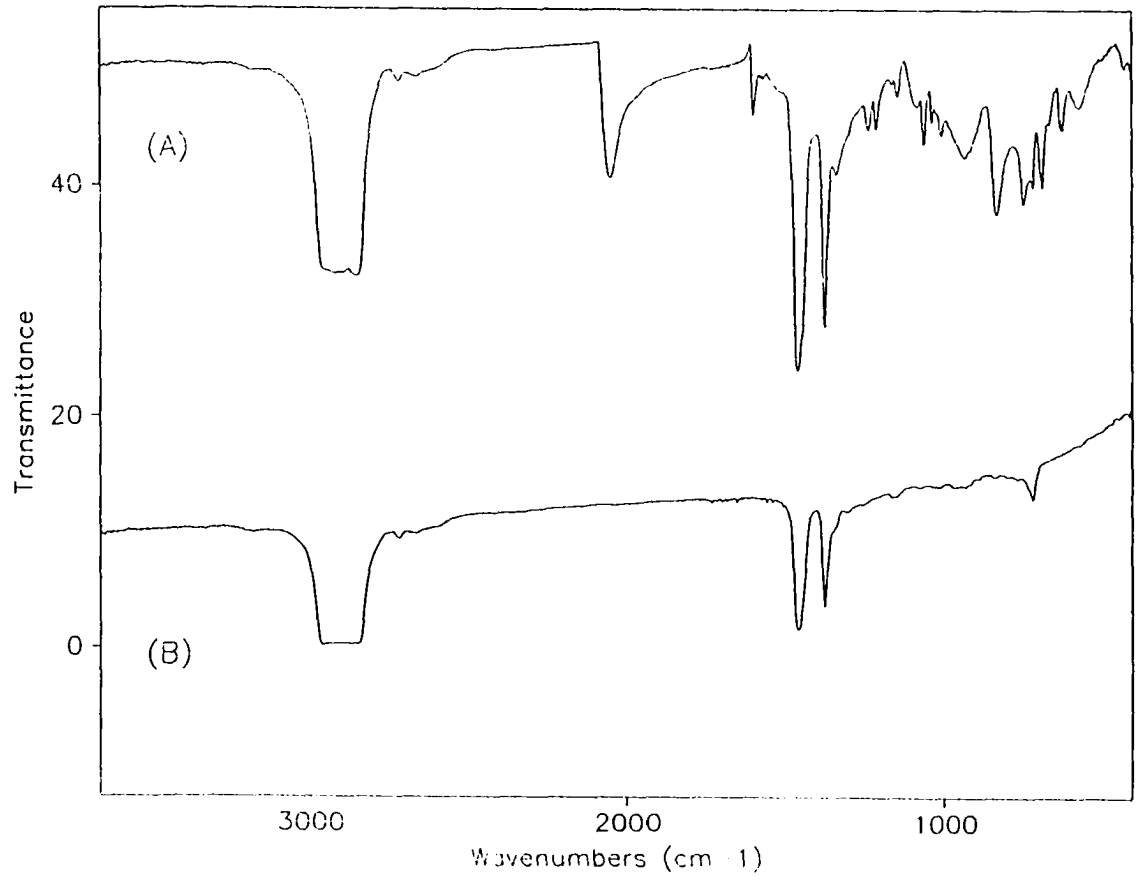

Figure IV-10. IR spectra (Nujol) of 1C and 3C, A and B, respectively, which illustrate the change in functionality in 1C as it is heated in ammonia to 280 °C to form a solid state molybdenum compound with a metal-nitrogen ratio of 4:7

RESULTS AND DISCUSSION

$Mo_2(O_2CCH_3)_4$ and $Mo_2Cl_4py_4$ Reactivity

Based on the similarities between the chemistry of chloride and the "pseudo halide," azide, one might expect the reaction of $Mo_2(O_2CCH_3)_4$ with excess TMSA to yield $Mo_2(N_3)_4py_4$, analogous to the product, $Mo_2Cl_4py_4$, formed from the reaction of $Mo_2(O_2CCH_3)_4$ with excess trimethylsilylchloride (TMSC). The molybdenum percentage in $Mo_2(N_3)_4py_4$ is 28.39, whereas the molybdenum composition in **1B, 1C, 2A** and **2B** is ca. 40 %. Obviously, the azide analog of $Mo_2Cl_4py_4$ is not formed in the reactions forming **1B-2B.** In related research, Chatt and Dilworth[15] began with the bis-dinitrogen compound of molybdenum, $Mo(N_2)_2(dppe)_2$ (dppe = $Ph_2PCH_2CH_2PPh_2$), and reacted it with TMSA to yield $MoN(N_3)(dppe)_2$. In a discussion of the probable pathway to azido-nitrido formation from both the molybdenum and tungsten bis-dinitrogen compounds, Leigh, et. al.[16] discussed a disproportionation from a postulated intermediate, $M(N_2)(N_3)(dppe)_2$, to produce both $M(N_2)_2(dppe)_2$ and $M(N_3)_2(dppe)_2$. The latter decomposes to $MoN(N_3)(dppe)_2$ and molecular nitrogen. Based on this result, one would reasonably expect $Mo_2(N_3)_4py_4$ to form as an intermediate in the synthesis of **1B, 1C, 2A** and **2B.** In the former study[15], the nitride-azide of molybdenum was characterized as having two

distinctive absorptions in the IR region. One corresponded with $\upsilon(N_3)$ at 2040 cm^{-1} and the other was assigned to $\upsilon(Mo{\equiv}N)$ at 980 cm^{-1}. In each of the spectra generated for compounds **1B - 2C** there is the distinctive peak attributed to $\upsilon(N_3)$ in the range 2051 - 2056 cm^{-1} and a less obvious, broadened band centered at 944 $cm,^{-1}$ but covering a range of 1000 - 900 $cm,^{-1}$ corresponding to the $\upsilon(Mo{\equiv}N)$.

There is some question as to the exact identity of **1B-2B**. All the products have the same IR spectral features and have the same molybdenum content (within experimental uncertainty), but they differ in their pyridine solubility. The $MoN(N_3)$py compound is obtainable from the molybdenum acetate or the chloride dimers. The XPS spectra comparing the N-1s emissions of **1B** (insoluble in pyridine) and **1C** (soluble in pyridine) is given in Figure IV-11, while the XPS spectra of the Mo-3d emissions for the same compounds are given in Figure IV-12. In Figure IV-12, the two Mo-3d peak intensities and shapes are essentially identical for **1B** and **1C**, which indicates that each molybdenum is in a similar environment and oxidation state. With the empirical formula of $MoN(N_3)$py, it is highly unlikely that the material is monomeric. More consistent with the elemental data is the formation of a double dimer with multiple bonded nitrogen bridges connecting the dimers.

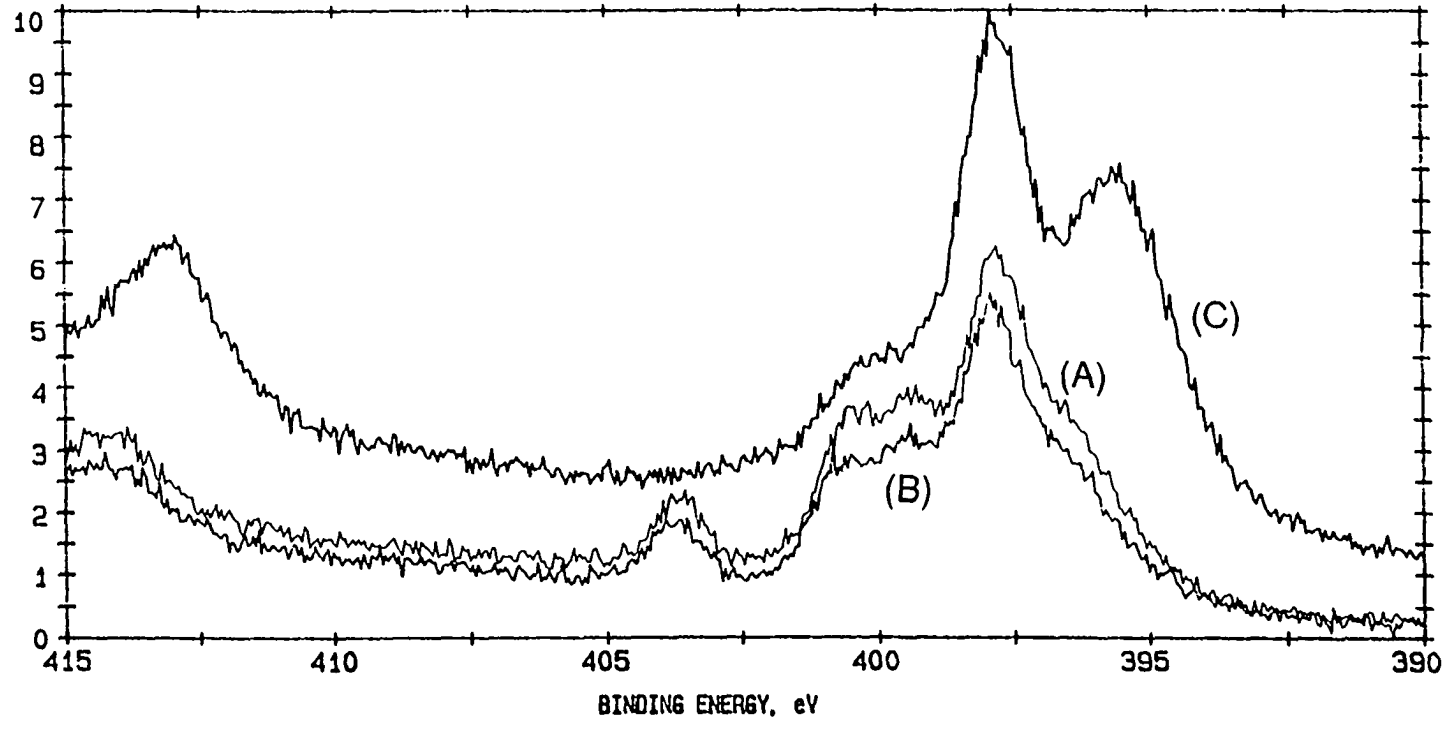

Figure IV-11. X-ray photoelectron spectra of N 1s emissions for related materials. **1B** (A) and **1C** (B) were made from the same reaction but differ in their solubility in pyridine. The peak at 395 eV for **3B** (C) is formed as a result of thermal decomposition and represents a nitride-like nitrogen

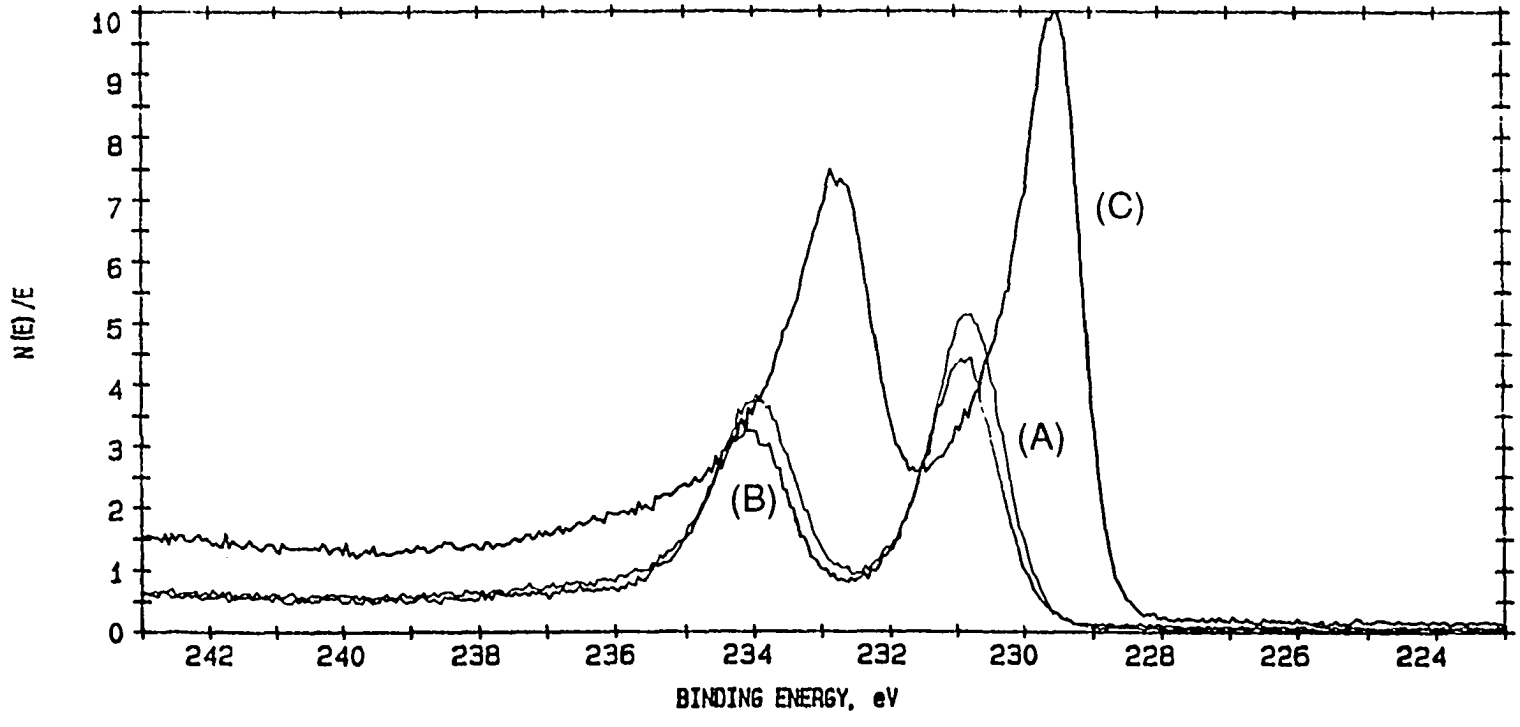

Figure IV-12. XPS spectra of the Mo 3d leveis. **1B** (A) and **2B** (B) are very similar in molybdenum environments while the **3B** (C) peaks have shifted to lower binding energies, indicative of condensed nitrides

^1H NMR Studies of $Mo_2(O_2CCH_3)_4$ and $Mo_2Cl_4py_4$ Reactivity

The reactions between the two molybdenum compounds, $Mo_2(O_2CCH_3)_4$, $Mo_2Cl_4py_4$ and TMSA has been followed by ^1H NMR in $py(d_5)$ (see Fig. IV-5,6 for $Mo_2(O_2CCH_3)_4$ and $Mo_2Cl_4py_4$ reactions, respectively). The mole ratio of dimer to azide was 1:8 in the reactions. A contrast is seen between the spectra for the two reactions. In Figure IV-5 the largest peak in the 3 hour spectrum corresponds to TMSA while after 5 days at ambient temperature the azide peak was reduced significantly, which resulted in the peak corresponding to the product of the metathesis, $(CH_3)_3SiO_2CCH_3$, becoming much larger. In the case of $Mo_2Cl_4py_4$ (see Fig. IV-6), the peak identifying the TMSA protons does not decrease noticeably relative to the azide peak in the 3 hour spectrum. In fact, it is only after the chloride material is brought to refluxing temperatures that $Mo_2Cl_4py_4$ reacts with TMSA to form TMDC. It was observed that after three days the solvent for the $Mo_2(O_2CCH_3)_4$ reaction was deeply colored, with no evidence of the molybdenum acetate. After three days, the solvent in the $Mo_2Cl_4py_4$ NMR tube was only weakly colored and most of the red molybdenum chloride could be seen unreacted in the tube. The observation that both the $Me_3SiO_2CCH_3$ and Me_3SiCl were formed in the reactions indicates that the tetraazidomolybdenum dimer may form as an intermediate before

decomposition to the mononitride.

Thermal Decomposition of $MoN(N_3)py$.

1B was placed in a reaction tube and heated at 5 °C/min, from 25 °C to 590°C, in a reduced pressure environment. A thick-walled glass capillary tube connected the reaction tube to a Finnigan mass spectrometer which evaluated the volatile components of the pyrolysis (see Fig. IV-13). The masses giving the highest ion current were 79 and 28 corresponding to pyridine and nitrogen, respectively. The azide decomposes at 257 °C, according to the mass spectral data. Some variability in determination of the azide decomposition temperature resulted from the placement of the thermocouple and the atmosphere present during decomposition of the azide. The agreement between the mass spectral and TG\DTA data (Fig. IV-8) is reasonable even though the decompositions were conducted in vacuum and argon, respectively. In the TG/DTA plot the two exotherms occur at 220 and 420 °C. The former temperature correlates with the azide decomposition occurring at 257 °C. A large amount of carbon was retained in the thermolysis product when **1B** was decomposed in an inert atmosphere. The decomposition of the $MoN(N_3)py$ was complicated by pyridine retention in the molecular precursor and in the final material after decomposition. **3A** was produced when **1B** was heated in an argon

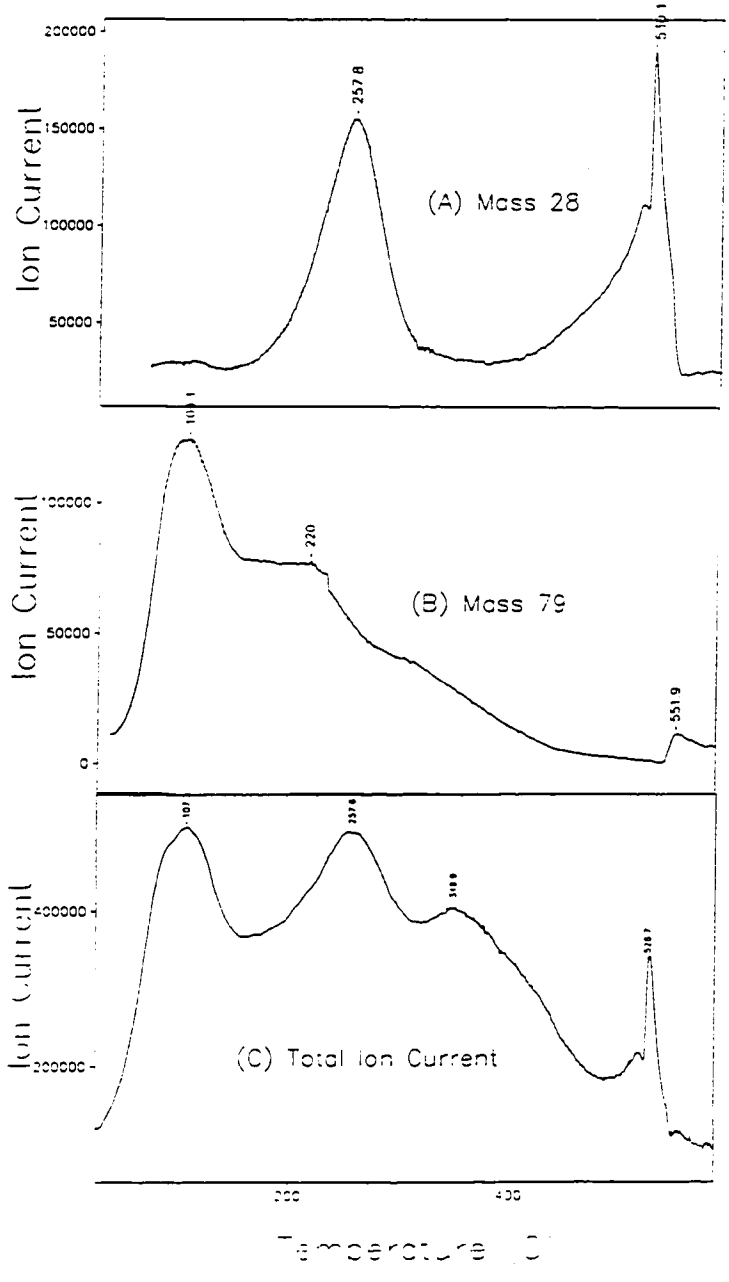

Figure IV-13. A mass spectral thermal decomposition study of 1B under dynamic vacuum. 1B was heated at a ramp of 5°/min from 25 to 590 °C and the volatile components were analyzed with a Finnigan mass spectrometer. Ions with masses 28 and 79 were predominant at temperatures under 300 °C

atmosphere. The final product contained a high percentage of C. The N and C analyses for **3A** were 16 and 24, respectively. The retention of carbon was also seen in samples heated under vacuum. Again, in Figure IV-13, the total ion current was very intense at 350 °C. The ions accounting for this current are mostly carbon fragments from organic materials used in the reaction. The fact that there was a significant amount of carbon containing materials being evolved after the azide decomposition, leads to the conclusion that the carbon levels would be relatively high in the product of $MoN(N_3)py$ decomposition at 280 °C under reduced pressure.

It has been shown that the carbon levels in the decomposition products **3B** and **3C** are significantly reduced. The N and C percentages are 18 and 5, respectively for both **3B** and **3C**. This reduction in carbon percentage is due to the ammonia atmosphere used when heating the molybdenum azides. The fact that there was still C present in the system is less than ideal but the Mo:N ratio of 1:1.8 is highly encouraging. XPS spectra of the N 1s peak and the Mo 3d emissions were obtained for **1B**, **1C** and **3B** (see Figures IV-11,12). In Figure IV-11, sample **3B** shows a similar type of nitrogen to **1B** and **1C** at a binding energy of 398 eV. However, the N peak at 395 eV for **3B** is unique among the three samples. A new type of nitrogen is being produced by the decomposition of the azide. This nitrogen at lower binding energy is very close to the value reported for WN of 395 eV,[17] in contrast to alkyl ammonium nitrogen at 399-

400 eV.[18] In Figure IV-12, the molybdenum 3d peaks are shifted to lower binding energies for the decomposition product, **3B**. Although, one expects a general increase in binding energy as oxidation state increases, this reasoning only applies for compounds in similar environments. Reasonable comparisons for the binding energy of **3B**, can be found in molybdenum oxides. For comparative purposes, the $3d_{5/2}$ binding energies for the iow energy 3d peak of Mo, MoO_2 and MoO_3 are 227.9, 229.3 and 232.6 eV,[19] respectively, while the $3d_{5/2}$ B.E. of **3B** is 229.5 eV. Based on this, it is probable that molybdenum in **3B** is in an oxidation state from +3 to +5.

CONCLUSION

By the apparent metathetic substitution of azide for acetate and chloride in $Mo_2(O_2CCH_3)_4$ and $Mo_2Cl_4py_4$, respectively, and subsequent decomposition of the metal azide, a new molybdenum nitride azide with the empirical formula $MoN(N_3)py$, has been synthesized. The same product is produced by using either molybdenum dimer, although $Mo_2(O_2CCH_3)_4$ is a more facile reactant because of its higher pyridine solubility, relative to that of $Mo_2Cl_4py_4$. Because the azide decomposition is occurring on a molecular level, one could expect extremely high surface areas in materials isolated immediately after decomposition. Due to the high expected surface areas of these compounds, their catalytic properties may be of interest. The observation of a molybdenum (II) azide decomposition into a molecular molybdenum nitride azide has been reported.[15,16] This finding lends support for a $Mo_2(N_3)_4py_4$ intermediate which decomposes at refluxing temperature to give "$MoN(N_3)py$" as the observed product. $MoN(N_3)py$ can be decomposed thermally at 250 °C, in an atmosphere of ammonia, to evolve nitrogen and form a molybdenum-nitrogen compound with Mo:N, 1:1.8. When $MoN(N_3)py$ was decomposed in an inert gas environment or under reduced pressure, the solid has been shown to retain at a high level of carbon, based on elemental analyses and mass spectral information correlated with $MoN(N_3)py$ thermal decomposition.

REFERENCES

1. Shah, V. K.; Brill, W. J. *Proc. Nat. Acad. Sci.* (U.S.), **1977**, 74, 3249.

2. Boyer, L. L.; Krakaur, H; Klien, B. M.; Pickett, W. E.; Wang, C. S.; *Physica B+C* **1985**, 135, 252.

3. a) Watanabi, R.; Yazaki, I.; Igarashi, Y. ; Toyota, N., Noto, K. *J. Mater. Sci. Lett.* **1986**, 5, 255 b) Papconstantopoulos, D. A.; Pickett, W. E.; *Phys. Rev. B. Condens. Mater.* **1985**, 31, 7083 c) Papconstantopoulos, D. A.; Pickett, W. E.; Klein, B. M.; Boyer, L. L; *Phys. Rev. B. Condens. Matter* **1985**, 31, 572 d) Linker, G.; Smithey, R.; Meyer, O.; *J. Phys. F* **1984**, 14, L115

4. Bezinge, A.; Yvon, K.; Muller, J.; Lengauer, W.; Ettmayer, P. *Sol. State Commun.* **1987**, 63(2), 141.

5. Ettmayer, P. *Monatsc. Chem.* **1970**, 101, 127.

6. Jehn, H,; Ettmayer, P; *J. Less-Common Metals*, **1978**, 58, 85.

7. Schönberg, N. *Acta Chem. Scand.* **1954**, 8(2), 2047.

8. Boudart, M.; Volpe, L. *J. Solid State Chem.* **1985**, 59, 332.

9. Jaggers, C. H.; Michaels, J. N.; Stacy, A. M. *Chem. Mater.* **1990**, 2, 150.

10. Lengauer, W. *J. Cryst. Growth* **1988**, 87, 295.

11. Fix, R. M.; Gordon, R. G.; Hoffman, D. M.; *J. Am. Chem. Soc.* **1990**, 112, 7833.

12. McCarley, R. E.; Templeton, J. L.; Colburn, T. J.; Katovic, V.; Hoxmier, R. J.; *Adv. Chem. Serv.*, **1976**, 150, 318.

13. Elwell, W. R.; Wood, D. F. *Analytical Chemistry of Molybdenum and Tungsten*; Permangon Press: New York; 1971.

14. Bremner, J. M.; Mulvaney, C. S. *Methods of Soil Analysis, Part 2. Chemical and Microbiological Properties - Agronomy Monograph* no. 9, 1982, 595.

15. Chatt, J.; Dilworth, J. R. *J. Chem. Soc., Chem. Comm.,* **1975**, 983.

16. Bevan, P. C.; Chatt, J.; Dilworth, J. R.; Henderson, R. A.; Leigh, G. J. *J. Chem. Soc. Dalton Trans.*, **1982**, 821.

17. Colton, R. J.; Rabalais, J. W. *Inorg. Chem.* **1976**, 15, 237.

18. Schwartz, W. E.; Gray, R. C.; Carver, J. C.; Taytu, R. C.; Hercules, D. M. *Spectrochemica Acta.* **1974**, 30A, 1561.

19. Sarma, D. D.; Rao, C. N. R. *J. Electron. Spect. Related Phen.* **1981**, 20, 25

SUMMARY

The tetrameric compound, $[WNCl_3]_4$, has been characterized structurally by single crystal X-ray diffraction techniques. $WNCl_3$ appears to coordinate DCE solvent molecules in a 4:1 ratio ($WNCl_3$:DCE) to produce a phase differing from uncoordinated $WNCl_3$. The reaction of $WNCl_3$ with TMSA, yields a material corresponding to the formula, $WN(N_3)Cl_2$. The thermal decomposition of $WN(N_3)Cl_2$ follows a pathway inconsistent with the formation of WN_2, the desired product. This decomposition appears to reduce the metal as the azide is oxidized to N_2. In related work, evidence for the anion, $WN_2Cl_3^{3-}$, has been found from the reaction of $WNCl_3$ and Li_3N in coordinating and non-coordinating solvents.

Ammonium tungsten bronze, $(NH_4)_{0.28}WO_3$, has been synthesized through a new route involving the ammonolysis of $WNCl_3$. The utility of this procedure was found in a tungsten imide intermediate, which increases the potential of isoelectronic imido substitution for oxide in the bronze, relative to conventional syntheses. Even though the tungsten bronze was made with a nitrogenated reactant, it was found, from a Rietveld refinement of neutron data for the bronze, that imide does not substitute for oxide to a measurable degree, in the ammonium bronze phase.

A new molybdenum azide, $MoN(N_3)py$, was synthesized by apparent

decomposition of the intermediate $Mo_2(N_3)_4py_4$. Two separate routes, using $Mo_2(O_2CCH_3)_4$ or $Mo_2Cl_4py_4$ reacted with TMSA, produce the same material, $MoN(N_3)py$. Thermal decomposition of $MoN(N_3)py$ in argon, at 250 °C, results in a material containing 24 percent C, and 16 percent N. When $MoN(N_3)py$ is decomposed thermally in ammonia, at 200 to 280 °C, the resulting product has the percent composition: N, 18; C, 5; Mo, 70. The ratio of Mo to N is 1:1.8. of The products from the thermal decomposition of $MoN(N_3)py$ have low densities, and therefore, may be of interest in catalytic applications.

REFERENCES

1. Rao, C.N.R.; Gopalakrishnan, J. *New Directions in Solid State Chemistry,* Cambridge University Press; Cambridge, UK, 1986, p 116-124.

2. Hench, L.L.; West, J.K. *Chem. Rev.* **1990,** 90, 33-72.

3. Brinker, C.J.; Clark, D.E.; Ulrich, D.R., Eds. "Better Ceramics Through Chemistry"; Elsevier: New York, 1986.

4. LaDuca, R. L.; Wolszanski, P. T. Received for publication, *Inorg. Chem.* Oct, 1991

5. Livage, J.; Henry, M.; Sanchez, C. *Prog. in Sol. St. Chem.* **1988,** 18, 289-342.

6. Toth, L.E. *Transition Metal Carbides and Nitrides,* Academic Press: New York, 1971.

7. Vidyasagar, K.; Gopalakrishnan, J.; Rao, C. N. R. *Inorg. Chem.* **1984,**23, 1206.

8. Brinker, C. J.; Scherer, G. W. *Sol-Gel Science: The Physics and Chemistry of Sol-Gel Processing* Academic Press, San Diego,1990.

9. Volpe, L; Boudart, M. *J. Solid St. Chem.***1985,** 59, 332.

10. Lengauer, W. *J. Cryst. Growth* **1988,** 87, 295.

11. Nagata, S.; Shoji, F. *Jap. J. Appl Phys.* **1971,** 10, 11.

12. Gicquel, A.; Bergongnan, M. P.; Amouroux, S.; *Proc. Electrochem. Soc.* **1983,** 83, 169.

13. Lyutaya, M. D. *Soviet Powder Metall. Metal Cer.* **1979,** 190

14. Lakhtin, Yu. M.; Kogan, Ya. D; Borovskaya, T. M.; Solodkin, G. A. *Russ. Metall.* **1979,** 4, 158.

15. Khirtrova, V. I. *Soviet Phys. Cryst.* **1962,** 6(4), 439.

16. Fix, R. M.; Gordon, R. G.; Hoffman, D. M. *J. Am. Chem. Soc.* **1990,** 112, 7833.

17. Carlson, C. D. Ph.D Dissertation, Iowa State University, 1990, Section I.

ACKNOWLEDGEMENTS

I want to thank Professor Robert E. McCarley for his support, encouragement and insight, and teaching, by example, the importance of thorough scientific investigation blended with concern for others. I wish to thank ISU instrument services personnel, Victor Young for crystallography assistance, Steve Veysey and Jan Beane for mass spectra expertise and Vinko Rutar and Dave Scott for NMR training and assistance. Matt Peterson's assistance on the molybdenum azide research was helpful and appreciated. Special thanks are due to Jim Anderegg for XPS analyses and Dr. Scott Chumbley's group for X-ray powder diffractometer use. In addition, I express my apreciation to Harold Hall, Trond Forre and Eldon Ness for excellent workmanship and timely delivery of specialized projects.

My sincere appreciation goes to those that I can call friends. Your support, love, encouragement and unlimited faith has made a significant difference. My family deserves my deepest gratitude. I appreciate my sons, Carson, Collin and Laine for making time away from school truly enjoyable. I am extremely grateful for the love and support of my mother, who sacrificed many things in order for me to attend college. I will always remember the encouragement, love, patience and faith of my beautiful wife, Sherron, during our "UV" days.

DOE Report IS-T 1608. This work was performed at Ames Laboratory under Contract W-7405-eng-82 with the U.S. Department of Energy.